The Impact of Surface Chemistry on Macrophage Polarisation

Submitted by

Hassan Muhammad Rostam, M.Sc.

Thesis submitted to the University of Nottingham for the degree of Doctoral of Philosophy

December 2016

ABSTRACT

Background: Antigen presenting cells (APCs) such as macrophages play a crucial role in orchestrating immune responses against foreign materials. The activation status of macrophages can determine the outcome of an immune response following implantation of synthetic materials, towards either healing or inflammation. A large range of biomaterials are used in the fabrication of implantable devices and drug delivery systems. These materials will be in close contact with APCs and characteristics such as surface chemistry may have a critical role in polarising macrophages towards pro- or anti-inflammatory immune phenotype. Each phenotype can be characterised by their cytokine profile, transcription factors, surface markers or even morphology.

Objectives: The overall objective of this study was identifying novel chemistries that are able to induce differentiation of human monocytes towards macrophages with distinct pro or anti-inflammatory phenotypes. To achieve this, a combination of different surface chemistries has been generated using oxygen plasma etching as well as acrylate and acrylamide polymer libraries.

Methods: Fluorescent microscopy, real time-PCR, multiplex assay, ELISA, macrophage phagocytic activity were used for macrophage phenotype identification. Libraries of acrylates and acrylamide polymer microarrays (first generation microarray of 141 polymers and second generation of 442 polymers), and oxygen plasma etching of polystyrene used as two different techniques for making different

surface chemistries. CellProfiller software was used for analysing images and was used for machine learning for phenotype identification.

Results: polystyrene with highly hydrophobic surfaces are shown to suppress expression of M1-associated surface markers and cytokines while promoting M2-associated markers. However, highly hydrophilic surfaces seem to have the opposite effect as evidenced by promoting M1-associated marker expression and pro-inflammatory cytokine production while suppressing M2-associated marker expression and anti-inflammatory cytokine production. Also, the protein thickness was proportional with the hydrophilicity of the surface, which had impact on cell polarisation.

Furthermore, co-polymers 157 from the second generation array was the most M2 biased polymer among the first and second generation of microarray polymers by induction of MR (M2 marker) cell expression, while co-polymers 217 and 123 from the second generation had impact to increase calprotectin (M1 marker). Also, cell adherence and morphology were affected by polymers surface chemistry.

Conclusion:

Surface chemistry without using polarising cytokine can polarise macrophage towards pro-inflammatory and anti-inflammatory phenotypes.

PUBLICATIONS AND PRESENTATIONS

Publications

1- **Rostam, H.M.**, Singh, S., Vrana, N. E., Alexander, M. R., and Ghaemmaghami, A. M. (2015) Impact of surface chemistry and topography on the function of antigen presenting cells. Biomaterials science 3, 424-441

2- **Rostam, H.M.**, Singh, S., Salazar, F., Magennis, P., Hook, A., Singh, T., Vrana, N. E., Alexander, M. R., and Ghaemmaghami, A. M. (2016) The impact of surface chemistry modification on macrophage polarisation. Immunobiology

3- **Rostam, H. M.**, Reynolds, P. M., Singh, S., Alexander, M. R., Gadegaard, N., and Ghaemmaghami, A. (2016) Image based machine learning for identification of M1 and M2 macrophages. The Journal of Immunology 196, 126.125(abstract)

4- **Rostam H.M.**, Reynolds P M, Singh S, Alexander M R, Gadegaard N , and Ghaemmaghami A. Image based Machine Learning for identification of M1 and M2 macrophages. (Submetted to Scientific Reports)

5- **Rostam H.M.**, Hook A, Singh S, Alexander M R, and Ghaemmaghami A. The modulation of macrophage polarisation by members of an acrylamide and acrylate polymer library (manuscript)

6- Singh S., Htwe Su, **Hassan M.R.**, Awuah D., Rajchagool B., Cha B.H., Kim D., Khademhosseini A., Ghaemmaghami A. Effect of gelatin methacryloyl (GelMA) hydrogel topography and stiffness on human macrophages (manuscript)

Presentations

1- The Impact of Surface Water Contact Angle on Macrophage Polarisation (poster), Life Sciences Symposium, 5th July 2014, University of Nottingham, UK

2- The impact of polystyrene surface wettability on macrophage polarisation (poster), Second international Scientific Conference for Kurdish Student , 15th September 2014, University of Nottingham

3- The impact of polystyrene surface wettability on macrophage polarisation (poster), Dendritic Cells and Macrophages Reunited, 8th –13th March, 2015, Quebec, Canada

4- The Impact of Polystyrene Surface Chemistry on Macrophage Polarisation (Talk), Life Sciences Symposium, 14th and 15th July 2015, University of Nottingham, UK

5- Image based Machine Learning for identification of M1 and M2 macrophages (poster),American Association of Immunologist (AAI) annual meeting 13th - 17 May,2016, Seattle, USA

Awards

1- Travel Award from the British Society for Immunology (BSI)

2- Travel Award from the School of Life Science/ University of Nottingham

3- Human Capacity Development Program (HCDP) / Kurdistan

DEDICATION

To the soul of my dad and mum

To my wife, Awat

To Maria, Muhammad and Rawa

To my brothers and sisters

ACKNOLEDGEMENTS

Firstly, I would like to express my sincere gratitude to my supervisor Prof. Amir Ghaemmaghami for the continuous support of my Ph.D. study and related research for, his motivation patience, and immense knowledge. His guidance helped me in all the time of research and writing of this thesis. My sincere thanks also go to Prof. Morgan R Alexander for his advice, enthusiasm, and his useful suggestions, and he provided me an opportunity to join his team. Without his precious support it would not be possible to conduct this research.

Special Thanks for Dr. Sonali Singh for her support and encouragement, also for Salazar Fabian, Andrew Hook, Taranjit Singh, Peter Magennis and Cato Paul and Adam David Celiz for their assistance. I thank my fellow lab mates in for the stimulating discussions, working together, encouragement, and for all the fun we have had in the last four years.

Its pleasure to acknowledge, Nikolaj Gadegaard, Paul M. Reynolds and Nihal Engin Vrana for their collaboration and assistance.

Acknowledge NEXUS Newcastle (http://www.ncl.ac.uk/nexus/) for XPS analysis, David Scurr with ToF-SIMS measurements, Human Capacity Development Program (HCDP) / Kurdistan Government for providing Scholarship, School of life Sciences and British Society for Immunology (BSI) for providing travel award.

Last but not the least; I would like to thank my wife, Awat, and my children; Maria, Muhammad and Rawa.

TABLE OF CONTENTS

TABLE OF FIGURES

LIST OF TABLS

ABBREVIATIONS

AA	Acrylic acid
AFM	Atomic Force Microscopy
APCs	Antigen presenting cells
ARG1	Arginase 1
BDEDTC	Poly(benzyl *N*,*N*-diethyldithiocarbamateco- styrene)
CCL18	Chemokine (C-C motif) ligand 18
CCR7	Chemokine (C-C motif) receptor 7
Chi3l2 or Ykl39	Chitinase 3-like 2
CHO	Chinese Hamster Ovarian
Cox2	Endoperoxide synthase-2
CTLs	Cytotoxic T cells
DCs	Dendritic cells
DG	Glycol dimethyl ether
DMAPAAmMeI	Methiodide of poly(dimethylaminopropyl-acrylamide)
D-PHI	Degradable polar hydrophobic ionic polyurethane
DSA	Drop shape analysis
DVO	Divinyl oligomer
EC	Vascular endothelial cell
ECM	Extracellular matrix
ES	Mouse embryonic stem
FBGCs	Foreign body giant cells
FBR	Foreign body reaction
GM-CSF	granulocyte macrophage colony-stimulating factor
GPCR	G-protein coupled receptor
hASCs	Human adipose stem cells
hBMSCs	Human Bone Marrow Stromal Cells
hMSCs	Mesenchymal stem cells
hNSCs	Human neural stem/progenitor cells
IFN-γ	Interferon gamma
IL-1RA	IL-1 receptor antagonist
Klf4	Kruppel-like factor 4
LPS	Lipopolysaccharide
M-CSF	Macrophage colony-stimulating factor
MDI	4,4’-methylene bisphenyl diisocyanate
MDM	Human monocyte-derived macrophages
MHC	Major histocompatibility complex
MIONs	Magnetic iron oxide nanoparticles
MMP	Matrix Metalloproteinase
MR	Mannose receptor

NK	Natural killer
NO	Nitric oxide
O2-PSs	O2 plasma etched polystyrene surfaces
OD	Octadiene
PAAm	Polyacrylamide
PAANa	Sodium salt of poly(acrylic acid)
PBMCs	Peripheral blood mononuclear cells
PCA	Principal Component Analysis
PDGF	Platelet-derived growth factor
PDL2	Programmed death ligand 2
PEG	Poly(ethylene glycol)
PEO	Polyethylene oxide
PET	Polyethylene terephthalate
PLGA	Poly-DL-lactide-co-glycolide
pMAs	Polymethacrylate
PRRs	Pathogen recognition receptors
PS	Un-treated polystyrene
Ptgs2	Prostaglandin- 2
RELMα	Resistin-like molecule-α
RGD	Arginine-glycine-aspartate
ROS	Reactive oxygen species
SAMs	Self-assembled monolayers
Si	Silicon
SNR	Signal to noise ratio
STAT	signal transducer and activator of transcription
TCP	Tissue culture polystyrene
TGFβ1	Transforming growth factor-β1
T_H2	T helper 2
TIMP1	Metalloproteinases 1
TNF	Tumour necrosis factor
TOF-SIMS	Time-of-Flight Secondary Ion Mass Spectrometry
TSLP	Thymic stromal lymphopoietin
UVO	Ultra-violet Ozone
WCAs	Water contact angles

Chapter One: General Introduction

1.1. Introduction

Some of the early evidence for using implants come from ancient Egypt back in 2500 BC, when they used gold ligature wire to stabilize teeth(1). During the past decades in line with advances in materials and biological sciences we have seen significant improvements in the biomaterials used in medical applications (2). However, in parallel with increased use of implantable medical devices we have also seen a variety of complications associated with their use (3). Implant complications can be due to a number of causes including biomechanical failure, Loss of integration (4) prosthesis instability (5), infection (6), inflammation and adverse immune responses leading to their encapsulation or rejection (7).

One of the early events upon implanting a foreign material inside the body is nonspecific adsorption of different types of protein such as albumin, complement, fibrinogen, vitronectin, fibronectin, and γ globulin on its surface (8). Water-mediated hydrophobic, hydration forces and electrostatic interactions are considered as the major factors determining protein adsorption (9).

Protein adsorption on the surface of biomaterials is therefore considered as the first step of foreign body reaction (10), playing a significant role in determining the extent and degree of the subsequent development of the immune response against biomaterials (11).

1.2. The body's response to implanted biomaterials

The foreign body reaction is the last step of inflammation and wound healing process which occurs after implantation of biomaterials, this process consists of several phases(12); recognition and inflammation, adsorption of plasma proteins, macrophage adhesion, macrophage fusion (foreign body giant cell formation) and crosstalk between foreign body giant cell and other cells.

1.2.1. Recognition and inflammation

Foreign body reaction (FBR) to implanted biomaterials is an immune-mediated, inflammatory, multifactorial process that involves different cell types and mediators (13,14). Exposure of implantable biomaterials to the host tissues can initiate acute innate immune responses through rapid neutrophil infiltration and instantaneous adsorption of different host proteins to biomaterials. Then, circulating polymorphonuclear leukocytes and monocytes move to the implant area. Subsequently, opsonins and soluble factors are release by attacking leukocytes (12) (**Figure 1.1**).

1.2.2. Adsorption of plasma proteins

Following implantation and the initial contact with the host blood, proteins such as complement, fibronectin and vitronectin adsorb on the implant surface according to the specific chemical and physical properties of the surface (8) (**Figure 1.1**).

1.2.3. Macrophage adhesion

Monocytes extravasate from blood stream and migrate to the implanted area under the effect of chemokines, then differentiate to macrophage (15). Macrophages β integrin cell receptor mediates cell adhesion via binding to the adsorbed protein on biomaterials (16) (**Figure 1.1**).

1.2.4. Macrophage fusion (foreign body giant cell formation)

As time passes, macrophages and their aggregates, known as foreign body giant cells (FBGCs) and multinucleated giant cells, are recruited to the interface between the tissue and the materials (17). This sequence of events leads to a foreign body reaction (FBR), which is the last stage of the inflammatory response to an implanted material (8). This in turn induces the adhesion of monocytes and macrophages under the

influence of soluble mediators such as IL-4 and IL-13, which released by mast cells and later by T helper 2 (T_H2) cells (8) (**Figure 1.1**).

1.2.5. Crosstalk between foreign body giant cell and others

Secreted inflammatory mediators such growth and angiogenic factors by macrophages and foreign body giant cells play an important role in regulation of fibroproliferation. Secretory factors from macrophages recruit and stimulate fibroblasts to form the fibrous capsule around the implanted biomaterials. Also, interaction between lymphocytes and macrophages play a critical role in the foreign body reaction which occurs at the tissue/material interface (8) (**Figure 1.1**).

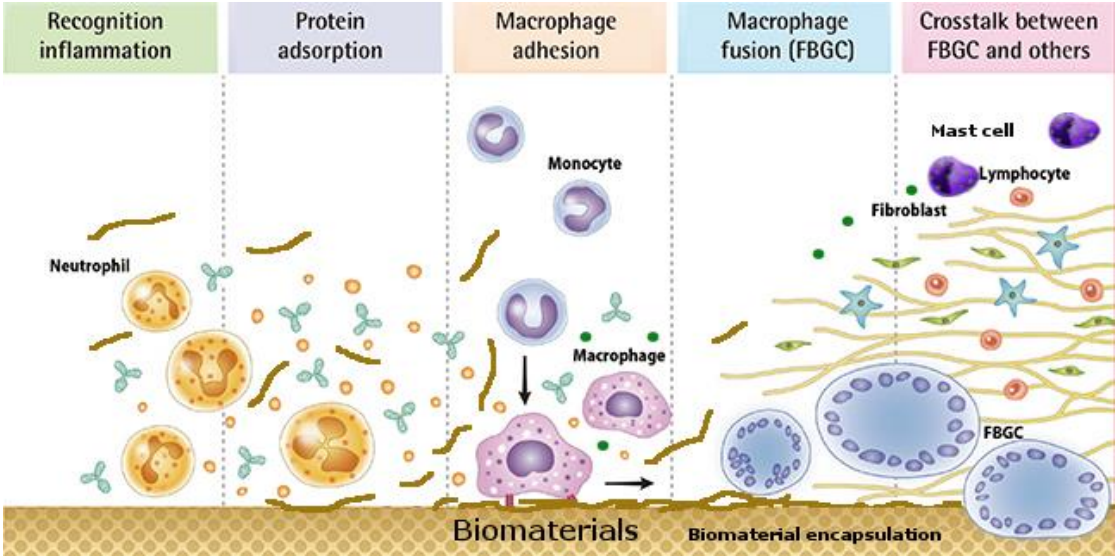

Figure 1.1: Different types of protein adhere to biomaterials; β2 integrin from cells can mediate cell adherence at the biomaterial surface. IL-4 and IL-13 from mast cell and T_H2 cell stimulate macrophage aggregation and FBGC formation, which secrete primary mediators for immune cells and fibroblasts, causing fibrogenesis and encapsulation of the implanted biomaterial. The figure has been taken from Lee *et al*. 2015 with modification (12).

1.3. Foreign body reaction in summary

Preclinical biocompatibility studies ensure that such acute responses can be avoided. However, implants can still induce subtle inflammatory responses that in the long term can have detrimental effects on the function of the implant (e.g. loosening of metal implants) and cause damage to the surrounding tissues. Antigen presenting cells (APCs), particularly macrophages (18) and dendritic cells (DCs) (19) play a central

role in orchestrating immune responses to foreign substances including biomaterials (20).

Contact with implanted materials may enhance inflammation by provoking macrophages to release cytokines that cause immune responses by other immune cells such as DCs and lymphocytes. Development of such pro-inflammatory microenvironment could typically lead to chronic inflammation, tissue damage/fibrosis, which is one of the major causes of implant failure.

Macrophages have a sensitive and rapid response against foreign material including biomaterials that are implanted in different tissues (18). Macrophages and FBGCs are the primary mediators of FBR, inducing the infiltration and stimulation of immune cells (e.g. lymphocytes) and stromal cells (e.g. fibroblasts) and fibrinogenesis at the implant site (8). At the end of the FBR, the implant can be encapsulated by a fibrous capsule and cut off from the host. This not only creates mechanical and functional problems, but for implanted devices, such as electrodes, can mean the end of their functional life-time.

Although macrophages and FBGCs can cause chronic inflammation and osteolytic activity (21), they also play an important role in regeneration and healing processes via extracellular matrix (ECM) modulation and phagocytosis (ingestion) of microbes, dead cells, and debris as well as promoting vascularisation (18). Macrophages mediate biodegradation of bioresorbable material and control the differentiation, proliferation, and recruitment of other tissue cells such as osteoblasts, fibroblasts, keratinocytes, and endothelial cells during the healing process (18).

1.4. Biomaterial surface modification

Mechanical, physical and chemical methods have been used to modulate biomaterial surface (22), which affects the interaction between the biomaterial surface and

macrophages to reduce inflammatory reactions (23). In this context, it is interesting to note that different surface modifications have been shown to be able to induce specific cellular response in other cell types such as mesenchymal stromal cells (24).

Many different types of implantable biomaterials are used in clinical practice such as intraocular lenses (25), coronary stents (26), degradable sutures (27), catheters (28), vascular grafts (29), prosthetic joints (30), cochlea (31) and pace maker replacements (32). Also many biodegradable biomaterials have been developed for tissue engineering applications (33). Most of the biomaterials which are widely used clinically have been selected due to their "bio-inertness", i.e. they are known to induce a lesser degree of immune response. But for the new generation of biomaterials where efficient integration and tissue remodelling is a crucial component, control of the immune response rather than its dampening is more appropriate. It is well-known that the surface chemistry of these materials has a significant influence on cellular responses (24), but this relationship is complex and still not fully understood, especially for immune cells including macrophages.

Here initially it is first discussed how different surface chemistries could influence cell behaviour, particularly in the context of innate immune responses by macrophages as antigen presenting cells (APCs) when interface with implanted materials. Better understanding of cell-material interactions will allow the development of new strategies for modification of implant surfaces to modulate immune responses towards anti-inflammatory and healing phenotypes.

1.5. Antigen Presenting Cells

The adaptive immune response by T cells depends on activation signals received from APCs (34), which include monocytes, macrophages, DCs and B cells (35) **(Figure 1.2).** APCs are sentinels of the immune system that can detect and capture foreign

antigens in the periphery. APCs process and present these antigens to T cells in the context of major histocompatibility complex (MHC) molecules (36). T cell activation by APCs, which typically takes place in the lymph nodes, requires at least two signals: the first signal is delivered by MHC-antigen peptide complex that interacts with T cell receptors, and the second signal is provided by co-stimulatory molecules such as CD80 and CD86 that interact with CD28 on T cell surface. Depending upon the APC's cytokine profile and maturation status, T cells may differentiate to different subsets with distinct functions (37).

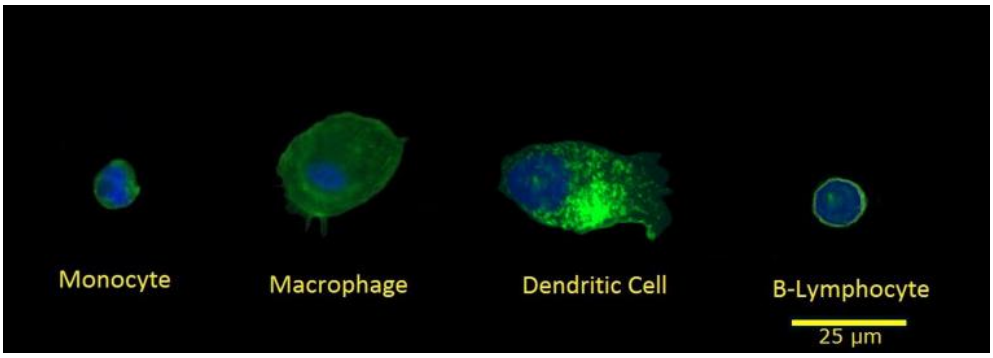

Figure 1.2: Different types of antigen presenting cells. Monocyte, naïve macrophage (human monocyte treated with GM-CSF for 6 days), dendritic cell (human monocyte treated with IL-4 /GM-CSF for 6 days), B-Lymphocyte. F-actin and cell nuclei immunostaining were performed by phalloidin Alexa Fluor 488 (green) and DAPI (blue) respectively. Scale bar = 25 µm.

The mononuclear phagocyte system includes a subgroup of leukocytes that originate from myeloid progenitor cells in the bone marrow (38). Monocytes derived from these progenitors circulate through blood vessels and migrate into tissues in response to pro-inflammatory cytokines, growth factors, or microbial products (39). Once in tissues, monocytes differentiate into DCs or macrophages (39). Monocytes as APCs are able to uptake antigen in bone morrow or in the blood vessels (40), but compared to macrophages and particularly DCs they have lower capability of antigen presentation and phagocytic activity (41).

Since their discovery by Steinman and Cohn (42), DCs have been shown to be the most potent APCs (43). DCs are found in different tissues in the body and monitor any signs of threat in the microenvironment, using a host of different pathogen recognition receptors (PRRs) (44). Typically, DC interaction with foreign antigens leads to the maturation of DCs and their migration to the local lymph nodes where they prime naïve T cells towards distinct functional subsets (45,46). In addition, DCs play a vital role in maintaining tolerance towards self-antigens (47).

The importance of the behaviour of distinct APC subsets and the ability to control their polarization have garnered the attention of the researchers in the biomaterials field (48). However, due to the diversity of materials and conditions used, lack of clear definitions and scarcity of mechanistic details, many aspects of how different biomaterials can modulate macrophage and DC function have remained elusive.

1.6. Effect of surface chemistry on cell function

1.6.1. Non-Immune cells

Different aspects of cell biology such as adhesion, differentiation, proliferation, and migration can be influenced extensively by the physical and chemical properties of biomaterial surfaces (49).

Surface chemistry has been reported to have significant effect on neural tissue regeneration (50) (**Table 1.1**). In the body, radial glial cells naturally guide nerve cells in a growing brain, inducing the linkage and directional outgrowth of nerve cells (51). Accordingly, it has been reported that micro-groove width and surface chemistry have a significant effect on both neuron and radial glia response, radial glia cells were found to prefer extreme hydrophilic and hydrophobic chemistry and microgroove surface less than 10 μm (50). In addition, hydrophilic polystyrene enhanced corneal epithelial cell attachment more than a hydrophobic surface chemistry, but after day 7, cell attachment and growth were similar (52). Also, the effects of 100 combinations of

surface topography and wettability on 3T3 dermal fibroblasts proliferation were examined by Yang *et al.*, (53) (**Table 1.1**). In these experiments different groove widths, varying from 5 μm to 95 μm, were used where each groove presented a gradient of different wettability from most hydrophilic to most hydrophobic. They concluded that surface wettability influences fibroblast proliferation more than groove widths (53). Moreover, Liu *et al.*, have shown human adipose stem cells (hASCs) can respond to different surface chemistries of substrate. In these studies, a variety of surface chemistries were obtained by depositing monolayers of alkanethiolates on gold which provide surfaces with a range of functional groups such as CH_3, COOH, OH, NH2, SH, Br and Phenyl. NH_2 surface was the most and CH_3 surface had lowest influence on cell growth rate among other surfaces. Br surface caused hASC differentiation towards adipogenic, while NH_2 promoted osteogenic differentiation, and chondrogenic differentiation was induced by SH and phenyl surfaces (54). Other studies have reported the effect of different surface chemistries on the function and development of primary human osteoblasts. Hofstetter *et al.*, seeded cells on gold, chromium, zirconium, titanium, tantalum and niobium. Results indicated that, these surfaces had little modulatory effect on cell differentiation, viability, and gene expression. Therefore, they related cell behaviour to peri-implant tissue which regulates the microenvironment more than surface chemistry (55). Silicon (Si) nano-scale roughness enhanced fibroblast cell adhesion independently of surface chemistry, but change of surface wettability affected cell adhesion behaviour (56) Cantini *et al.*, observed that super-hydrophilic polystyrene surface can influence protein adsorption and myoblast differentiation (57). On the other hand, Shen *et al.*, found that the wettability has the opposite effect on cell adhesion/migration of

vascular endothelial cells (EC) when they observed that hydrophilic surfaces enhanced cell adhesion but inhibited cell migration and vice versa (58) (**Table 1.1**).

Table 1.1 summarises examples of how the function/phenotype of different cell types can be modulated through changes in the surface chemistry where the main set of effects are the chemical groups available on the surface layer and the wettability of the surfaces. Different cell types show different tendencies towards their interaction with the surface wettability and chemical groups, which can be exploited to control their behaviour.

Table 1.1: The impact of surface chemistry on non-antigen presenting cells

Material	Sample generation method	Surface chemistry	Cell type	Effect on cellular response
Polymers with graduated amine-hydrocarbon chemistry	Micro-patterns were achieved by hot embossing against a silicon master. Surface chemistry modification was obtained by plasma polymer coating.	Surface chemistry combined with series of microgrooves (width scaled from 5-95 µm and with a depth of 3.4 µm) orthogonally	Primary neurons And radial glia	-Mid-range wettability in grooved surfaces (width 5–10 µm) caused axonal alignment. -Radial glia cells were found to prefer extreme hydrophilic and hydrophobic chemistry in groove width of 6-35 µm (50).
Polymer chemical gradients	Micro-patterns were formed by hot embossing against a silicon master. Surface chemistry modification was achieved by plasma polymer coating	Parallel grooves with widths scaled from 5 µm to 95 µm, each groove combined with WCA˚ varying from 55-95 (Chemistry=amine-hydrocarbon)	NIH 3T3 fibroblasts	-Cells aligned with grooves and coverage increased at WCA˚ 68 – 76, groove width 40–60 µm area -Surface wettability influences fibroblast coverage more than groove widths (53)
Silicon (Si)	Ultrafast laser structuring	Gradient dual-scale roughness at micro- and the nano-scale combined with different wettability	NIH 3T3 fibroblasts	Small ratios of roughness enhanced cell adhesion independently of surface chemistry but change of surface wettability by silanization to super-hydrophobic and oxidization to super-hydrophilic for the same degree of roughness affected cell adhesion (56).
Polystyrene	Super-hydrophobic surfaces achieved using one phase separation methodology Super-hydrophobic surfaces achieved using Argon plasma	Super-hydrophilic Super-hydrophobic	Myoblasts	Super-hydrophilic can influence protein adsorption and myoblast differentiation(57)

Material	Sample generation method	Surface chemistry	Cell type	Effect on cellular response
Silicon wafers	SiOx plasma coating	Range of hydrophilic (WCA˚~ 26) to hydrophobic (WCA˚ ~98.)	Vascular endothelial cell (EC)	Wettability had opposite effect on cell adhesion/migration of vascular endothelial cell (EC) when they observed that hydrophilic surfaces enhanced cell adhesion but inhabited cell migration and vice versa (58).

1.6. 2 Antigen Presenting Cells

1.6.2.1. Dendritic Cells

The effect of biomaterial surface chemistry on DC maturation and inflammatory behaviour is typically studied by culturing immature DCs derived from human peripheral blood monocytes on different biomaterial films. PLGA and chitosan films have been shown to enhance DC maturation (up-regulation of CD80, CD86, CD83, HLA-DQ and CD44) and to stimulate them to secrete pro-inflammatory cytokines (59). In addition, alginate films have been shown to induce mature DCs to release higher amounts of pro-inflammatory cytokines than immature DCs, whereas DCs cultured on hyaluronic acid films exhibited less expression of co-stimulatory molecules and HLA-DR, while agarose films did not affect DC function (59). In a similar study by Kou *et al*., the relationship between DC phenotype and biomaterial properties was investigated by assessing the response of DCs derived from human peripheral blood monocytes to 12 different polymethacrylate (pMAs) surface chemistries (60). In that study, cytokine profile and surface markers were investigated. The investigators found a strong association between DC maturation and carbon- and oxygen-treated pMA surfaces where oxygen treatment maintained immature DC phenotype, whereas carbon-treated surfaces induced strong DC maturation (60). Furthermore, the surface chemistry of biomaterials can influence DCs and differentiate them towards DC1 (pro-inflammatory) or DC2 (anti-inflammatory).

Hume *et al*., showed that magnetic iron oxide nanoparticles (MIONs) stimulated immature DCs and macrophages in mice towards DC1 and M1 phenotypes respectively. Both cell types secreted different T_H1 inducing cytokines such as IL-12 and TNF-α (61). In contrast, functionalised poly (ethylene glycol) hydrogels with immobilised immunosuppressive factors (TGF-β1 and IL-10) have been shown to decrease murine DC maturation as evidenced by suppression of IL-12 production and expression of major histocompatibility complex-II (MHCII) (62).

1.6.2.2. Macrophages

The impact of surface chemistry on macrophage phenotype and function has been investigated by different groups**.** Neutrally charged (not cationic or anionic) and hydrophilic polyacrylamide (PAAm) surfaces have been shown to induce minimal pro-inflammatory changes in human macrophages including FBGC formation *in vitro* (63) (**Table 1.2**). In addition, such surfaces cause an increase in the production of the anti-inflammatory cytokine IL-10 and a decrease in the production of pro-inflammatory cytokines IL-1β and IL-6, in adherent macrophages after 10 days of incubation. In a similar study, McBane *et al.*, observed that a degradable polar hydrophobic ionic polyurethane (D-PHI) surface affected human monocyte-derived macrophages (MDM) by inducing a decrease in the level of pro-inflammatory cytokines (TNF-α, IL-1β and HMGB1) and an increase in the anti-inflammatory cytokine, IL-10 in comparison with tissue culture polystyrene (64) (**Table 1.2**). Similarly, in another study by Schutte *et al.*, human monocytes/macrophages were seeded on different surface chemistries: polyurethane, polyethylene, polymethyl, expanded polytetrafluoro-ethylene, 1-vinyl-2-pyrrolidinone, a hydrogel copolymer of 2-hydroxyethyl methacrylate, and polyethylene glycol acrylate in tissue culture polystyrene plates. IL-1β, IL-1rα, IL-6, IL-8, IL-10, TNF-α, MCP-1, MIP-1α, and

VEGF were measured at different stages and overall they observed an increase in chemokines, cytokines, and growth factors, as an indicator of monocyte differentiation to macrophages with pro-inflammatory cytokines up-regulated. Surprisingly, production of cytokines was only slightly affected by different surface chemistries (65).

In another study Dadsetan *et al.*, showed a significant effect of hydrophobic (WCA˚ ~120) PDMS film on protein adsorption and reduction of human macrophage adhesion (66) (**Table 1.2**). In contrast, in similar research by Jones *et al.*, they found that the number of adherent cells on polyacrylamide hydrophilic and neutrally charged surfaces was decreased in comparison with hydrophobic surfaces (63) which was accompanied by a phenotypic switch from pro-inflammatory to anti-inflammatory phenotype where adherent cells showed an increase in anti-inflammatory (i.e., IL-10) and a decrease in pro-inflammatory (i.e., IL-1β and IL-6) cytokine production over time. In another study, researchers examined responses of human macrophages and monocytes to two surfaces with a terminal methyl group among 14 silane modified glass surfaces. In that study, IL-4 was used to induce formation of FBGC, and GM-CSF was used to enhance adhesion of macrophages. Interestingly they found that, the contact angle and surface energy did not have a significant effect on FBGC formation (67). In a different set of experiments, Alfarsi *et al.* combined surface chemistry with topography. Different surface chemistries of titanium such as polished (SMO) micro-rough sand blasted, acid etched (SLA) and hydrophilic-modified SLA (modSLA) were shown to differentially regulate macrophage function. For instance, SLA and SMO surfaces elicited up-regulation of 16 pro-inflammatory genes, but modSLA surface down-regulated the expression of 10 genes (TNF, IL-1α and β, CCL1, CCL3, CCL19 and CCL20, CXCL1 and CXCL8, and IL-1 receptor type 1) (68).

Table 1.2: The effect of surface chemistry on macrophage function

Material	Sample generation method	Surface chemistry	Cell source	Effect on cellular function
Polymer	Polyethylene terephthalate film (Mylar1, PET) is coated with poly(styrene-co-benzyl N,N-dimethyldithiocarbamate) (BDEDTC)	PET coated with BDEDTC (WCA˚ ~70) and polymerised with: -Polyacrylamide (PAAm) WCA˚ ~46±12 -Sodium salt of acrylic acid, (AANa) WCA˚ ~24 -Methyl iodide salt of N-(3-(dimethylamino) propyl) acrylamide, (DMAPAAmMeI) WCA ~31˚	Human monocytes	Polyacrylamide (PAAm) enhanced adherent cells to: Anti-inflammatory cytokine IL-10 ↑ Pro-inflammatory cytokines IL-1β and IL-6 ↓ Cell adherence density ↓ (63)
Polyurethane	D-PHI film preparation were formed by combining divinyl oligomer (DVO),methyl methacrylate (MMA) and methacrylic acid (MAA)	-D-PHI coated and non-coated with collagen -Tissue culture polystyrene (TCPS) coated and non-coated with collagen	Human monocyte	-Collagen coated D-PHI and TCPS had more DNA than the uncoated TCPS after 7days -There was more esterase activity for cells on TCPS than D-PHI (±collagen) after 7 days -D-PHI stimulated the decrease of pro-inflammatory cytokines (TNF-α, high mobility group box 1 protein (HMGB1) and IL-1β)and the increase of anti-inflammatory IL-10 secretion over time when compared to TCPS (64)
Modified silicon	Polymer films were prepared by extrusion	Polycarbonate urethane (Bionate® 80A with WCA˚ ~62)	Human monocytes	Hydrophobic PDMS stimulated spreading of adherent macrophage ↓ By adding IL-4, mannose receptor (MR) expression ↑ in comparison Bionate® 80A (66).
	Silastic_ BioMedical Grade ETR Elastomer Q7-4765	PDMS film with advancing contact angle of 120 °		

1.7. Clinical implications of APC-Biomaterials cross-talk

Immune response related problems are one of the most common reasons that biomaterial based implants fail (7). The dominant practice to minimise such adverse immune responses is the use of different anti-inflammatory strategies in order to improve the clinical outcomes. These include i) introduction of anti-inflammatory drugs (both steroidal and non-steroidal) and their controlled release from implant surfaces ii) development of surface coatings that decrease the immune response iii)

angiogenic agents to facilitate the integration of the implanted structures (69). Although, these approaches have provided a fair amount of success and they generally contribute to the improved functionality of implants, in many cases, they are not sufficient for the successful integration and functionality of an implant, particularly in the long term.

The problems related to such approaches mainly stem from the original understanding of biocompatibility where the immune response to a biomaterial was considered detrimental which should be kept at a minimum or suppressed (70). For example, *in vitro*, poly-ethyleneglycol (PEG) coatings were shown to induce monocyte detachment via a Matrix Metalloproteinase (MMP) dependent manner, which can explain the relatively low level of immune reaction to PEG-coated structures (71). This can be related to the highly hydrophilic nature of PEG as a general repellent for cell adhesion. However, this approach cannot be applied to biomaterials based structures such as engineered tissues as they need to be remodelled and integrated where the immune response, particularly from monocytic cells like macrophages, play an indispensable part. Thus, the new paradigm in biomaterials research is to communicate with the immune system rather than trying to avoid it. Due to their crucial role in the foreign body response, APCs are the most common target of such approaches. Better understanding of events at the interface between different biomaterials and APCs could pave the way for the rational design of new strategies to harness local immune response to biomaterials to enhance clinical outcomes.

In this context APCs can be targeted to create a favourable cytokine microenvironment (e.g. high IL-10 and TFG-β) to promote healing and implant integration. One possibility to achieve this could be delivering optimally activated

APCs to the site of implant via encapsulation. This would be similar to the delivery of insulin producing Langerhans cells used in the treatment of type 1 diabetes (72).

1.8. Macrophage phenotypes Identification

A number of different macrophage phenotypes with distinct functional properties have been identified with a spectrum of activities. The two best studied macrophage phenotypes are M1 or classically activated macrophages and M2 or alternatively activated macrophages. M1 macrophages have pro-inflammatory and anti-tumour activities, while M2 macrophages have anti-inflammatory and pro-wound healing activities (73) **(Figure 1.3).** Interferon gamma (IFN-γ) (produced by T helper 1 (T_H1) cells and $CD8^+$ T cells (adaptive immunity) or natural killer (NK) cells (innate immunity) in the presence of microbial products such as lipopolysaccharide (LPS) induces differentiation of M1 macrophages. On the other hand, interlukin-4 (IL-4) and/or IL-13, which mainly originate from T_H2 cells (adaptive immunity) (74) or from polymorphonuclear cells such as mast cells (75) (innate immunity), induce differentiation of M2 macrophages (76). However, the classification of M2 macrophages is made more complex by the fact that different studies have used the term "M2 macrophage" for macrophages activated with a diverse range of agents: e.g. immune complexes, apoptotic cells, prostaglandins, glucocorticoids, macrophage G-protein coupled receptor (GPCR) and IL-10 (77). There has been an effort to acknowledge the differences between these disparate M2 macrophage types by subdividing them into M2a, M2b, and M2c macrophages or defining a third category of "regulatory macrophages" (78). A recent review by a consortium of macrophage biologists, calls for standardisation of macrophage activation protocols and nomenclature, proposing a revised system of nomenclature that explicitly identifies the activating agent – e.g. M(IFN-γ), M(IL-4), M(IL-10), etc. (78). However, to avoid

confusion, in this study it was referred to macrophages with pro or anti-inflammatory functions as M1 or M2 respectively.

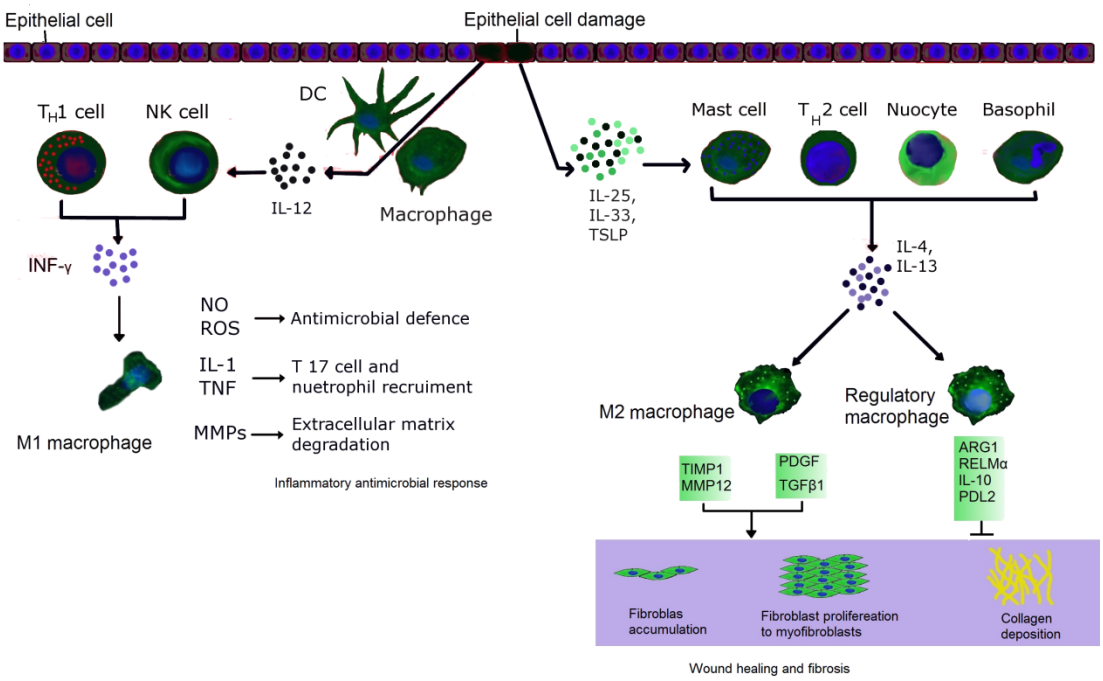

Figure 1.3: Inflammatory monocytes are recruited to the injured tissue from blood vessels. Under the effect of interferon-γ (IFN-γ) from natural killer (NK) and T_H1 cells, monocytes differentiate into pro-inflammatory M1 macrophages. M1 macrophages express reactive oxygen species (ROS) and nitric oxide (NO), and release tumour necrosis factor (TNF), interleukin-1 (IL-1) and matrix metalloproteinases (MMPs). Thymic stromal lymphopoietin (TSLP), alarmins, IL-25 and IL-33 secretion by damaged tissue induce T_H2 cells, nuocytes, basophils and mast cells to secrete IL-4 and IL-13, which stimulate macrophage polarisation to M2 or regulatory phenotypes. M2 macrophages promote wound healing via secretion of soluble mediators such as platelet-derived growth factor (PDGF), tissue inhibitor of metalloproteinases 1 (TIMP1), MMP12, transforming growth factor-β1 (TGFβ1). Regulatory macrophages express programmed death ligand 2 (PDL2), arginase 1 (ARG1), resistin-like molecule-α (RELMα) and secrete IL-10, which contribute to the wound healing process (79).

Unlike in murine macrophages where M1 and M2 activation results in distinct marker profiles, in human macrophages, there is some overlap in the expression of markers between the two activation states. For example, Arginase-1 (Arg1), which has been used as an "M2 marker" in murine macrophages, has been detected in both M1 and

M2 human macrophages (80). In addition, MR and chemokine (C-C motif) ligand 18 (CCL18) (M2 markers) can also be expressed by stimulation of monocytes with GM-CSF or IFN-γ, and LPS, respectively (81). Thus, it appears that in human macrophages, differences between marker expression in M1 and M2 phenotypes are more quantitative rather than qualitative (82).

Given the complexity of M1/M2 identification in human macrophages, an alternative approach that would be simpler, less resource-intensive, and hence, more widely adoptable is required. Studies that focussed on the morphology of different macrophage phenotypes (81,83-88) have led to the hypothesis, that cell morphology could be an indicator of macrophage activation status.

Pelegrin and Surprenant reported that murine peritoneal macrophages that are polarised to an M1 phenotype *in vitro* were distended cells with multiple lamellar processes, elongated filopodia, and distributed F-actin in the cytoplasm. On the other hand, *in vitro* polarisation of these macrophages to an M2 phenotype resulted in cells that were similar in shape to unpolarised macrophages, with less lamellar processes and paranuclear-compacted F-actin (85). Vereyken *et al*. also observed a relationship between macrophage activation and morphology in murine bone marrow-derived macrophages albeit reporting different morphologies for M1 and M2 cells. Their data suggested that M1 macrophages appeared large, rounded, flat cells, while M2 macrophages were stretched and elongated cells (88). Further, a recent study by McWhorter *et al*. succeeded in polarising murine bone marrow-derived macrophages towards an M2 phenotype by inducing the cells to adopt an elongated morphology on micropatterned grooves with a width of 20 μm (87). These data suggest that not only do different macrophage phenotypes have distinct morphologies, but also that altering

the morphology of macrophages can itself trigger alterations in the activation status of these cells.

Morphological differences have also been seen in differentially activated human macrophages. Using the human monocyte-like cell line THP-1, Lee *et al*. observed a correlation between cell morphology and the production of the pro-inflammatory cytokine TNF-α (86). Porcheray *et al*. also found that different pro- and anti-inflammatory cytokines induced distinct morphologies in human primary monocyte-derived macrophages, although in their study, there was no correlation between macrophage morphology and surface expression of a selection of M1 (e.g. MIP-1α) and M2 (e.g. MR, CD163, CCL18) markers, highlighting the limitations of relying on surface markers for determining macrophage phenotype (81). It is therefore reasonable to assume that morphological attributes of macrophages are influenced by their functional properties and can be used for their functional classification.

1.9. Aims of the project

The wettability can clearly influence macrophage polarisation in some systems, it is not a specific enough measure to be able to rationalise cell response between different classes of materials. For example hydrophilic polyacrylamide (63) and hydrophobic ionic polyurethane (64) can both induce the production of anti-inflammatory cytokines by macrophages.

Given the diversity of methods used for generating macrophages and different readouts used for determining their functional phenotype, it is not surprising that some investigators have reported that surface chemistry does not have any significant effect on macrophage polarisation (89),(67). This highlights the need for more detailed and systematic studies in this area involving multiple material systems.

Polystyrene has been used widely in the cell culture industry and it is important to understand the impact of polystyrene surface properties on immune cell phenotype.

Furthermore, the interface between cells and biomaterials is extremely complex, and it is difficult to hypothesise the start point from which materials induce immunomodulatory behaviour. Consequently, an unbiased screening approach to identify materials with immunomodulatory potential, by using inductive or data high driven approaches which cover a wide range of materials, was undertaken.

Polymer microarrays of commercially available acrylate and acrylamide libraries are ideally suited to that strategy.

Thus, the overall aim of this project was to investigate the effect of different chemistries on human monocyte derived macrophages phenotype and function. This was achieved by:

1) Using O_2 plasma etching to develop different surface chemistries on a polystyrene substrate and investigating macrophage phenotype and function on each surface

2) High throughput screening of microarray libraries of acrylates and acrylamide polymer for their ability to modulate monocyte differentiation to different macrophage subsets.

It was hypothesised that changes in surface chemistry will lead to phenotypical and functional changes in macrophages. Hence providing means to control the outcome of immune response through modifying these parameters.

In addition to facilitate future attempts for image based high throughput classification of macrophages, it was attempted to develop an alternative approach for macrophage classification based on cell morphology.

Chapter Two: Materials and Methods

2.1. Surface chemistry modifications

2.1.1. Polystyrene surface modification with O_2 plasma etching

To obtain polystyrene slides with different wettability from hydrophilic to hydrophobic, polystyrene samples (4 cm^2) were made by cutting sections from an un-treated polystyrene (PS) petri dish (Greiner bio-one Ltd., UK) with a scalpel.

Two different O_2 plasma etched polystyrene surfaces (O_2-PSs) were made by etching un-treated PS with oxygen plasma following the conditions listed in **Appendix I** using radio frequency powered equipment. Also polystyrene tissue culture plates (TCP) (Corning) were used, which have proprietary treatment as the third type of surface chemistry (90).

2.1.2. Microarray polymer Array Synthesis

Polymer microarrays were formed using an XYZ3200 dispensing station (Biodot) and homo-polymer metal pins (946MP6B, Arrayit). The printing conditions were O_2 < 2000 ppm, 25 °C, and 35% humidity. Polymerisation solution was composed of polymer (50%, v/v) in dimethylformamide with photoinitiator 2,2-dimethoxy-2-phenyl acetophenone (1%, w/v). Three replicates were printed on each slide. Polymers were purchased from Aldrich, Scientific Polymers and Polysciences and printed onto epoxy-coated slides (Xenopore) dip-coated with poly(2-hydroxyethyl methacrylate) pHEMA (4% w/v, Sigma) in ethanol (95% v/v in water) to avoid cell adhesion on the slide except the arrays. Arrays were sterilised by exposure to UV light for 15 minutes. Scale up polymer coupons were formed by pipetting polymerization solution (6µL) onto a pHEMA coated slide and irradiating for 10 mins at O_2 < 1300 ppm with a long wave UV source. Once formed, polymers were dried at <50 mTorr for 7 days (91-94).

2.2. Surface chemistry characterisation

2.2.1. Water contact angle measurement

Water contact angle (WCA) measurement on surfaces was performed on an automated DSA100 (Krüss, Germany) instrument by using pico-litre ultrapure water. Water droplets with a volume of 400 pl were dispensed on surfaces using a piezo-driven print head, repeating capture of images in a frame set at 18 ms for 5 s. Drop shape analysis (DSA 4) version 1.1 software was used to capture images. WCA was measured at the first appearance of water droplet on the surface. Averages of six measurements were obtained from each sample (95).

2.2.2. Time-of-Flight Secondary Ion Mass Spectrometry (TOF-SIMS)

ToF-SIMS experiments were carried out to detect adsorbed molecules on polystyrene surfaces. An IONTOF GmbH ToF-SIMS IV equipped with a bismuth liquid metal ion gun and a single-stage reflection analyser was used for these experiments. Polystyrene samples were adhered to double-sided tape to produce an immobile surface suitable for the instrument. By operating a Bi_3^+ primary ion source at 25 kV exhibiting a pulsed target current of ~1 pA. Both positive and negative secondary ions spectra were collected (mass resolution of >7000 at m/z = 29). 4 replicates on each sample were scanned in area patches of 500 µm × 500 µm, each patch acquired 15 frames at 1 shot/pixel. To maintain static SIMS conditions, the primary ion dose was retained below 1×10^{12} ions/cm^2. Due to the non-conductive nature of the samples, a low energy (20 eV) electron floodgun was used for charge compensation. Ion masses were determined using a high resolution TOF analyser allowing accurate mass assignments. The experiment was done with the help of David Scurr. ToF-SIMS data was acquired and analysed using SurfaceLab 6 software (ION TOF, GmbH).

2.2.3. X-ray photoelectron spectroscopy (XPS)

Chemical elements on the polystyrene surfaces were detected by XPS analysis, which was carried out using a Theta Probe MKII spectrometer with a micro-focussed monochromated X-ray Al Kα source at 15mA emission current and 10 kV anode potential Polystyrene samples were adhered to double side tape. Three points were analysed in the centre of each samples. Surveys and high resolution C1s, O1s and N1s spectra were collected at all points. Charge neutralisation was used throughout the analysis. The experiment was carried out by NEXUS Newcastle (http://www.ncl.ac.uk/nexus/). Following the data acquisition, elemental quantification was carried out using CASA XPS software (version 2.3.16 PR 1.6) with standard Scofield library.

Measured XPS N1s at% can be converted into protein layer thickness using the equation[3]:

$$d_{\mathrm{N(1s)}} = -L_{\mathrm{N(1s)}} \cos\theta \ln\left(1 - \frac{[\mathrm{N}] - [\mathrm{N}]_0}{[\mathrm{N}]_\infty - [\mathrm{N}]_0}\right)$$

Where L = electron attenuation length (3.02nm), cos(θ) =1, [N] = measured nitrogen fraction, $[N]_\infty$ = atomic fraction of nitrogen in the pure protein (15%) and $[N]_0$ = nitrogen fraction on substrate (0%) (96).

2.3. Multivariate Analysis

To determine the linear correlation between chemical molecules and polystyrene surfaces, principle component analysis (PCA) was carried out using PLS_Toolbox (ver. 5.2; Eigenvector Research, Manson, WA., USA) for Matlab (Mathwords, Inc., Natick, MA, USA) to minimizes the mean square error of approximating data was mean centred before analysis(97). PCA was performed with the help of Andrew Hook.

2.4. Atomic Force Microscopy (AFM)

AFM was used to obtain polystyrene surface topography data, it was carried out on a Dimension^{TM} 3000 AFM equipped with a NanoScope IIIa controller (Veeco Instruments ltd USA) operating in tapping mode in air. The images were processed and analysed with Nanoscope 5.30r2 software version. Then multiplatform Gwyddion software was used to process AFM data and display them to 3D images with their dimensions, also it was used to find roughness of the different polystyrene surfaces.

2.5. Monocyte isolation and culture

Buffy coats were obtained from the National Blood Service following Ethics committee approval (National Blood Services, Sheffield, UK; 2009/D055). Peripheral blood mononuclear cells (PBMCs) were obtained from buffy coats by Histopaque-1077 (Sigma-Aldrich) density gradient centrifugation. Monocytes were isolated from PBMCs using the MACS magnetic cell separation system (positive selection with CD14 MicroBeads and LS columns, Miltenyi Biotec) (98,99). This method routinely yielded 95% pure monocytes as determined by flow cytometric analysis of CD14 expression.

Purified monocytes were suspended in RPMI-1640 medium supplemented with 10% FBS, 2 mM L-glutamine and 100 U/ml penicillin and 100 µg/ml streptomycin (all from Sigma-Aldrich) (henceforth referred to as "complete RPMI medium") with the cell density of 1 x 10^6 cells/ml. 3 ml of the suspension (=3 x 10^6 monocytes) was seeded on polystyrene surfaces(O_2-PS surfaces, PS, and TCP surfaces) or 15 ml (15 x 10^6 monocytes) were seeded on microarray surface, then incubated at 37˚C, 5% CO_2 in a humidified incubator for six days.

2.6. Immunofluorescent staining

2.6.1. Phenotypical marker staining

On day 6 all adherent cells on polystyrene slides were fixed in 4% paraformaldehyde (EMS Diasum) in PBS, then blocked with 3% BSA (Sigma-Aldrich) and 1% Glycine (Fisher Scientific) in PBS. Subsequently, another blocking step was done using 5% goat serum (Sigma) in PBS. Adherent cells were stained with 2 µg/ml anti-human calprotectin mouse IgG1 Ab (Thermo Scientific), and with 1 µg/ml rabbit CD206 (MR) anti human primary Ab (Abcam) followed by 1 h incubation at room temperature. After washing, cells were stained with 8 µg/ml Rhodamin-x goat anti-mouse IgG (H+L) secondary Ab (Invitrogen), and 8 µg/ml Alexa flour-488 goat anti-rabbit IgG(H+L) secondary antibody (Invitrogen) for another hour at room temperature. Then nuclei were stained with 250 ng/ml DAPI (4',6-Diamidino-2-Phenylindole) (Invitrogen). Slides were covered with FluorSave™ anti-fade medium (Calbiochem) and mounted with Fluoromount™ (Sigma-Aldrich). Arrays were imaged using an automated fluorescence microscope (IMSTAR) and by using CellProfiler cell image analysis software (http://www.cellprofiler.org/) to identify the number of positively MR and calprotectin-stained cells from array or from polystyrene surfaces.

2.6.2. Morphological analysis of different cell types

Cells were fixed with 4% paraformaldehyde in PBS as described in phenotypical marker staining section, washed twice with PBS (5 min per wash), then permeabilized by 0.2 % Triton-X100 (Sigma-Aldrich) in PBS for 20 min. All the steps in this procedure were carried out at room temperature. After 2 washes with PBS, non-specific binding was blocked with 5% goat serum in PBS as described in the previous section. This was followed by 2 washes with PBS and cytoskeleton staining of F-actin

with 5 µg/ml Alexa Fluor® 488 Phalloidin (Cell Signalling Technology) in 1% goat serum and 0.1% sodium azide (Sigma-Aldrich) for 30 min, cells were then washed 3 times with PBS and stained with 250 ng/ml DAPI (4',6-Diamidino-2-Phenylindole) (Invitrogen) in PBS for 5 min, washed 3 times with PBS, then embedded with anti-fade medium, and finally mounted on a slide followed by imaging using a florescent microscope (LEICA)(**chapter 5**) or with IMSTAR (**chapter 3 and 4**).

2.6.3. Determining M1 and M2 phenotype identification criteria using fluorescence microscopy

Cells of different activation states were produced using cytokine addition monocytes seeded on normal glass slides: for polarisation to M1 a mixture of 20 ng/ml IFN-γ (R&D Systems) and 50 ng/ml GM-CSF (Miltenyi Biotec) was added to a total volume of 1ml; for M2 differentiation 20 ng/ml of IL-4 (Miltenyi Biotec) and 50 ng/ml M-CSF (Miltenyi Biotec) were added to the well volume of 1 ml. The cells were incubated at 37ºC, 5% CO_2 in a humidified incubator for 6 days. On day 3 of incubation, 500 µl of the medium was replaced with fresh complete RPMI medium containing the same concentration and mix of cytokines that were used for cell stimulation at the beginning of culture. After six day of incubation M1 and M2 macrophages were stained with calprotectin (M1 marker) and MR (M2 marker) (see chapter two, phenotypical marker staining section). Images of both phenotypes were taken with an automated fluorescent microscope. Automated image analysis software (CellProfiler) was used to measure and record the maximum fluorophore intensity (to avoid false positive signal for each phenotypes) per image for nine different images. This was repeated for two different samples for the same biological donor and the average value of calprotectin in M2 and MR in M1 calculated. These values were used as threshold intensity values of calprotectin and MR in order to categorise cells not exposed to cytokines, with each cell exhibiting a fluorescence intensity above these

calprotectin and MR thresholds categorised as M1 and M2 respectively (**Appendix II).**

2.7. Cytokine analysis

IL-6, IL-10, and IL-1β production were measured using FlowCytomix bead-based multiplex system (eBioscience) with a slight modification to the manufacturer's instructions (100-102). Sample or standard (10 μl) was mixed with 10 μl of a cocktail of beads coated with primary antibodies for the detection of the cytokines of interest and 20 μl of a cocktail of biotin-conjugated secondary antibodies in a FACS tube and incubated for 2 h at room temperature in the dark. Tubes were then washed twice with 400 μl each of assay buffer to remove unbound beads and antibodies. 20 μl of diluted streptavidin-phycoerythrin (PE) conjugate was then added to each tube and the samples / standards incubated for 1 h at room temperature in the dark. Samples were washed twice with assay buffer as before and re-suspended in 400 μl assay buffer, stored at 4^{o}C, and analysed on a Beckman Coulter FC500 flow cytometer within 24 h. Results were analysed using the eBioscience FlowCytomix Pro 3.0 software.

CCL18 was measured using the human CCL18/PARC DuoSet ELISA kit (R&D Systems) as per the manufacturer's instructions (100-102).

2.8. RNA extraction, cDNA conversion and quantitative real-time PCR (qRT-PCR)

To quantify STAT1, ATAT6, SOCS1, SOCS3, IRF4 and IRF5 transcription factors, quantitative real-time PCR (qRT-PCR) was performed. Total RNA was extracted from cells using the RNeasy Plus Minikit (Qiagen). Cells were lysed with RLT buffer, and the lysates were homogenized by QIAshredder (Qiagen) and centrifuged at 8000 g for 2 min. The flow though was transferred to a gDNA eliminator spin column placed in a 2 ml collection tube and centrifuged at 8000 g for 30 s. A volume of 70% ethanol

was added to the flow though and mixed well by pipetting. The mixture was then transferred to an RNeasy spin column placed in a 2 ml collection tube and centrifuged at 8000 g for 15 s. The flow through was discarded and 500 µl of RPE buffer was added to the RNeasy spin column and centrifuged at 8000 g for 2 min. After discarding the flow through, the spin column was placed in a new collection tube and centrifuged at 8000 g for 1 min. The spin column was placed in a 1.5 ml centrifuge tube and added 30 µl RNeasy-free water. Subsequently, the spin column was centrifuged at 8000 g for 1 min to elute RNA.

The concentration of the total extracted RNA was measured using nanodrop ND1000 spectrophotometer (Thermo Scientific). cDNA was synthesized from 1 µg of total RNA using the superscript III first-strand synthesis kit (Invitrogen) according to the manufacturer's protocol. Using a LightCycler® 96 machine (Roche). qRT-PCR was performed based on TaqMan and SYBR chemistry. The data were analysed by LightCycler® 96 SW 1.1 software (Roche). Six different primers were used (**Table 2.1**).

Table 2.1: **Forward and reverse primer sequences used in qRT-PCR experiments**

Genes	Primers/probe	Sequence (5'-3')
GAPDH	Forward	GAGTCAACGGATTTGGTCGT
	Reverse	GACAAGCTTCCCGTTCTCAG
STAT1	Forward	GGAAGGGGCCATCACATTCA
	Reverse	GTAGGGTTCAACCGCATGGA
STAT6	Forward	CTCGCTGGACAGAGCTACAG
	Reverse	CCCTCTGCTGTCTTCTCCCT
SOCS1	Forward	CCCTGGTTGTTGTAGCAGCTT
	Reverse	TTGTGCAAAGATACTGGGTATATGT
IRF5	Forward	GCCATGAGCAGGGAAAGAAC
	Reverse	CCCTTAGGCAATTCCTCCTATACA
SOCS3	Life Technologies Hs02330328_s1 *(Taqman)*	
IRF4	Life Technologies Hs01056533_m1 *(Taqman)*	

For the normalization, *GAPDH* was chosen as the house-keeping gene (103). Relative expression of each gene of interest was calculated based on relative standard curve method. Standard curve for each gene was plotted based on Ct value and log concentration of five 2-fold-serial dilution of a pool of all cDNA samples. Equation for each gene was generated by linear regression analysis. The concentration of each gene was calculated from interpolation of the Ct value corresponding to the standard curve. The relative expression of the target gene was determined by the concentration of target gene divided by the concentration of *GAPDH*.

2.9. Phagocytosis activity

To detect phagocytic activity of monocytes on different polystyrene surfaces, monocytes seeded on PS and O_2-PS40 were incubated with Alexa Fluor 488-conjugated zymosan A (*Saccharomyces cervesiae*) BioParticles (Molecular Probes, Thermo Fisher Scientific) with the concentration of 25 particles/cell at 37 °C for 30 min and then cells were washed 5 times with PBS. Cells were imaged with a Zeiss LSM 880 confocal microscope using a 40x oil objective lens (NA = 1.30), a 488 nm argon laser, and 500–535 nm emission bandwidth. Images were captured using Zen digital imaging software.

2.10. Image analysis and machine learning for phenotype identification

Composite images of f-actin and DAPI staining were loaded into CellProfiler, and metadata detailing the cell type in the image was extracted from the file name. After optimisation of the primary detection of the cell nucleus (DAPI channel), followed by secondary detection of the cell body (f-actin channel) the full dataset of 93 images was analysed in 4 h on a high spec desktop computer (Dell XPS). The extent of each cell was then morphologically analysed for a broad range of descriptors such as area,

orientation, extent, shape, intensity, etc. A total of 228 measurements were acquired for each cell, and a database was established for the full experiment, which was comprised of 93 images. The machine learning step was then carried out in CellProfiler Analyst. Here, 50 cells were randomly selected from the training data set representing each of the different phenotypes. The software then performed a GentleBoosting algorithm to establish a set of 25 rules (**Figure 5.7** and **Figure 5.8**) capable of identifying the different phenotypes based on individual morphometric values for each cell. Progress was checked by cross validation of the classifier, after which the user could add further training data to improve accuracy.

2.11. Statistical analysis

The one-way ANOVA and unpaired Student t-test were employed within the GraphPad Prism 6 program for assessing statistical significance of differences between conditions. Pearson correlation was used to calculate the coefficient of determination (r^2) between variables. P values > 0.05 were considered statistically significant in all tests. Signal to noise ratio (SNR) is the ratio of the *mean value* of the signal and the *standard deviation* of the noise (104) SNR of 2 used as a threshold for cell phenotype differences (105). *n*= number of different biological donors.

Chapter Three: The Impact of Polystyrene Surface Chemistry Modification with Oxygen Plasma Treatment on Macrophage Polarisation

3.1. Introduction

Implanted biomaterials typically trigger an inflammatory immune response orchestrated by macrophages (106). Often this results in a cascade of inflammatory and fibrotic events known as the foreign body response (FBR) (107). FBR begins with protein adsorption on the implant surface, which promotes the adhesion of monocytes and macrophages (108). Macrophages are sensitive to micro-environmental changes and mount a rapid response to implanted materials, they can also fuse under the influence of the cytokines interleukin 4 (IL-4) and IL-13, forming foreign body giant cells (FBGCs). Macrophages and FBGCs induce infiltration and stimulation of immune cells (e.g. lymphocytes) and stromal cells (e.g. fibroblasts), leading to inflammation and fibrosis at the implant site (14). FBR can end with sequestration of the implant within a fibrous capsule (8). This creates mechanical and functional problems, and for devices such as electrodes, can mean the end of their functional life (69). Macrophages are extremely plastic cells, adopting a wide spectrum of phenotypes in response to different stimuli (109). The physical, chemical, and topographical characteristics of implanted materials can affect macrophage polarisation, resulting in macrophages that are either predominantly pro-inflammatory or anti-inflammatory (110).

The two best studied macrophage phenotypes are M1 and M2. M1 (classically activated) macrophages with pro-inflammatory and anti-tumour function (73) can be generated in vitro from monocytes by treatment with the T helper (T_H) 1 cytokine interferon gamma (IFN-γ) (111) and/or lipopolysaccharide (LPS) (112). The addition of granulocyte macrophage colony-stimulating factor (GM-CSF) during M1 polarisation augments the pro-inflammatory function of these cells (113,114). By contrast, M2 (alternatively activated) macrophages with anti-inflammatory and pro-

wound healing activities (73) can be generated in vitro from monocytes by treatment with the T_H2 cytokines IL-4 (111,115) and/or IL-13 (111). The addition of macrophage colony-stimulating factor (M-CSF) during M2 polarisation can enhance the anti-inflammatory function of M2 macrophages (111,115).

M1 macrophages produce high levels of pro-inflammatory cytokines such as IL-12, IL-23 (116), tumour necrosis factor alpha (TNF-α) (117,118), IL-6, and IL-1β (117). They are also characterised by elevated expression of the chemokine (C-C motif) receptor 7 (CCR7) (119), CCR2 (120), calprotectin (121), and nitric oxide synthase 2, inducible (NOS2) (122). In contrast, M2 macrophages secrete large amounts of anti-inflammatory and pro-fibrotic cytokines such as IL-10 (123), transforming growth factor (TGF-β) (118), and IL-1 receptor antagonist (IL-1RA) (124). In addition, these cells express high levels of mannose receptor (MR) (119,123,125) and the scavenger receptor CD163 (122,123).

Additionally, M1 macrophages express high levels of prostaglandin-endoperoxide synthase 2 (Ptgs2 or Cox2) and IL23p19 genes, and exhibit phosphorylation of signal transducer and activator of transcription 1 (STAT1). M2 macrophages can be identified by high levels of Kruppel-like factor 4 (Klf4) and chitinase 3-like 2 (Chi3l2 or Ykl39) gene expression, and STAT6 phosphorylation (79).

Appropriate regulation of macrophage activation post-implantation is extremely important, since these cells play a crucial role in the elimination of microbes and debris, biodegradation, tissue regeneration and vascularisation, and extracellular matrix reorganisation following tissue damage (18). Therefore, macrophages and FBGCs, either directly or through modulating the function of other cell types, can tip the balance between chronic inflammation and restitution /wound healing following biomaterial implantation (21).

In order to minimise implant-associated inflammation, various approaches have been used to modulate macrophage-biomaterial interactions (23,110). Biomaterial surface chemistry is one factor that impacts cellular responses (24) as it influences the amount, identity and conformation of protein adsorption on the surface (126), which in turn modulates cell behaviour. For instance, surfaces functionalised with the arginine-glycine-aspartate (RGD) peptide, chitosan, and vitronectin stimulate expression of CD147, CD98, MR, and CD13 (molecules related to macrophage fusion) in monocytes (66,127,128).

Modification of material surface chemistry has been used to change the functional properties and phenotype of different cell types (129,130), including immune cells (131,132). Such strategies would enable the development of materials with distinct cell-instructive properties that could be used for devices such as pace maker replacements (32), prosthetic joints (30), intraocular lenses (25), vascular grafts (29), degradable sutures (27), etc.

Many studies have focused on developing biomaterials with low attachment or anti-adsorbent properties to avoid cell adhesion. An alternative approach could be modifying biomaterials' surface properties to guide cells differentiation towards a specific phenotype (pro/anti-inflammatory). Clearly the prerequisite to achieving such a goal is to gain a better understanding of particular surface chemistries and protein adsorbates that are able to promote macrophage differentiation to a specific cell phenotype (M1 or M2 macrophages).

It was hypothesised that treating polystyrene by oxygen plasma etching can lead to changes in the surface chemistry of polystyrene, which affect the quantity and quality of adsorbed proteins, and subsequently stimulate signalling pathways of macrophages that can lead to macrophage polarisation to a particular phenotype.

The overall aim was therefore fabricating polystyrene with different surface chemistry using O_2 plasma etching, and investigate if any of the resulting surface chemistries could induce macrophage differentiation to pro-inflammatory/anti-tumour (M1) or anti-inflammatory/pro-healing phenotype (M2) macrophage phenotypes. In addition, characterisation of the protein layer on each surface could identify unique protein signatures associated with either pro or anti-inflammatory phenotypes.

In this study, O_2 plasma etching was employed (a process used routinely in the mass production of tissue culture ware (133)) to develop different surface chemistries using polystyrene as substrate. Then phenotype was characterised by cytokine profile, and functional properties of human monocytes that were cultured on these surfaces for 6 days. Finally, to better understand how these surface chemistries influence monocyte differentiation and macrophage polarisation, initial characterisation of protein adsorbates on each of the surfaces was conducted.

3.2. Material and methods

3.2.1. Material preparation

Radiofrequency plasma deposition of oxygen was used to achieve 4 different polystyrene samples (2 cm^2) (see **chapter 2.1.1.**). Water contact angle (WCA) measurements for 60 spots on each surface were then performed, using an automated DSA100 (Krüss, Germany). All polystyrene surfaces were washed with PBS and sterilised with UV with 254 nm wavelength for 20 minutes.

3.2.2. Surface chemistry and topography characterisation

Time-of-Flight Secondary Ion Mass Spectrometry (TOF-SIMS) An IONTOF GmbH ToF-SIMS IV instrument was used for adsorbed amino acid detection on different polystyrene surfaces (see **chapter 2.2.2.**). Principle component analysis (PCA) was carried out using PLS_Toolbox (see **chapter 2.3.**) for data analysis. In addition, X-ray

photoelectron spectroscopy (XPS) analysis was carried out using a Theta Probe MKII spectrometer with a micro-focussed monochromated Al Kα source to detect C1s, O1s and N1s. (see **chapter 2.2.3.**). Three different repeats for each surface condition were in one experiment.

Surface topography and surface roughness measurement has been carried out by Atomic Force Microscopy (AFM), DimensionTM 3000 AFM (see **chapter 2.4.**) Three different repeats were used for untreated PS and O2-PS40 surfaces.

3.2.3. Cell experiments

Monocytes isolated from Buffy coats were obtained from six different donors (see chapter 2.5.). Suspension 3 ml, 1 x 10^6 monocytes/1ml RPMI medium (supplemented with 10% foetal bovine serum (FBS), 2 mM L-glutamine, 100 U/ml penicillin, and 100 µg/ml streptomycin) were seeded on polystyrene surface. Prior cell seeding, surfaces were washed with PBS and sterilized with UV 254nm wavelength for 20 minutes and placed inside a 6-well TCP plate with three replicates per condition. Samples were incubated at 37˚C, 5% CO_2 in a humidified incubator for six days. On the second day of incubation, surfaces were moved to a new a 6-well TCP plate and the same volume of cell culture media was added. On day six of incubation, supernatants were collected for cytokine analysis IL-6, IL-10, IL-1β and CCL18 cytokine analyses, for 3 different donors (see **chapter 2.7.**). All adherent cells on polystyrene slides of one donor with three repeats were fixed and stained with fluorescent antibodies calprotectin (M1 cell marker) and MR (M2 cell marker) for fluorescent microscopy imaging by IMSAR fluorescent microscope (see **chapter 2.6.1.**). Then, the CellProfiler were used for processing and analysing the images. Furthermore, adherent cells on PS and O_2-PS40 surfaces for 3 different donors on day 6 of the experiment were used for STAT1, SOCS1, SOCS3, IRF4 and IRF5

transcription factors analysis by quantitative real-time PCR (qRT-PCR) (see **chapter 2.8.**). In addition, monocytes seeded on PS and O_2-PS40, were exposed to phagocytosis activity experiment after six days of incubation for 3 different donors (see **chapter 2.9.**).

3.2.4. Statistical analysis

The one-way ANOVA and unpaired Student t-test were employed within the GraphPad Prism 6 program for assessing statistical significance of differences between conditions. Pearson correlation was used to calculate the coefficient of determination (r^2) between variables. P values > 0.05 were considered statistically significant in all tests.

3.3. Results

3.3.1 Characterisation of polystyrene surface wettability

Polystyrene surface wettability was determined by measuring the WCA of each surface in air[1] (air-water contact angle). On day 0 of plasma treatment, untreated PS was the most hydrophobic (WCA=84˚±4˚), followed by O_2-PS8 (59˚±4.7˚), commercial TCP (38˚±9˚), and the most hydrophilic surface, O_2-PS40 (10˚±2˚) (**Figure 3.1**). After six days of oxygen plasma etching, the WCA had remained the same on all surfaces. However, on all surfaces after six day of incubation in RPMI medium (containing 10% FBS, 2 mM L-glutamine, 100 U/ml penicillin and 100 µg/ml streptomycin) WCA was approximately 18º (**Figure 3.1**).

[1] Surfaces with high surface energy (hydrophilic) in air-water contact angle, while it has low interface energy (hydrophilic) when it measured in oil-water contact angle and vice versa (140).

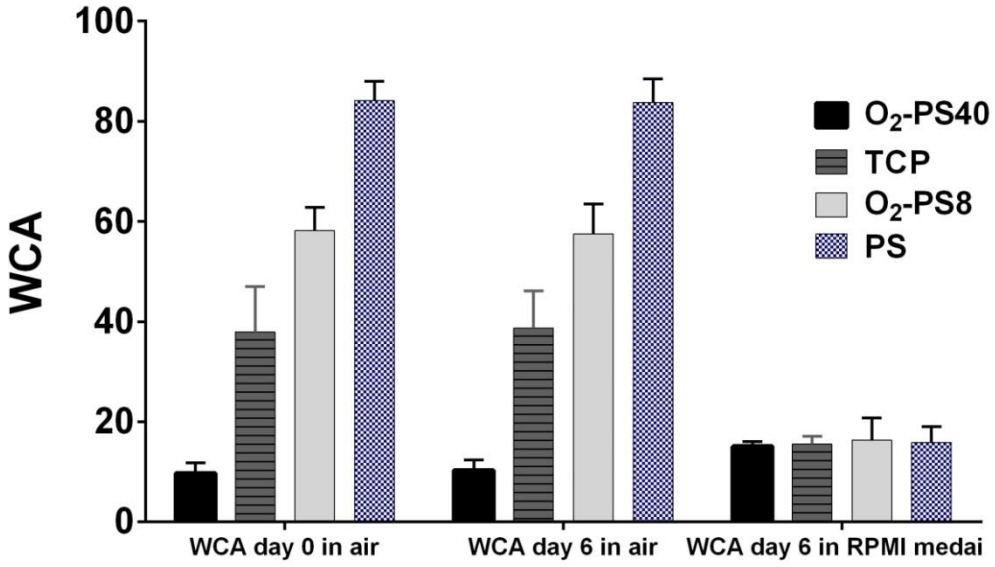

Figure 3.1: Water contact angle (WCA) of polystyrene and TCP surfaces. The graph depicts the mean WCA ± SD for *n*=4 different experiments for WCA day 0 in air, and *n*=1 experiment for other 2 conditions (there were 3 different repeats for each samples). Oxygen plasma-etched polystyrene (O_2-PS40 and O_2-PS8), tissue culture plastic (TCP), and untreated polystyrene (PS).

3.3.2. The effect changes in surface wettability on monocyte attachment and expression of calprotectin and mannose receptor

The number of monocytes adherent to the 4 surfaces after 6 days of incubation was compared. There were significant differences in the number of adherent cells on O_2-PS8 compared to O_2-PS40 (p=0.0027) and PS (p=0.0015) (**Figure 3.2**)**.** Differences between the other conditions were not significant.

Furthermore, the ratio of MR^+ to calprotectin$^+$ cells on each surface was measured as an indication of M2 vs. M1 polarisation, respectively. The highest ratio of M2/M1 marker expression was observed in PS followed by O_2-PS40 (**Figure 3.2**). O_2-PS8 showed the lowest M2/M1 ratio. Also, it had the highest number of naïve (non-polarised) cell when compared with cell on other surfaces (**Figure 3.2**). In terms of total number of cells expressing M1 or M2 markers, the only statistically significant

difference was higher number of calprotectin+ cells on TCP compared to PS (p=0.0483).

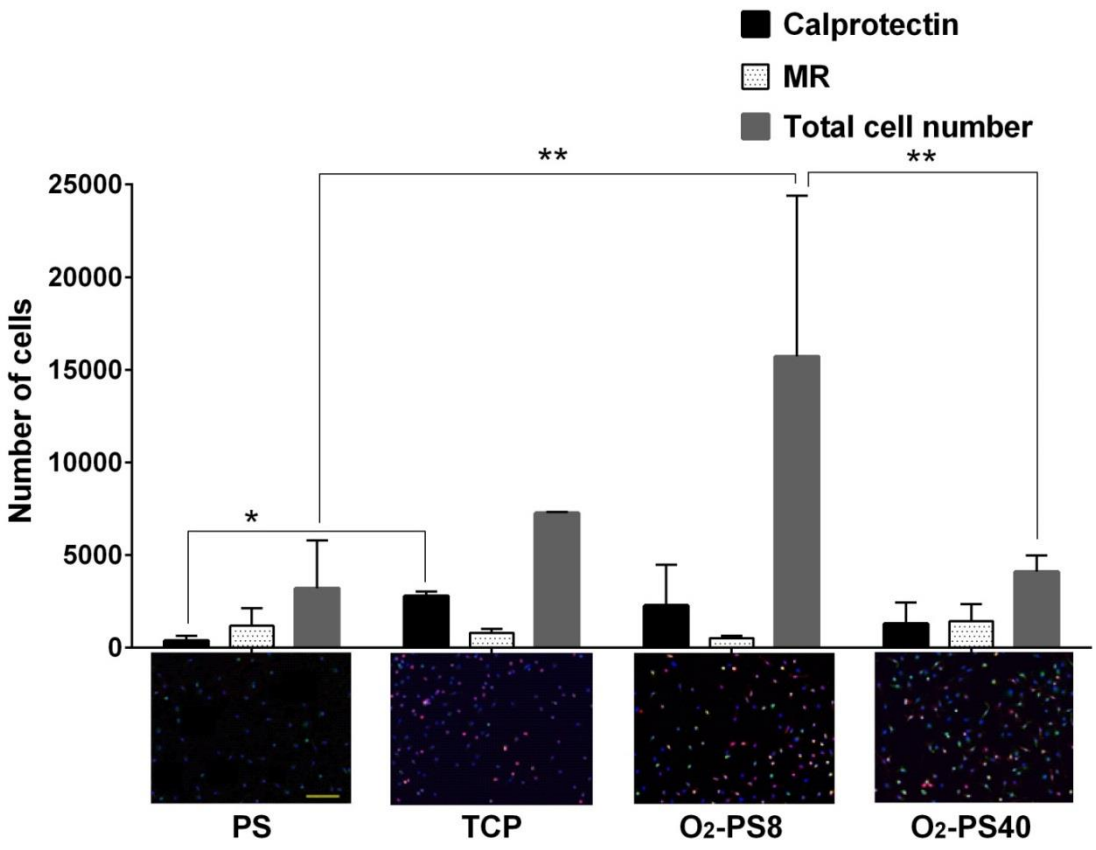

Figure 3.2: Monocytes seeded on polystyrene and TCP surfaces for 6 days. The number of adherent cells and calprotectin-MR cell markers expression on PS, O_2-PS and TCP surfaces was measured after 6 days of culture. The graph depicts mean cell number ± SD for *n*=6 different experiment (O_2-PS40 and PS) and *n*=2 different experiment, (O_2-PS8 and TCP) one donor with three repeats has involved in each experiment. Cells were stained with rabbit anti-human MR primary antibody and goat anti-rabbit secondary antibody conjugated with Alexa Fluor 488 (green), mouse anti-human 27E10 primary antibody (against calprotectin) and goat anti-mouse secondary antibody conjugated with Rhodamine red-X (red), and DAPI (blue) to visualise the nucleus. Scale bar=200 µm, all images are at the same magnification. Calprotectin and mannose receptor analysed quantitatively by using CellProfiler (**see appendix III**). Significance calculated by one-way ANOVA with Tukey's post-test: *, $p \leq 0.05$; **, $p \leq 0.01$.

3.3.3. A highly hydrophobic surface induces production of IL-10 but not CCL18 by macrophages

Cells on PS produced significantly higher levels of IL-10 compared to O_2-PS40 (p=0.0008), TCP (p=0.0050), and O_2-PS8 (p=0.0022) (**Figure 3.3A**). By comparison, cells on O_2-PS8 produced significantly more CCL18 than cells on any other surface (**Figure 3.3B**). Cells on O_2-PS40 produced the highest levels of IL-6 and IL-1β, with negligible levels produced by cells on PS (**Figure 3.3C, D).** Cytokine data was not been normalised with cell number on each surface, because the same number of the cells were seeded on each surface and the cells were not proliferative.

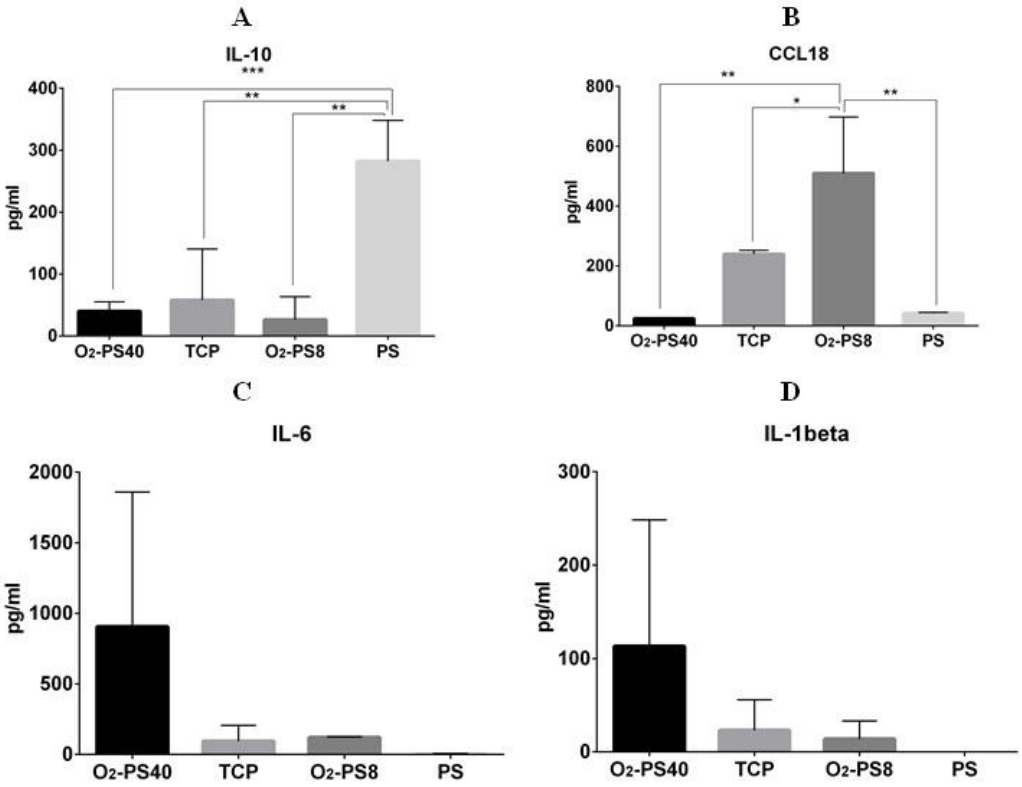

Figure 3.3: Cytokine analysis of monocytes seeded on polystyrene and TCP surfaces for 6 days. (A) IL-10, **(B)** CCL-18, **(C)** IL-6 and **(D)** IL-1β. The graphs depict mean cytokine production ± SEM for monocytes seeded on O_2-PS40 and PS (*n*=4), O_2-PS8 and TCP (*n*=3) surfaces, (*n*) is number of donors with 2 repeats, the experiment has been done once. Significance calculated by one-way ANOVA with Tukey's post-test: *, p≤0.05; **, p≤0.01; ***, p≤0.001.

3.3.4. A highly hydrophilic surface supports differentiation of monocytes towards pro-inflammatory macrophages

qRT-PCR was used to determine the relative expression of activation state-associated transcription factor mRNA in monocytes differentiated on O_2-PS40 and PS surfaces. Significant increases in the expression of pro-inflammatory transcription factors STAT1 ($p<0.0001$) and IRF5 ($p=0.0059$) were seen in monocytes on O_2-PS40 compared to those on PS (**Figure 3.4A, C**). Also, there were significant differences in SOCS1 expression ($p=0.0239$), but not IRF4 expression ($p=0.0786$), between monocytes seeded on O_2-PS40 and PS surfaces (**Figure 3.4D, E**). The difference between SOCS3 transcription factor expression on the two surfaces was significant (**Figure 3.4B**).

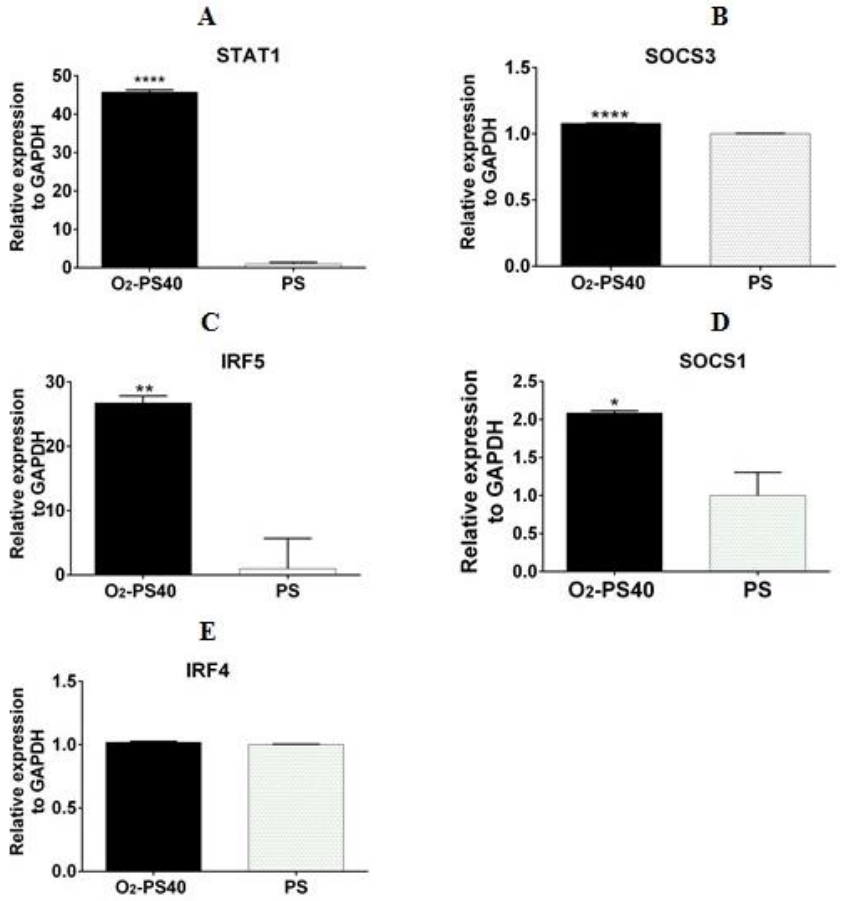

Figure 3.4: Comparison of transcription factor mRNA expression in monocytes seeded on un-treated polystyrene (PS) with water contact angle 84.2° and oxygen plasma etched

polystyrene (O_2-PS40) with water contact angle 9.8°. qRT-PCR analysis of **(A)** STAT1, **(B)** SOCS3, **(C)** IRF5, **(D)** SOCS1, **(E)** IRF4 relative mRNA expression in monocytes on PS and O_2-PS40 macrophages after 6 days of culture. All values are reported relative to the house-keeping gene GAPDH. The graphs depict mean gene expression ± SEM of 3 different donors (3 technical replicates performed for each donor). Significance calculated by Student's t test: *, p≤0.05; **, p≤0.01; ****, p≤0.0001.

Furthermore, presented data shows monocytes differentiated on O_2-PS40 were highly phagocytic as evidenced by the engulfment of fluorescently labelled zymosan particles. Cells differentiated on PS showed negligible phagocytic activity (**Figure 3.5**).

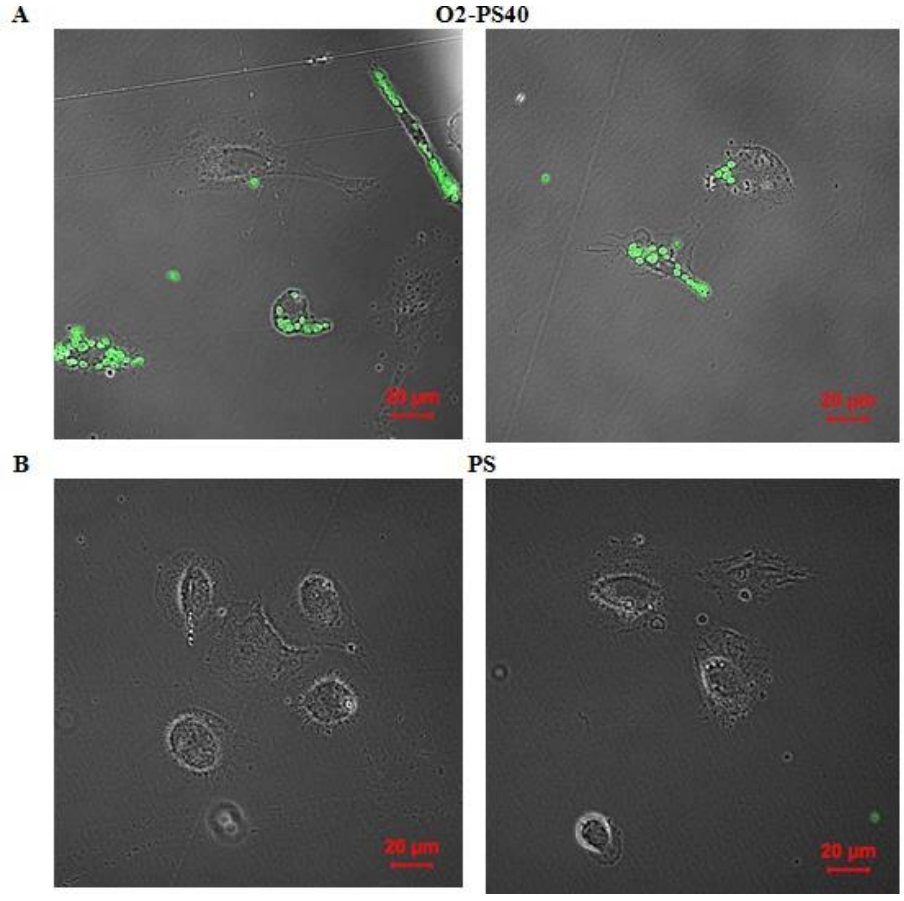

Figure 3.5: Phagocytic activity of monocytes cultured on O_2-PS40 and PS surfaces for 6 days. On Day 6 of culture, monocyte-derived macrophages on **(A)** O_2-PS40 and **(B)** PS were treated with Alexa Fluor 488-labelled zymosan particles for 30 min at 37°C, 5% CO_2. All images were taken from the same experiment. The images are representative for 2 experiments, each experiment with one donor and 2 replicates. Scale bar=20 µm.

3.3.5. Characterisation of surface chemistry and protein adsorbate quantification on hydrophobic and hydrophilic surfaces

The oxygen concentration determined by XPS on the surfaces was 2.5±0.2% on PS, 5.3±1.1% on O_2-PS8, 6±1.2% on TCP and 12.0±1.4% on O_2-PS40 (**Table 3.1**). Significant differences in the oxygen concentration of the different surfaces were observed (**Figure 3.6A**). The surface oxygen introduced by plasma etching and proprietary TCP treatment correlated positively with surface hydrophilicity (**Figure 3.6**B, r^2=0.9212, p=0.0402).

Table 3.1: Carbon (C), Oxygen (O), and Nitrogen (N) atomic percentage concentration on polystyrene and TCP surfaces before and after incubation with culture medium. Data presented are mean of *n*=3 different donor with 3 replicates in one experiment.

	Elemental concentration (Atomic %) before incubation with culture medium			**Elemental concentration (Atomic %) after incubation with culture medium**		
	C	**O**	**N**	**C**	**O**	**N**
PS	96.4	2.5	1.1	81.3	11.1	7.5
O_2-PS8	94.0	5.3	0.6	75.9	15.1	9.0
TCP	93.1	6.0	0.8	77.7	13.5	8.8
O_2-PS40	87.1	12.1	0.7	73.1	17.1	9.8

To characterise the surface chemistry of the materials under culture conditions, samples were incubated in culture medium without cells. The nitrogen concentration of each surface was used to quantify the amount of adsorbed protein (135). The protocol used retained strongly adsorbed protein species on the surface but removed weakly adsorbed ones prior to surface analysis

After incubation with the culture medium, significant elemental composition differences were observed for all surfaces (**Table 3.1**). The protein overlayer thickness also differed significantly between all the surfaces ($p \leq 0.0001$), except between TCP and O_2-PS8 surfaces (p=0.3390) (**Figure 3.6C**). The following hierarchy was

observed for protein overlayer thickness: PS, 2.11±0.06 nm < O_2-PS8, 2.76±0.01 nm < TCP, 2.67±0.11 nm < O_2-PS40, 3.19±0.03 nm. Further, the protein adsorption on these samples showed a strong but non-significant correlation with surface WCA (r^2=0.8727, p=0.0658) and oxygen atomic percentage before medium treatment (r^2=0.8825, p=0.0606) (data not shown).

By comparing the observed protein overlayer thickness to the size of the most abundant globular protein in serum, albumin, it can be seen that the protein layer ranges from 2.1 to 3.2 nm monolayers in thickness. Thus, even at the lowest protein coverage, the cells would likely encounter a completely covered polymer surface. Consequently, in an attempt to gain some insight into the composition of this protein layer surface mass spectral analysis using ToF-SIMS was carried out.

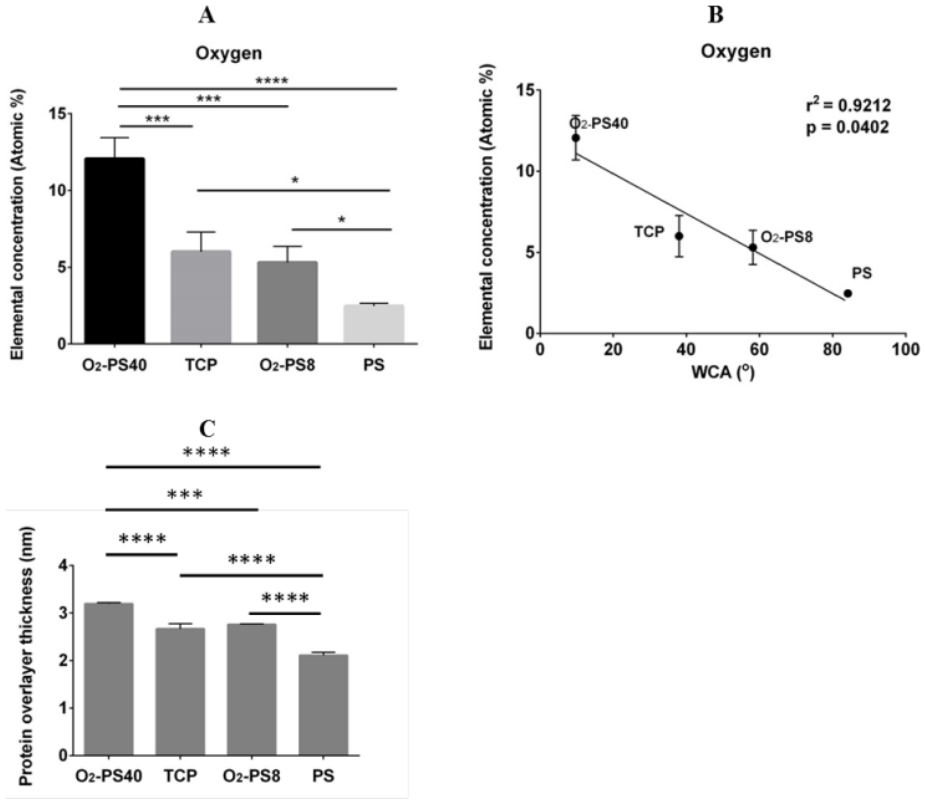

Figure 3.6: (A) Oxygen concentration (atomic percent) on polystyrene and TCP surfaces before incubation with cell culture medium (mean ± SD, *n*=3). Significance calculated by one-way ANOVA with Tukey's post-test. **(B)** Pearson correlation of surface oxygen concentration before incubation with medium vs. the WCA of the surfaces (mean ± SD, *n*=3). **(C)** Thickness

(nm) of protein overlayer on polystyrene and TCP surfaces. Surfaces were incubated with cell culture medium, following protein overlayer thickness was measured (mean ± SD, *n*=3 different donor with 3 replicates in one experiment). Significance calculated by one-way ANOVA with Tukey's post-test: *, p≤0.05; ***, p≤0.001; ****, p≤0.0001.

To effectively assess differences in the complex spectra between samples, PCA was used to identify the key variance across the datasets. Plots of PC1 and PC2 for the positively charged ions in the ToF-SIMS data discriminated between all 4 surfaces and replicate measurements clustered together, indicating similarity of the information contained in the spectra (**Figure 3.7A**). All 4 samples were separated from each other using the ions contained in PC2, while PC1 separated O_2-PS8 from the other surfaces (**Figure 3.7A**). For PC2, negative loadings for PC2 were associated with particular amino acids (**Figure 3.7B**) (135), suggesting that a significant contribution in the PS sample had a positive score, whereas the other 3 samples had negative scores, with TCP having a score between the other two samples. The majority of the ions with the highest positive or variance in surface chemistry is associated with differential protein adsorption and/or orientation. Specifically, secondary ions associated with tyrosine and phenylalanine, lysine, histidine, valine, and methionine (**Figure 3.7C**) had positive loadings, indicating a higher intensity of these amino acids on PS samples. For the positive PC2 loadings, it was also notable that there were ions that could have derived from polystyrene, m/z=55.0548 (C4H7+); m/z=77.0377 (C6H5+); m/z=105.0699 (C8H9+), suggesting that there may be areas uncoated by proteins. Ions associated with arginine, alanine, and proline had negative loadings for PC2, indicating that these amino acids were present at a higher intensity on O_2-PS8, TCP, and O_2-PS40 samples. Thus, the surface protein composition was substantially different on the 4 surfaces.

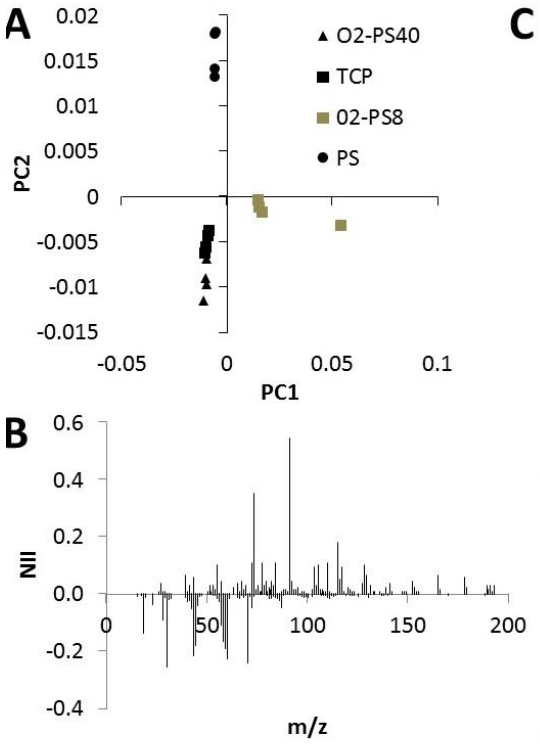

C

Loading	m/z	Assignment	Associated amino acid
0.55	91.0567	$C_7H_7^+$	Tyrosine, phenylalanine
0.35	73.0643	$C_2H_7N_3^+$	
0.18	115.0518	$C_4H_7N_2O_2^+$ $C_9H_7^+$ $C_5H_9SN^+$	
0.11	84.088	$C_5H_{10}N^+$	Lysine
0.11	110.078	$C_5H_{10}N^+$	Histidine
0.11	72.0856	$C_4H_{10}N^+$	Valine
0.11	77.0377	$C_6H_5^+$	
0.11	105.0699	$C_8H_9^+$	
0.10	55.0548	$C_4H_7^+$	
0.10	128.0509	$C_5H_6N^+$ $C_6H_{10}SN^+$ $C_6H_8O_3^+$	
0.10	117.0617	$C_5H_{11}SN^+$ $C_8H_7N^+$ $C_4H_9N_2O_2^+$	
0.10	103.0508	$C_3H_7N_2O_2^+$ $C_8H_7^+$ $C_4H_9SN^+$	Methionine
0.07	165.0663	$C_8H_9N_2O_2^+C_6H_7N_5O^+$	
-0.25	30.0368	CH_4N^+	
-0.24	70.0707	$C_4H_8N^+$	Proline, Arginine
-0.23	60.0554	$CH_6N_3^+$ $C_3H_8O^+$	
-0.22	43.029	$CH_3N_2^+$	
-0.19	59.049	$CH_5N_3^+$ $C_3H_7O^+$	Arginine
-0.18	44.0509	$C_2H_6N^+$	Alanine
-0.17	58.0676	$C_3H_8N^+$	
-0.14	18.0363	H_4N^+	
-0.09	28.0203	CH_2N^+	

Figure 3.7: ToF-SIMS analysis of polystyrene and TCP surfaces after incubation with cell culture medium. (A) Scores plot for PCs 1 and 2 using positive ions only. (B) Loading plots for PC2. List of ions with the highest **(C)** positive or negative loadings for PC2 with corresponding assignments and associated amino acids. *n*=3 different donor with one 2 replicates in one experiment

PS and O_2-PS40 surfaces from either ends of the WCA spectrum were selected for topographical characterisation using AFM. Both surfaces had similar roughness, r_a=11.4 nm and 11.2 nm respectively (**Figure 3.8**).

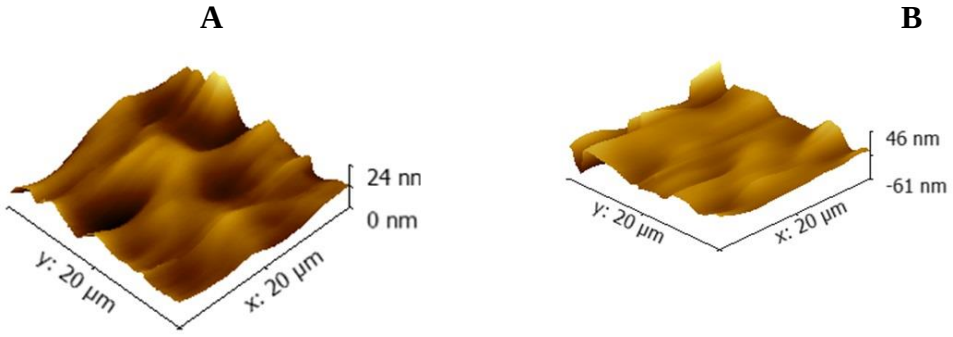

Figure 3.8: Atomic force microscopy (AFM) images of polystyrene surfaces before treating with cell culture medium. (A) PS surface**. (B)** O2-PS40. Representative images of *n*=2 different donor with 3 replicates in one experiment.

3.4. Discussion

In this study, it was observed that monocyte differentiation towards different macrophage phenotypes in response to altered surface chemistry in the absence of exogenous polarising cytokines. Given its widespread use for tissue culture, polystyrene was used for surface modification studies. Using O_2 plasma etching 4 surfaces were developed with distinct chemistries that were graded by their surface wettability (measured as WCA). Untreated PS was the most hydrophobic and O_2-PS40 the most hydrophilic. Presented data show that the hydrophilic surface O_2-PS40 stimulated monocyte polarisation towards a pro-inflammatory M1-like phenotype while the hydrophobic surface PS had the opposite effect.

The ratio of MR+ (M2-marker (119,123,125) cells to Calprotectin+ (M1-marker (121)) cells was ~3 on PS and decreased to ~1 on O_2-PS40. This was in line with the cytokine profile of the cells where monocytes cultured on PS secreted significantly higher levels of the anti-inflammatory cytokine IL-10 (21). Also, phagocytic activity in PS-cultured cells was negligible compared to O_2-PS40-cultured cells (136). The effect of macrophage polarisation on phagocytosis depends upon whether the phagocytosis is Fc-mediated or mediated by a specific pathogen recognition receptor (77,137). Fc-mediated phagocytosis is reduced in M1 macrophages, while non-Fc-mediated phagocytosis of yeast (e.g. Candida albicans) is increased in M1 macrophages (77). In this assay, phagocytosis would be mediated both through Fc receptors due to the presence of FBS in the medium as well as through zymosan-specific receptors such as the mannose receptor (MR), complement receptors and β-glucan receptors (138).

Analysis of transcription factor expression gave a more mixed picture of surface-induced macrophage polarisation. IRF4 was expressed at similar levels in monocytes on both O_2-PS40 and PS surfaces. This corresponds to previous reports of IRF4 gene

expression being similar in M-CSF and GM-CSF-induced human macrophages (139). Cells on O_2-PS40 expressed highly significant levels of the pro-inflammatory transcription factors STAT1 (77,140) and IRF5 (139,141) compared to cells grown on PS. However, O_2-PS40-cultured cells also expressed significantly more SOCS1 (142,143) than PS-cultured cells. SOCS1 is associated with M2 macrophage activation as it downregulates IFN-γ-driven JAK2/STAT1 and TLR/NF-κB signalling, and promotes arginase 1 expression (142). Interestingly, Whyte *et al*. reported that SOCS1 can inhibit IL-10 secretion (143). This may explain the significant increase in IL-10 production by SOCS1-low cells on PS vs. SOCS1-hi cells and lower IL-10 secretion on O_2-PS40 surfaces. Given that the balance of SOCS1 and SOCS3 expression in macrophages affects their activation state (142), data from this study suggest that macrophages cultured on polystyrene display a unique phenotype that may be directed towards a more pro-inflammatory or anti-inflammatory state by modifications to surface wettability.

Given the potential impact of surface chemistry on protein absorption, it was hypothesised that the impact of different polystyrene surfaces on macrophage polarisation is due to differences in the identity and conformation of proteins adsorbed on these surfaces (126). To test this hypothesis, surface chemistry characterisation of all surfaces was carried out by XPS and ToF-SIMS. The XPS data showed that the greatest total amount of protein was adsorbed on hydrophilic O_2-PS40. Similar results were reported by Grinnell and Feld when they found that fibronectin adhesion to hydrophilic glass was more than to hydrophobic functionalised glass. However, others have reported that fibronectin binds to hydrophobic polystyrene surfaces more than to hydrophilic surfaces (144). Furthermore, ToF-SIMS data confirmed that ions assigned to amino acids arginine, alanine, and proline were more prevalent on O_2-PS40, while

ions assigned to tyrosine, phenylalanine, lysine, histidine, valine, and methionine were (135) more prevalent on PS.

From this surface characterisation data, it is reasonable to propose that the adsorbed protein, controlled by the polystyrene surface chemistry, influences the macrophage response. An example of known interaction with proteins is macrophage engagement of fibronectin and fibrinogen on implanted biomaterial surfaces through leukocyte β2 integrin receptors (particularly αMβ2 (Mac-1) mediator (145,146)), which initiates signalling pathways leading to macrophage activation and secretion of inflammatory cytokines such as IL-6, IL-1α, TNF-β (147), and chemotactic factors such as IL-8 and macrophage inflammatory protein 1 beta (MIP-1β) (63). In addition to the type of adsorbed proteins, their orientation on a surface can affect the type of macrophage response (148).

Polarizing cells with chemically modified polystyrene surfaces, without using exogenous cytokines, and discovering the amino acid correlated with each surface, were important findings in these experiments.

3.5. Conclusions

Data from this study clearly show that changes in surface chemistry resulting from O_2 introduction by plasma treatment affect protein adsorption on the material. This in turn appears to influence monocyte polarisation towards macrophages with distinct phenotypes. Specifically, hydrophobic PS was shown to suppress expression of M1-associated markers and cytokines while promoting M2-associated markers. On the other hand, highly hydrophilic O_2-PS40 had the opposite effect. Protein overlayer thickness and amino acid profiles were different on hydrophilic and hydrophobic polystyrene, suggesting differences in protein adsorption.

Therefore, it can be suggested that changes in the chemistry of material surfaces can be a powerful tool for modulating macrophage phenotype and function without using polarising cytokines. This has clear implications in biomaterial design and function with applications in cell culture and medical device fabrication amongst others.

Chapter four: the modulation of macrophage polarisation by members of an acrylamide and acrylate polymer library

4.1 Introduction

Macrophages play a key role in orchestrating immune responses against foreign bodies. These cells are able to directly phagocyte foreign bodies and secrete chemokine and cytokines, which are crucial in regulating inflammation and foreign body clearance or retention (149). At the site of inflammation they are also able to induce and control the recruitment and activation of other immune cells such as lymphocytes. These processes are crucial for tissue healing and remodelling after injury (150), as well as for the body's response to implanted biomaterials (106). Protein adsorption on the implanted surface stimulates monocyte and macrophage adhesion on the implants (107,108). Surface chemistry of biomaterial has impact on the identity of the adsorbed protein (151,152) which subsequently influences macrophage adhesion (153). Macrophages interact with adsorbed protein through integrin receptors (16). Integrin stimulation cause downstream signal transduction network lead to cytokine and growth factor activation (154) which in turn leads to inflammation and the fibrotic cascade, a phenomenon referred to as the foreign body (FBR) response. Interleukin-4 (IL-4) and IL-13 from mast cells and T helper 2 (T_H2) cells are the cytokines that predominantly influence adherent macrophages on the surface to aggregates and fuse to form foreign body giant cells and multinucleated giant cells. This, in turn, stimulates the infiltration of other immune cells such as lymphocytes and fibroblasts to implant site, leading to fibrinogenesis (14). This can create functional and mechanical issues for some implanted devices (69).

There are different markers for each macrophage phenotype; the pro-inflammatory (M1) phenotype is associated with a high level of calprotectin expression (121), while anti-inflammatory (M2) phenotype can be characterised by high levels of mannose receptor (MR, CD206) expression (119,123,125).

Macrophages exhibit a wide spectrum of phenotypes (109) in response to physical, chemical and topographical properties of substrates they come in contact with, which can promote pro-inflammatory or anti-inflammatory responses (16,154-159). Macrophage activation and FBGC formation in response to different polymer fibre diameter, (160,161) geometry (162), surface roughness (163,164) and surface topography (165). Recently poly(ethylene glycol), poly(acrylate), poly(acrylamide) and the sodium salt of poly(acrylic acid) have been reported to have an anti-inflammatory effect on macrophages, while methyl iodide of poly(3-(dimethylamino) propyl) acrylamide had a pro-inflammatory effect (166).

Polymeric materials in a high-throughput microarray format (94)have previously been used to study the interaction of between hundreds to thousands of unique polymers with bacteria (167), stem cells (168,130) and epithelial cell attachment (169), and would be suitable for identifying novel materials that alter the phenotype of macrophages without requiring a prior understanding of the biological-material interaction.

The complexity of interface of biology and biomaterials is so great that no plausible hypothesis exist to direct an experimentalist to a starting point from which immunomodulatory behaviour might be elicited from the material. Consequently, in the quest for materials which have immunomodulatory potential, an unbiased screening strategy similar to what was described by Douglas Kell in his 2003 bioassay arguing for using inductive or data high driven approaches to locating the starting point was employed (170) to cover a wide range of materials.

Polymer microarrays are ideally suited to this approach when coupled with commercially available monomer libraries. Therefore, commercially available acrylate

and acrylamides were screened without regard to their identity, which enables a non-biased screening of the available chemical space (171).

In this study, a wide screen on a first generation homo-polymer library consisting of 141 monomers (meth)acrylates and (meth)acrylamides for their ability to induce the differentiation of monocytes to distinct macrophage phenotypes was carried out. A second generation library consisting of co polymers of the hit monomers identified from the first generation was then investigated. Monocytes were seeded on the first generation arrays of 141 homo-polymers for six days and the 10 most effective polymers for cell polarisation toward the M1 or M2 phenotypes and cell adherence were chosen to produce a second generation of 442 co-polymers. From the second generation polymer array, 'hit' polymer formulations were identified that were able to influence the M1 and M2 phenotypes in macrophages.

4.2. Materials and methods

4.2.1. Polymer Array Synthesis

Polymer microarrays were synthesized using methods described in **chapter 2.1.2.** Microarray slides were placed inside a Petri dish, washed with PBS and then sterilized with UV with wavelength of 254 nm for 20 minutes.

4.2.2. Cell experiments

Monocyte isolated from buffy from three different donors (see **chapter 2.5.**) and diluted to cell density of 1 x 10^6 cells/ml. Cell suspension 15 ml;1 x 10^6 monocytes/1ml RPMI medium with 10% foetal bovine serum (FBS), 2 mM L-glutamine, 100 U/ml penicillin, and 100 µg/ml streptomycin) were seeded on microarray slides with four and three replicates on homo-and co-polymer slides respectively, and incubated at 37˚C, 5% CO_2 in a humidified incubator for six days. On the second day of incubation, surfaces were moved to a new Petri dish with the

same amount of RPMI medium. All adherent cells on microarray slides were fixed and stained with fluorescent antibodies calprotectin (M1 cell marker) and MR (M2 cell marker) (see **chapter 2.6.1.**). In addition, cells incubated for six days on another slide using cells from the same donor were used for observing the morphological differences of cells on microarray polymers, by fixing them and staining the actin cytoskeleton of the cells with phalloidin Alexa Flour 488 and their nucleus with DAPI (see **chapter 2.6.2.**).

All arrays were imaged using an automated fluorescence microscope (IMSTAR) and CellProfiler analysis software (http://www.cellprofiler.org/) was used for proccing and analysing the images.

4.2.3. Determining significance on the micro array using a signal to noise ratio (SNR) threshold

To understand when the mean value of cell number or fluorescence from the three replicates was significant relative to the variance observed across those individual measurements a test comparing the magnitude of the mean to the measured variance was applied. Cell data from the first and the second generation of micro array were tested using the SNR which is the ratio of the *mean value* of the signal and the *standard deviation* of the noise (104). An SNR of 2 was used as a threshold for differences in cell phenotype (105), adherence and cell morphology, below which the data were excluded.

4.2.4. Statistical analysis

Statistical significance was calculated using ANOVA, $p \leq 0.05$ was considered significant for morphological differences between the cells.

4.3. Results

4.3.1. First generation wide chemical space homo-polymer microarray

Monocytes from three different healthy donors were cultured on the first generation arrays composed of 4 replicates of 141 unique homo-polymers for 6 days. The list of monomers and their numerical codes used in this study is presented in (**Appendix IV**). After 6 days of cell culture the arrays were washed and immune stained for M1 (i.e. calprotectin) and M2 (i.e. MR) markers. Cells were also stained for actin cytoskeleton (phalloidin Alexa Fluor 488, green) and nucleus (DAPI) of macrophages in order to assess total cell adhesion and cell morphology. All these parameters were considered together to identify the optimal material for influences the macrophages towards a M1 or M2 phenotype.

Using fluorescence microscopy the number of MR^+ and $calprotectin^+$ cells was quantified for each homo-polymer. Using the M1 and M2 identification criteria developed on cytokine differentiated naïve macrophages which were polarised with M2/M1 ratio of about 0.1 and 3.5 respectively. When average M2/M1 ratio of 3 different donors were compared homo-polymer number 101 (N,N'-methylenebismethacrylamide) was the most effective at polarising the cells towards the M2 phenotype, with 2.5 times more cells expressing MR with a high degree of cell attachment (67.7±68.8 cells) was also observed on this homo-polymer as seen in **Figure 4.1A**. The highest M2/M1 ratio were observed with in the second donor on homo-polymer number 35 (hexyl acrylate) and 143 (dimethylamino-propyl acrylate) which scored M2/M1 ratio of (13.2±4.4) and (8.9±2.5) fold respectively, both polymers had high number of cell attachment of (111±12) and (104±50) cells respectively. Other materials in the first donor were polarising cells towards the M2 phenotype included homo-polymer numbers 42 (cyclohexyl methacrylate) and 21

(tetraethylene glycol dimethacrylate), with ratios of MR^+ to $calprotectin^+$ cells of (1.9± 0.6) and (1.9±0.8)-fold, respectively (**Figure 4.1B**). Homo-polymers 26 (butyl acrylate), 51(hydroxy-3-phenoxypropyl acrylate) and 60 (tricyclodecane-dimethanol diacrylate) in the first donor were with average M2/M1 ratio of around 1 (**Figure 4.1A**). Homo-polymers 69 (butanediol diacrylate), 70 (furfuryl methacrylate), 113 (heptadecafluorodecyl methacrylate), and 141 (dimethylamino-ethyl methacrylate) from the third donor were the most effective at polarising cells towards the M1 phenotype whilst still supporting the attachment of more than 50 cells, with 4 times more $calprotectin^+$ cells than MR^+ cells (**Figure 4.1D**). Furthermore, homo-polymers 61 (ethylhexyl methacrylate) and 47 (n-(tris(hydroxymethyl)methyl)acrylamide) exhibited high MR+ /calprotectin+ ratio (37 and 29 respectively) and, homo-polymer 73 (n-phenylmethacrylamide) showed low ratios (0.45), but their mean values were < 2 the inter and intra spot variance and therefore they were considered unreliable.

Cell adhesion varied across the polymer library by over 1 order of magnitude from 9.8±3.9 cells observed on homo-polymer 39 (tridecafluorooctyl methacrylate) to 229.7±64.8 cells observed on homo-polymers 42 (cyclohexyl methacrylate). Homo-polymers 133 (norbornyl methacrylate), 90 (di(ethylene glycol) diacrylate), 103 (hexyl methacrylate), 21 (tetraethylene glycol dimethacrylate), 94 (3-hydroxy-2,2-dimethylpropyl 3-hydroxy-2,2-dimethylpropionate diacrylate), 69 (butanediol diacrylate), 96 (carboxyethyl acrylate), 92 (n-dodecylacrylamide) and 33 (hexanediol ethoxylate diacrylate) also showed high levels of adherent cell, with values of 209±47.5, 197±69.2, 171.3±32, 168.6±17.8, 167.6±32.6, 146.6±8.2, 137.2±52.8, 132±38.5 and 127.1±25.3 cells, respectively. Other polymers with low cell attachment included homo-polymer 91 (n-hydroxyethyl acrylamide) (13.1±4.4 cells), 62 (propargyl acrylate) (17.3±6.3 cells), and 10 (29±10.1 cells) (**Figure 4.1I-K**).

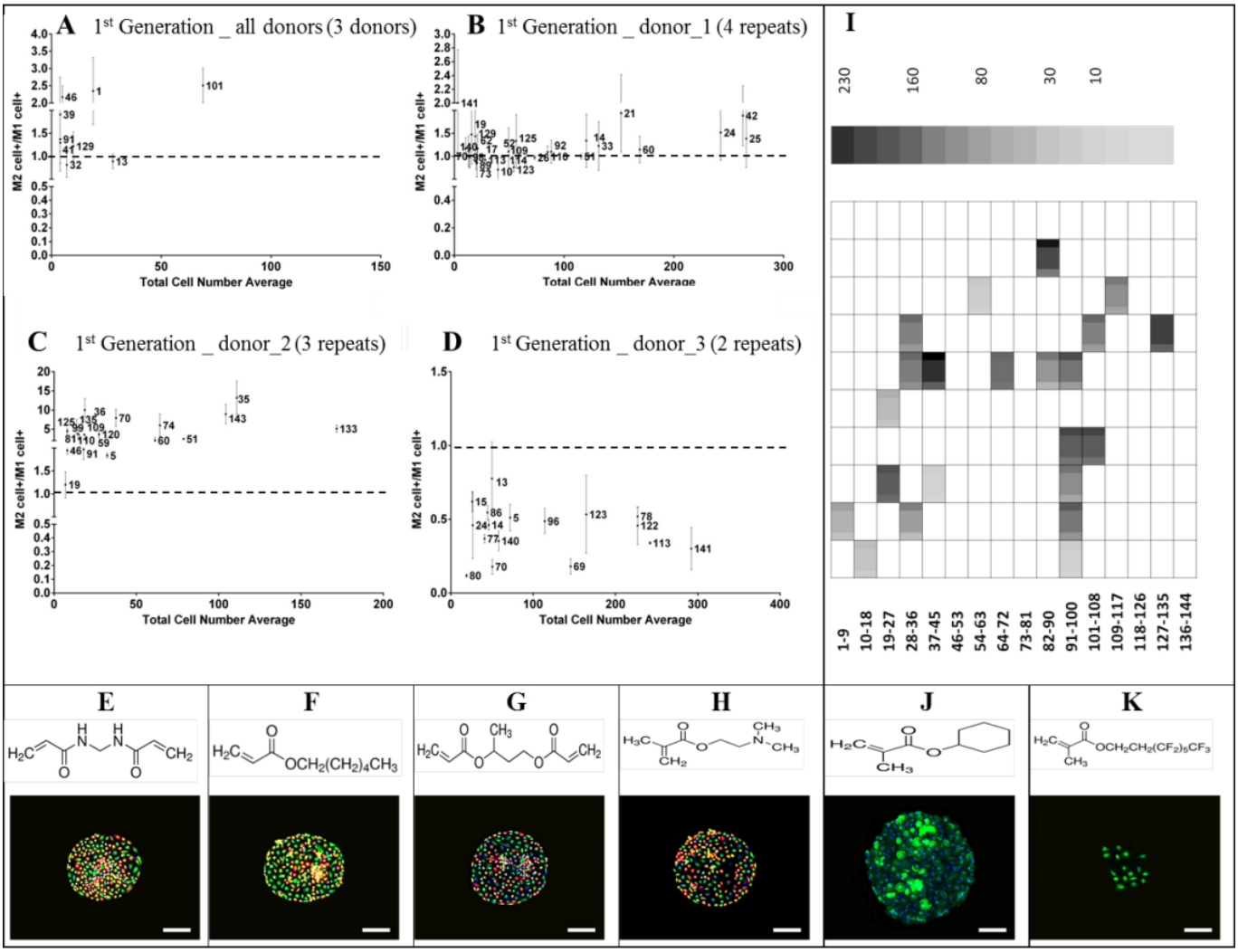

Figure 4.1: First generation microarray homo-polymers on macrophage polarisation and cell adherence. (A-D) Scatter plot for three different donors of M2 cell$^+$/M1 cell$^+$ average on homo-polymers, x-axis average total cell number on homo-polymer ,Y-axis is average of cells expressed MR$^+$(M2- phenotype)/ number of cell expressed calprotectin (M1- phenotype) on homo-polymer after six days of incubation. Dotted line is cells with M2- cells (MR$^+$ cells)/M2- cells (calprotectin$^+$ cells) =1.(A) Inter donor M2/M1 cell+ ratio average between all three donors. **(B)** Intra donor M2/M1 cell+ ratio average in donor number 1 (average of 4 repeats), **(C)** donor number two (average of 3 repeats), and **(D)** donor number 3 (average 2 repeats). (**E-H**) Effective homo-polymers (chemical structure) on macrophage polarisation, fluorescent images of cells stained for calprotectin (27E10 antigen, red), and mannose receptor (MR, green) and nucleus (DAPI blue) on most effective homo-polymers **(E)** homo-polymer 101(N,N'-methylenebismethacrylamide). **(F)** homo-polymer 35(hexyl acrylate). **(G)** homo-polymer 69 (butanediol diacrylate). **(H)** homo-polymer 141(dimethylamino-ethyl methacrylate). **(I-K) Cell adherence on homo-polymers**. **(I)** Average number of adherent cells on different polymers. Numbers indicate the homo-polymer identity. The large shaded area within each outlined area indicates the mean value, and the mean ±1 SD. unit is presented in the narrow columns to the top (plus) and bottom (minus) of the mean, *n* = 3. Colour

scale shown on the top. (**J, K**) Effective homo-polymers (chemical structure) on cell adherence, fluorescent images of cells stained for actin cytoskeleton of macrophages (phalloidin Alexa Fluor 488, green) and nucleus (DAPI blue) on macrophage adherence. After six days of incubation **(J)** homo-polymer 42 (cyclohexyl methacrylate) was one of the most adherent and **(C)** homo-polymer 39 (tridecafluorooctyl methacrylate) was one of the least adherent homo-polymers.
Data below SNR threshold (mean/SD≥2) were excluded (**Appendix IV** show the first generation micro array library with their code), n= 3 Three different experiment, for three different biological donors; donor_1 (4 replicates), donor_2 (3replicates) and donor_3 (2 replicates). Scale bar = 200 µm.

4.3.1.1. Cell morphology

The morphology of macrophages has been linked with their differentiation (87), thus, cell area, nucleus area, cell length and width were measured for each cells on each polymer (**Figure 4.2**).

Cells seeded on homo-polymers 41 (hexafluorobutyl acrylate), 113 (heptadecafluorodecyl methacrylate), and 30 (3-sulfopropyl methacrylate potassium salt) had the largest average cell area of 164.9±60.8 μm^2, 140.7±63.5μm^2 and 136.9±60.1 μm^2, respectively. Cells on homo-polymer 4 (ethyl methacrylate) had the smallest average cell area of 51.9±18.1μm^2, followed by homo-polymers 95 (hydroxyethyl methacrylate) and 86 (methyl 3-hydroxy-2-methylenebutyrate) with average cell areas of 69.9±31.7μm^2 and 71.4±35.5μm^2, respectively. Thus, a statistically significant ($p<0.0001$) change in cell area was observed for macrophages in response to material surface chemistry when small and large cell area groups were compared (**Table 4.1** and **Table 4.2**).

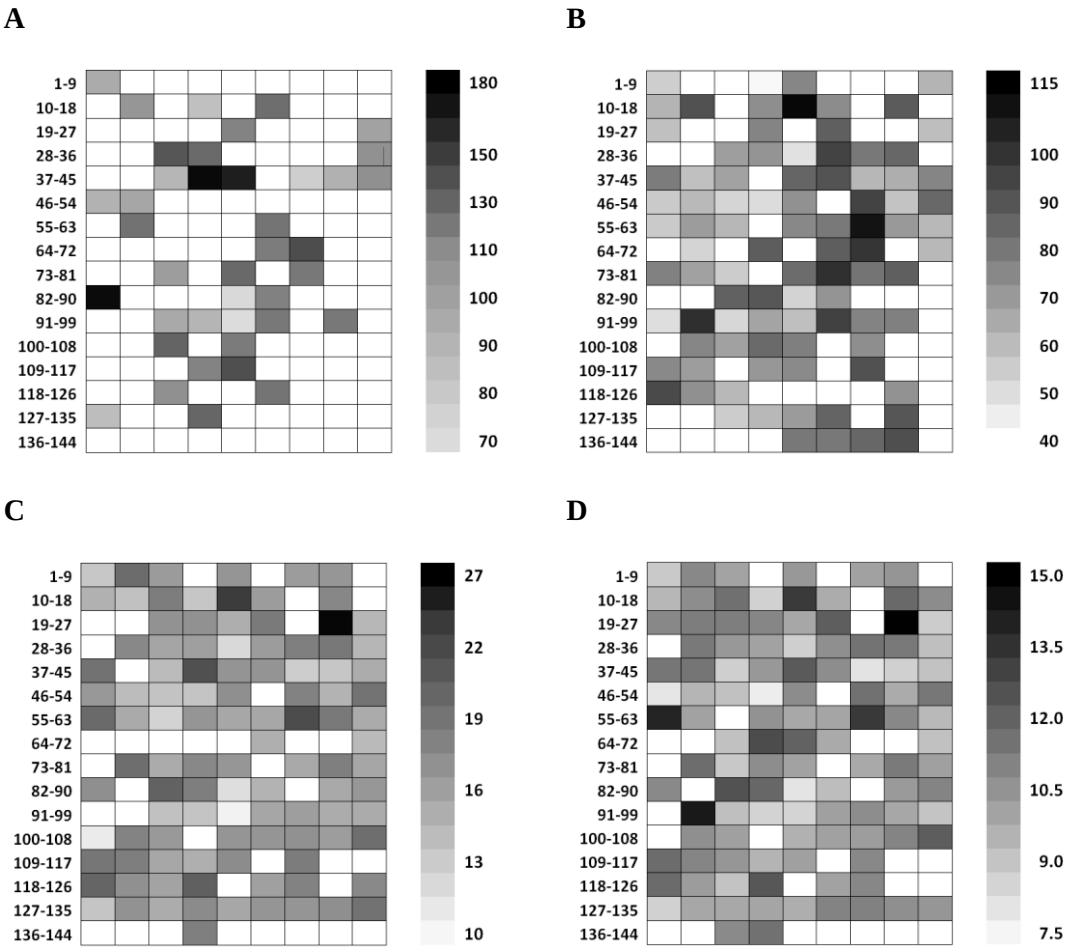

Figure 4.2: (A-D) The impact of microarrays homo-polymers first generation on cell morphology. (A) Cell area and **(B)** nucleus area of the cell (μ^2). **(C)**Major axis length and **(D)** Minor axis length of the cell (μ). Numbers (left) indicate the homo-polymer identity. The large shaded area within each outlined area indicates the mean value. Colour scale shown on the right. Data below SNR threshold (mean/SD≥2) were excluded (**Appendix IV** shows the first generation micro array library with their code). *n* = 3 different experiment, for three different biological donors; donor_1 (4 replicates), donor_2 (3replicates) and donor_3 (2 replicates).

Table 4.1: The most effective top 10 homo-polymers in first generation microarrays on largest cell area (^{L}), and smallest cell area (^{S}) arranged in descending order of cell area, with their nucleus area, major axis length, and minor axis length. Mean ± SD *n*= 3 different experiment, for three different biological donors; donor_1 (4 replicates), donor_2 (3replicates) and donor_3 (2 replicates).

Homo-polymers	Cell area (μ^2) ± STDEV(μ^2)	Nucleus Area(μ^2) ± STDEV(μ^2)	Major axis length(µ) ± STDEV(µ)	Minor axis length(µ) ± STDEV(µ)
41^{L}	164.9±60.8	85.5±9.8	16.8±4.2	12.3±3.1
113^{L}	140.7±63.5	74.7±37.0	17.3±5.0	10.1±2.4
30^{L}	136.9±60.1	68.6±34.1	15.6±3.6	10.3±1.8
101^{L}	129.8±37.6	67.8±17.9	16.4±3.4	10.1±1.4
130^{L}	128.9±48.7	60.9±24.2	17.4±5.9	9.9±2.0
77^{L}	127.5±25.1	83.4±22.9	16.7±2.9	10.0±1.4
31^{L}	127.1±56.5	71.6±23.5	16.0±4.2	10.0±2.4
15^{L}	125.1±54.6	73.8±30.8	16.3±4.2	9.7±2.6
56^{L}	122.8±54.8	69.1±34.1	15.3±3.3	10.1±1.7
60^{L}	122.0±59.8	79.6±35.5	15.5±4.1	9.9±2.7
1^{S}	94.2±43.4	54.6±15.0	13.3±3.5	8.8±1.8
44^{S}	91.2±34.2	64.0±16.6	13.3±2.9	8.6±1.6
46^{S}	90.7±26.4	55.8±12.1	16.5±6.9	7.9±1.1
94^{S}	89.1±24.0	67.0±14.3	13.5±2.1	8.5±1.1
39^{S}	89.0±29.5	67.4±26.3	14.1±4.3	8.6±1.1
13^{S}	83.7±28.4	73.2±32.8	13.3±4.0	8.6±1.6
43^{S}	76.6±31.9	61.4±20.0	12.8±3.3	8.0±1.7
86^{S}	71.4±35.5	53.1±11.1	11.7±3.9	8.0±1.8
95^{S}	69.9±31.7	58.9±15.7	10.2±2.3	8.5±2.3
4^{S}	51.9±18.1	42.3±8.3	9.3±1.5	7.2±1.4

Table 4.2: The top 10 homo-polymers in first generation microarrays with cells had largest cell area in comparison (^{L}), with 10 top homo-polymers with smallest cell area (^{S}). Significance calculated by one-way ANOVA with Tukey's post-test: *, p≤0.05; **, p≤0.01; ***, p≤0.001, ns (non-significant). Data below SNR threshold (mean/SD≥2) were excluded. *n*= 3 different experiment, for three different biological donors; donor_1 (4 replicates), donor_2 (3replicates) and donor_3 (2 replicates).

113^{L}	ns																		
30^{L}	ns	ns																	
101^{L}	ns	ns	ns																
130^{L}	ns	ns	ns	ns															
77^{L}	ns	ns	ns	ns	ns														
31^{L}	ns	ns	ns	ns	ns	ns													
15^{L}	*	ns	ns	ns	ns	ns	ns												
56^{L}	*	ns	ns	ns	ns	ns	ns	ns											
60^{L}	*	ns	ns	ns	ns	ns	ns	ns	ns										
1^{S}	****	**	*	ns	ns	ns	ns	ns	ns	ns									
44^{S}	****	**	**	ns	ns	ns	ns	ns	ns	ns	ns								
46^{S}	****	**	**	ns	ns	ns	ns	ns	ns	ns	ns	ns							
94^{S}	****	***	**	*	*	ns	ns	ns	ns	ns	ns	ns	ns						
39^{S}	****	***	**	*	*	ns	ns	ns	ns	ns	ns	ns	ns	ns					
13^{S}	****	****	***	**	**	*	*	*	ns	ns	ns	ns	ns	ns	ns				
43^{S}	****	****	****	***	***	***	***	**	**	**	ns	ns	ns	ns	ns	ns			
86^{S}	****	****	****	****	****	****	***	***	***	***	ns	ns	ns	ns	ns	ns	ns		
95^{S}	****	****	****	****	****	****	****	***	***	***	ns	ns	ns	ns	ns	ns	ns	ns	
4^{S}	****	****	****	****	****	****	****	****	****	****	*	*	ns	ns	ns	ns	ns	ns	ns
Homo-polymers	**41^{L}**	**113^{L}**	**30^{L}**	**101^{L}**	**130^{L}**	**77^{L}**	**31^{L}**	**15^{L}**	**56^{L}**	**60^{L}**	**1^{S}**	**44^{S}**	**46^{S}**	**94^{S}**	**39^{S}**	**13^{S}**	**43^{S}**	**86^{S}**	**95^{S}**

4.3.2. Second generation co-polymer microarray

The 10 homo-polymers which produced the greatest bias to the population of the M1 (32±12 cells) or M2 (56±24 cells) phenotype along with the 10 homo-polymers with the highest levels of cell attachment (188±42cells) were selected for a second generation array (**Appendix V**). This created 442 co-polymers for the second generation array polymer. Monocytes from three different healthy donors were incubated on second generation arrays composed of 3 repeats on single slide.

The number of MR^+ cells, calprotectin$^+$ cells, and the total number of adherent cells for macrophages taken from 3 different donors was assessed on the second generation array after 6 days of cell culture.

Cells cultured on co-polymer 157 (117-co-121) had a highest inter-donor percentage of MR-positive cells (M2 marker) with 2 times more cells than those classified as calprotectin-positive (M1) (**Figure 4.3A**) also, it scored 2.2 and 2.8 intra-donor M2/M1 ratio in the first and second donor respectively. Co-polymer 93 (90-co-88) induced the highest polarisation of monocytes towards M2 in first and second donor as evidenced by 10.7 and 7.8 fold respectively more MR^+ cells than calprotectin$^+$ cells (**Figure 4.3B,C**).

Co-polymers 118 (90-co-98), 419 (88-co-117), and 218 (47-co-125) had a similar number of MR^+ cells vs. calprotectin$^+$ cells (**Figure 4.3A).**

On other hand, co-polymers 193(15-co-41) polarised cells toward M1 as seen by the fact that calprotectin$^+$ cells outnumbered MR^+ cells by 5.8±0.08 folds (**Figure 4.3A**). In addition, copolymers 217 (35-co-141) and 123 (24-co-113) were induced M1 inter donor ratio by 3.5 and 2.5 folds respectively (**Figure 4.3A**), and they also, polarised the cells toward M1 in first and third donors in comparison with M2 cell$^+$ (**Figure 4.3B, D**).

In addition, co-polymers; 334 (61-co-61),264 (9-co-35), 288 (67-co-61), 131(22-co-125), 171(50-co-141), 222(22-co-126), 170(42-co-141) and 384(113-co-22) were with high MR^+ /$Calprotectin^+$ and co-polymers; 187(61-co-98), 303(24-co-42), and 292(67-co-22) with low inter-donor ratio but non-significant.

In the second generation of the array, co-polymer 222 (22 -co-126) in the second donor with the cell adherence of 510 ±13 was the largest M1 biased cell population, while co-polymer 162 (42-co-126) was the most adherent M2-biased co-polymer with cell number of 521±141 cells (**Figure 4.3C**)**.**

The co-polymer 56 (50-co-29) with average population of 411.2±143.3 cells had highest population of cells, followed by the co-polymer 386 (71-co-126) with average cell number of 362.7±99, then co-polymer 32 (25-co-67) with 356.9±166, and co-polymer 295 (94-co-71) with 346.9±165.6. However the co-polymer 358 (29-co-115) had lowest number of the cells with average 18.7±5.6 cells (**Figure 4.3 I-K**).

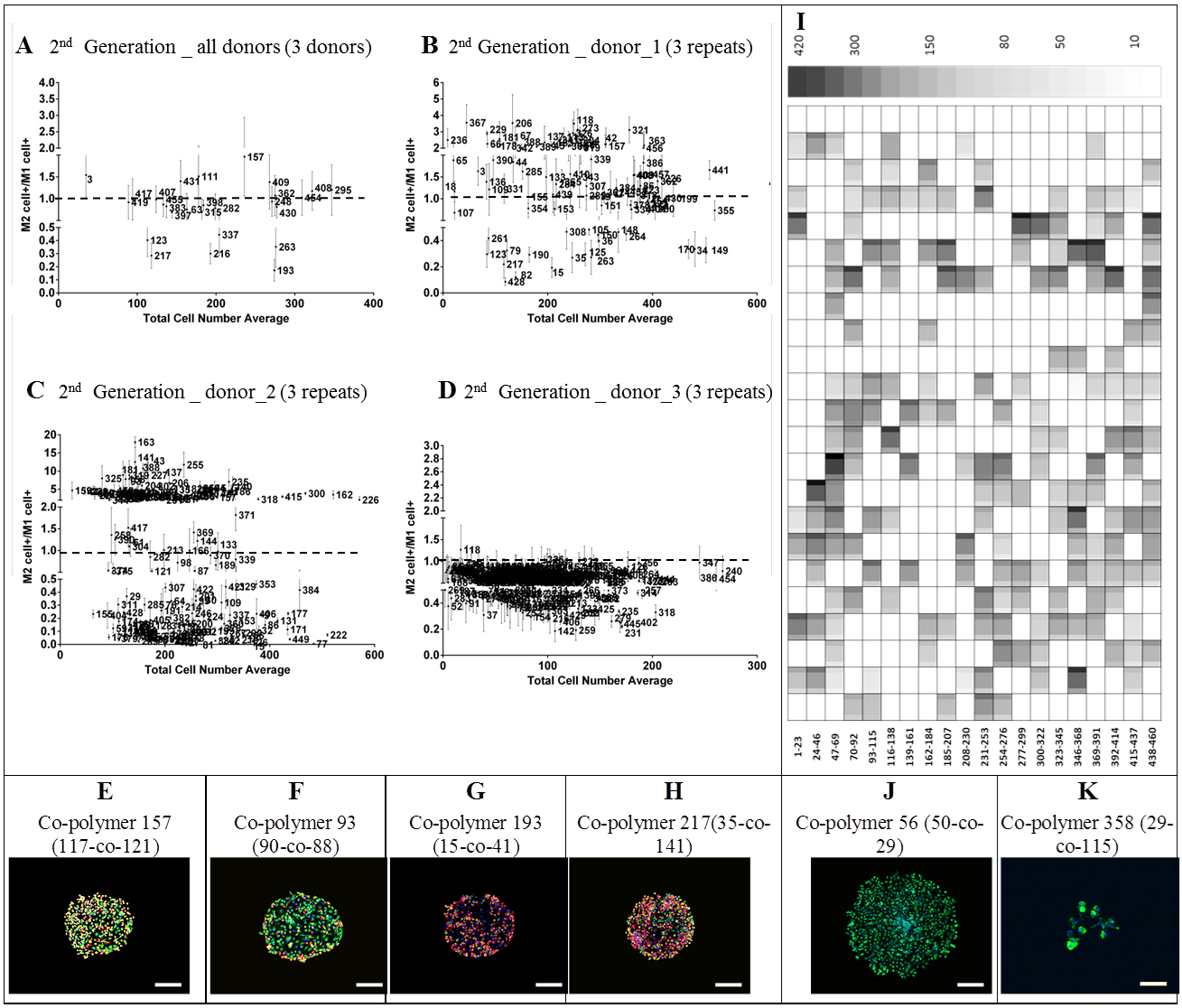

Figure 4.3: Impact of the second generation microarray co-polymers on macrophage polarisation and cell adherence .(**A-D**) Scatter plot for three different donors of M2 cell^{+}/M1 cell^{+} average on co-polymers, x-axis average total cell number on co-polymers ,Y-axis is average of cells expressed MR^{+}(M2- phenotype)/ number of cell expressed calprotectin (M1-phenotype) on co-polymer after six days of incubation. Dotted line is cells with M2- cells (MR^{+} cells)/M2- cells (calprotectin^{+} cells) =1.(**A**) Inter donor M2/M1 cell+ ratio average between all three donors. (**B**) Intra donor M2/M1 cell+ ratio average in donor number 1 (average of 3 repeats), (**C**) donor number two (average of 3 repeats), and (**D**) donor number 3 (average 3 repeats). (**E-H**) Effective co-polymers (their constituent) on macrophage polarisation, fluorescent images of cells stained for calprotectin (27E10 antigen, red), and mannose receptor (MR, green) and nucleus (DAPI blue) on most effective co-polymers (**E**) Co-polymer 157 (117-co-121). (**F**) Co-polymer 93 (90-co-88). (**G**) Co-polymer 193 (15-co-41). (**H**) Co-polymer 217(35-co-141). (**I-K**) **Cell adherence on co-polymers**. (**I**) Average number of adherent cells on different co-polymers. Numbers indicate the co-polymer identity.

The large shaded area within each outlined area indicates the mean value, and the mean ±1 SD. unit is presented in the narrow columns to the top (plus) and bottom (minus) of the mean, *n* = 3. Colour scale shown on the top. (**J, K**) Effective co-polymers (their constituent) on cell adherence, fluorescent images of cells stained for actin cytoskeleton of macrophages (phalloidin Alexa Fluor 488, green) and nucleus (DAPI blue) on macrophage adherence. After six days of incubation (**J**) Co-polymer 56 (50-co-29) was one of the most adherent and (**C**) Co-polymer 358 (29-co-115) was one of the least adherent homo-polymers. Data below SNR threshold (mean/SD≥2) were excluded **(Appendix IV)** shows the first and **(Appendix VI)** shows the second generation micro array library with their code, *n*= 3 different experiment, for three different biological donors, each donor with three replicates. Scale bar = 200 μm.

4.3.2.1. Cell morphology

In this study, there was impact of co-polymer library on cell morphology parameters such as cell area, nucleus area, cell major axis and minor axis (**Figure 4.4**). Cells incubated on co-polymer 403(67-co-15), 216(90-co-141), 215(9-co-113) had the largest average cell area of 220.5±91.9 μm^2, 220.2±104.9 μm^2 and 219.7±85.2, respectively. Cells on co-polymer 23(121-co-71) had the smallest average cell area of 78.4±18.6 μm^2, followed by co-polymer 298(133-co-133) with average cell area of 102.2±37.4 μm^2. Thus, there was a significant ($p<0.001$) difference between seeded cells in cell area average between small and large groups (**Table 4.3** and **Table 4.4**).

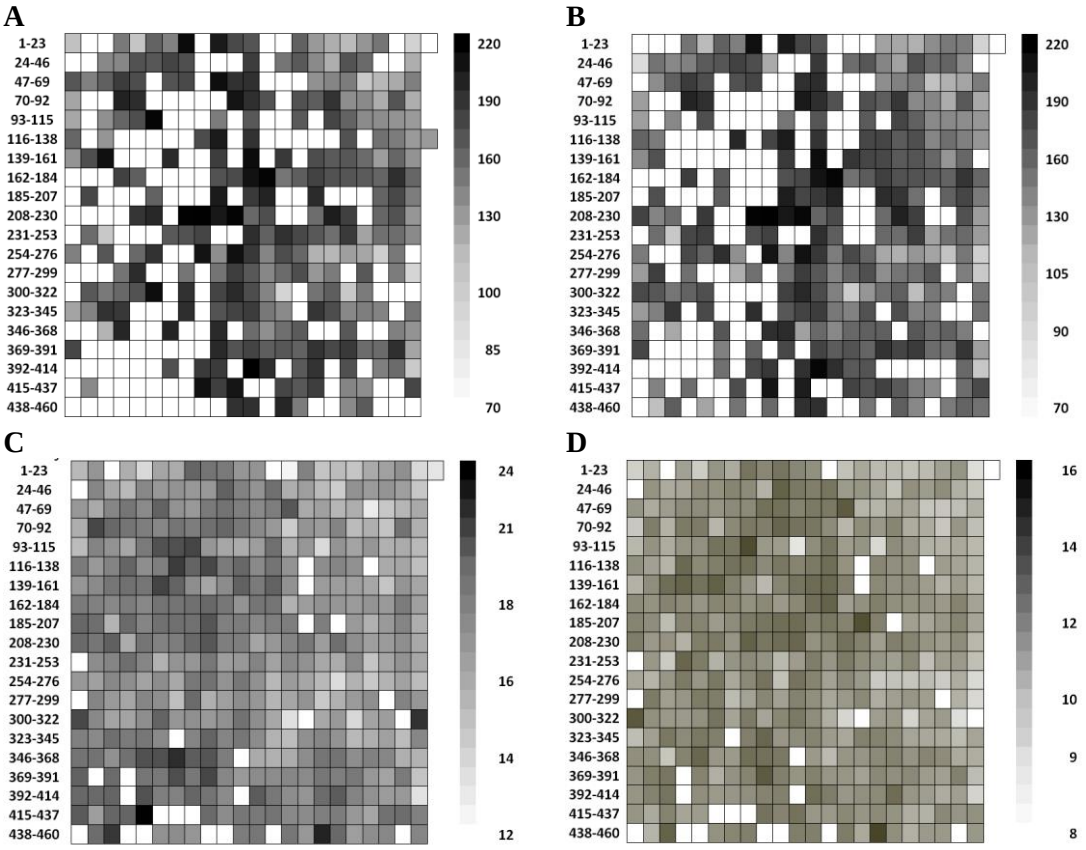

Figure 4.4: (A-D) The impact of microarrays co-polymers second generation on cell morphology. (A) Cell area and **(B)** nucleus area (μ^2). **(C)**Major axis length and **(D)** Minor axis length (μ). Average number of adherent cells on different co-polymers. Numbers (left) indicate the co-polymer identity. The large shaded area within each outlined area indicates the mean value. Colour scale shown on the right. Data below SNR threshold (mean/SD≥2) were excluded. **(Appendix IV and VI)** show the first and the second micro array library with their code and constituent. *n* = 3 different experiment, for three different biological donors each donor with three replicates.

Table 4.3: The most effective top 10 co-polymers in second generation microarrays on largest cell area and with 10 top co-polymers with smallest cell area(L), arranged in descending order of cell area, with their nucleus area, major axis length, and minor axis length. Mean ± SD. *n*=3 different experiment, for three different biological donors each donor with three replicates.

Co-polymers	Cell area (μ^2) ± STDEV(μ^2)	Nucleus Area(μ^2) ± STDEV(μ^2)	Major axis length(μ) ± STDEV(μ)	Minor axis length(μ) ± STDEV(μ)
403^{L}	220.5±91.9	216.5±97.6	19.7±3.7	13.9±4.0
216^{L}	220.2±104.9	219.6±105.4	19.9±6.1	13.7±3.6
215^{L}	219.7±85.2	218.6±86.8	19.1±3.4	14.5±3.7
174^{L}	218.6±91.8	217.3±93.4	18.5±3.8	14.4±4.0
218^{L}	218.4±103.7	216.0±104.9	18.1±4.7	14.3±3.8
8^{L}	214.5±98.2	210.9±102.4	19.3±4.6	13.8±3.8
150^{L}	214.1±95.6	212.2±97.6	18.3±4.2	14.1±4.2
264^{L}	211.6±99.5	209.6±102.3	18.4±4.5	13.8±4.0
423^{L}	211.0±89.8	208.0±93.2	19.0±4.1	13.8±3.5
173^{L}	210.9±87.9	208.8±90.5	18.5±3.4	14.0±3.9
5^{S}	110.7±44.5	107.4±44.7	13.8±2.5	10.3±2
233^{S}	109.4±23.2	99.2±23.6	17.7±2.5	10.4±1.1
317^{S}	109.4±50.9	105.8±51.6	13.9±3.7	10±2.8
65^{S}	108.6±38.3	103.1±36.9	12.9±2.5	10.6±1.9
413^{S}	107.9±37	99.3±34.1	13.4±2.1	10.1±2.3
273^{S}	105.9±26.1	102.4±26.6	15.6±2.0	10.4±1.5
22^{S}	103.8±35.3	93.0±36.3	13.8±2.0	9.7±1.8
313^{S}	102.6±26.2	96.5±30.0	13.5±1.2	10.0±2.2
298^{S}	102.2±37.4	98.5±38.9	16.9±4.3	9.9±1.5
23^{S}	78.4±18.6	65.9±22.9	13.2±3.6	8.4±1.0

Table 4.4: The top 10 co-polymers in first generation microarrays with cells had largest cell area in comparison (^{L}), with 10 top co-polymers had smallest cell area (^{S}). Significance calculated by one-way ANOVA with Tukey's post-test: *, p≤0.05; **, p≤0.01; ***, p≤0.001,****, p≤0.0001,ns (non-significant). *n*=3 different experiment, for three different biological donors each donor with three replicates.

Co-polymers	403^{L}	216^{L}	215^{L}	174^{L}	218^{L}	8^{L}	150^{L}	264^{L}	423^{L}	173^{L}	5^{S}	233^{S}	317^{S}	65^{S}	413^{S}	273^{S}	22^{S}	313^{S}	298^{S}
216^{L}	ns																		
215^{L}	ns	ns																	
174^{L}	ns	ns	ns																
218^{L}	ns	ns	ns	ns															
8^{L}	ns	ns	ns	ns	ns														
150^{L}	ns	ns	ns	ns	ns	ns													
264^{L}	ns	ns	ns	ns	ns	ns	ns												
423^{L}	ns	ns	ns	ns	ns	ns	ns	ns											
173^{L}	ns	ns	ns	ns	ns	ns	ns	ns	ns										
5^{S}	***	***	***	***	***	***	**	**	**	**									
233^{S}	***	***	***	***	***	***	***	**	**	**	ns								
317^{S}	***	***	***	***	***	***	***	**	**	**	ns	ns							
65^{S}	***	***	***	***	***	***	***	**	**	**	ns	ns	ns						
413^{S}	***	***	***	***	***	***	***	***	**	***	ns	ns	ns	ns					
273^{S}	****	****	****	***	***	***	***	***	***	***	ns	ns	ns	ns	ns				
22^{S}	****	****	****	****	****	***	***	***	***	***	ns	ns	ns	ns	ns	ns			
313^{S}	****	****	****	****	****	***	***	***	***	***	ns	ns	ns	ns	ns	ns	ns		
298^{S}	****	****	****	****	****	***	***	***	***	***	ns	ns	ns	ns	ns	ns	ns	ns	
23^{S}	****	****	****	****	****	****	****	****	****	****	ns	ns	ns	ns	ns	ns	ns	ns	ns

4.4. Discussion

Biomaterial surface chemistry has previously been shown to modulate macrophage adhesion and function. (172). Studies have related surface wettability (63,66) and surface molecule ionic charge with macrophage adhesion (128). Data from the previous chapter showed the impact of surface chemistry of polystyrene on macrophage polarisation towards M1 and M2 phenotypes. This highlighted the importance of materials' chemistry on macrophage phenotype providing a rationale for screening a wider range of commercially available polymers for their immune modulatory properties (173).

In this study using a high throughput screening strategy the effect of a combinatorial library of polymers on human monocyte differentiation was investigated. A range of macrophage responses were observed to the various polymers including changes in cell attachment, cell morphology and macrophage phenotype.

Interestingly, low cell attachment was observed on the first generation of the array which was more diverse chemically. Homo-polymer 42 (230±65 cells) ,133 (209±47 cells) , 90 (197±69cells) and in the first generation and co-polymers 56 (50-co- 29) (411±143 cells), 386 (71-co-126) (363±99 cells) and 32 (25-co-67) (357±166 cells) in the second generation of the array were the most adherent polymers for the cells, while co-polymer 358 (29-co-115) from the second generation array had lowest cell number average of 19 cells. All above mentioned polymers had no significant effect on cell polarisation. Furthermore, M2 biased homo-polymer 29 (81±40) and M1 biased co-polymer 263 (88-co-24) (276±66) were the most adherent biased polymers, while M2 biased homo-polymer 39 (9.8±3.9 cells) and M1 biased co-polymer 123 (24-co-113) (113.2±48 cells) were the least adherent biased polymers. Difference in

chemical nature of polymers can influence cell attachment (63,128,174), through the differences in adsorbed proteins (127).

Co-polymers 56 (50-co-29) (411.2±143.3 cells), 386 (71-co-126) (362.7±99 cells), 32 (25-co-67), 347 (3-co-126) (328.2±125.5 cells) and 295(94-co-71) (346.9±165.6 cells) from the second generation array had the highest number of attached cells, non-of their constituent had a significant high rate of cell attachment in the first generation array. Co-polymers 358 (29-co-115) (18.8±5.6), 209 (35-co-126) (46.8±22.1), 434 (35-co-123) (51.2±16.9), 94 (35-co-47) (54.1±8.6) and 48 (50-co-47) (55.7±18.5) had the lowest number of attached cells. Their constituent homo-polymers also had no significant cell attachment with low rate in the first generation of the array. Interestingly, monomer 35 (hexyl acrylate) was found in constituent of the second, third and fourth least adherent co-polymers.

Overall, the attached cell number in the second generation is more than first generation suggesting a synergistic effect of the individual monomers when combined as a co-polymer, which was led to cell attachment improvement.

Adsorbed protein plays a key role on macrophage attachment to surfaces (175). Anionic carboxylate groups have been observed to be particularly effective at inducing protein adsorption to improve macrophage adhesion (176). Carboxylate ions from acrylamides (177) or from meth acrylates (178) may play a role in macrophage adhesion. Co-polymers and homo-polymers of methacrylamides have previously been reported to stimulate antibody production in mice (179). Co-polymers of poly(ethylene glycol) and poly(lactide) (MPEG-b-PLLA) influenced Human Bone Marrow Stromal Cells (hBMSCs) proliferation and adhesion(180). This study has identified a number of polymers that can stimulate monocyte differentiation towards distinct macrophage phenotypes. Monocytes seeded on co-polymer 157 (117-co-121)

had the highest level of MR (M2 marker) expression. However, co-polymers 217 (35-co-141) and 123 (24-co-113) in induced high levels of calprotectin (M1 marker) expression.

The nature of bio-adsorbate layers themselves are clearly influenced by the chemical properties of each polymer spot (57,63,64,66,128). Also, quality and quantity of adsorbed protein can be influenced by the surface chemistry property (see chapter three) There are a variety of proteins in FBS (181) and so because the adsorbed protein identity is a key mediator of cell activity and behaviour (182), each type of protein can polarise macrophages toward a particular phenotype. For example, arginine, proline and alanine were found to be more related on M1-biased polystyrene surfaces, while phenylalanine, tyrosine, histidine, lysine, methionine and valine were more associated with M2-biased surfaces (see chapter three). While the exact molecular basis of such polymer induced macrophage polarisation is yet to be elucidated, it is reasonable to suggest that the distinct bio-adsorbate from the media and cell-secreted biomolecules on each of these polymer spots is responsible for the cell differentiation towards a particular phenotype.

The synergistic effect of copolymerisation by a number of co-polymers from the second generation of the microarray created a new or improved ability to stimulate the cell to a particular phenotype as their predecessors had no or less ability in the first generation microarray experiments.

Co-polymer 157 (117-co-121) in the second generation microarray (made from 66% monomer 117 and 33% monomer 121) polarised cells towards an M2 phenotype as evidenced by 2 fold higher expression of MR than calprotectin (M1 marker). In the first generation microarrays both homo-polymers 117 and 121 had no significant impact on macrophage polarisation. In addition, co-polymers 217 (35-co-141) and

123 (24-co-113) induced the M1 inter donor cell ratio by 3.5 and 2.5 folds respectively, while their constituent had no significant effect on inter donor M2/M1 cell ratio. However, homo-polymers 141, 24 and 113 were M1biased, and 35 were M2 biased in one donor of all three donors of the first generation.

The most consistent M2 biased co-polymer was 157, and the most M1 biased were co-polymer 217 and 123. They were not only biased to particular phenotype in the inter donor M2/M1 ratio, but they were also biased in intra donor M2/M1 ratio of 2/3 of all 3 donors.

The efficiency of M1 phenotypical polarisation by cytokines was higher than the M1 biased hit polymers polarisation effect by about 5.8 times, but hit M2-biased polymers were less efficient than cytokine polarised one by about 45%. However, M2 biased 255 (88-co-25) M1 222 (22-co-126) biased co-polymer in the second donor stimulated the cells to express their phenotypical cell marker more than cytokine polarised M2 and M1 by about double.

That mean M2 biased co-polymer 157, and M1 biased co-polymers 217 and 123 can be considered as robust polymer, which can used in design of biomaterials that are able to trigger desired immunological outcomes and thus support the healing(M2) or anti-tumour (M1) process.

Previous studies have reported the change of macrophage morphology under the influence of biomaterials surface chemistry (see **chapter one**) (86,183). Here in this study, morphological parameters such as cell area, nucleus area, average major axis length and average minor axis length have been reported. Top 10 homo-polymers influenced the seeded cells to have large cell area ranged between (122-165 μm^2), they had significant differences with other group of 10 homo-polymers which stimulated cell to have small cell area arranged between (52-94 μm^2). Furthermore,

top 10 co-polymers with large (210-220 μm^2) and small (78-107 μm^2) had larger cell area in comparison with their counterparts on homo-polymers. That can be due to the synergic effects of copolymerisation. But there were not significant differences of cell morphology between cells on M1biased and M2 biased hit polymers.

Polarizing macrophage toward M1 and M2 by copolymers (217 and 123) and (157) respectively, without using exogenous cytokines or binding was an important finding in this experiment. However, it is not possible to discern any monomer molecular structure-preference (cellular) relationship by hydrophobicity or hydrophilicity.

Nevertheless these findings are important in the sense that they have already identified materials with the ability to bias macrophage polarisation towards M1 or M2 phenotype paving the way for future attempts in developing immune-instructive medical devices.

4.5. Conclusions

Co-polymer 157 was the most potent polymer for induction of M2 phenotype while co-polymers 217 and 123 influenced high levels of calprotectin (M1 marker) expression. In addition, second generation co-polymers influenced the cell attachment by double in comparison with the first generation homo-polymers.

M2 hit co-polymer stimulated seeded cells to express M2 cell marker by about half of cytokines polarised M2. Also, M1 cytokine polarised cells expressed M1 marker by about 6 fold higher than M1 hit polymers **(Appendix VII).**

The experiment could be followed up by making uniform surfaces of polymers with M1 and M2 induction ability to allow scaling up of cell culture experiments. This will enable more detailed functional studies such as investigating of polarised cells cytokine and gene profile. Such data will enable better classification of polarized

macrophages on these surfaces. In parallel it will be of great interest to characterise the nature of different bio-adsorbate layers on selected polymer spots. Such data will allow elucidating the molecular basis of polymer induced macrophage polarisation. It is expected that collectively such data could enable the rational design of surface chemistries with tuneable immune instructive properties.

Chapter Five: Image Based Machine Learning for Identification of M1 and M2 Macrophages

5.1. Introduction

As a component of the innate immune system, macrophages play a central role in defence against pathogens as well as maintaining the body's haemostasis. They achieve these by contributing to a number of functions including clearance of dead cells and microorganisms, recruitment of other immune cells, and acting as antigen presenting cells (APCs) where they are able to provide necessary signals for T cell activation(34,77,184). Different macrophage phenotypes with distinct functional properties have been identified (73). For instance, M1 (classically activated) macrophages are induced by interferon gamma (IFN-γ) from T helper 1 (T_H1) cells, $CD8^+$cytotoxic T cells (CTLs) or natural killer (NK) cells in the presence of microbial products such as lipopolysaccharide (LPS) (74). M1 macrophages have pro-inflammatory and anti-tumour functions (73) and secrete high levels of pro-inflammatory cytokines such as interleukin 12 (IL-12) and IL-23 (116). On the other hand, M2 (alternatively activated) macrophages are induced by IL-4 and/or IL-13, which are mainly secreted by T_H2 cells (74) or polymorphonuclear cells such as mast cells (75). M2 macrophages have anti-inflammatory and pro-wound healing activities (73) and secrete large amounts of the anti-inflammatory cytokine IL-10 (185).

In vitro, monocytes can be polarised towards M1 phenotype by IFN-γ (111) or LPS (112). The addition of granulocyte macrophage colony-stimulating factor (GM-CSF), which acts as a priming signal for macrophages (113,114) during M1 polarisation augments the pro-inflammatory function of these cells (111,115). By contrast, M2 polarisation can be achieved by the addition of IL-4 (111). As with GM-CSF and M1 polarisation, macrophage colony-stimulating factor (M-CSF) can enhance the anti-inflammatory function of M2 macrophages (111,115).

Human macrophages express the intracellular marker CD68 and this is often used to identify them in tissue samples (186). In order to determine the activation status of macrophages, typically a panel of markers, cytokines, metabolites or transcription factors are employed. For instance, M1 macrophages can be identified by the production of high levels of pro-inflammatory cytokines such as IL-12, IL-23 (116), IL-1β, IL-6 and tumour necrosis factor alpha (TNF-α) (117,118). These cells have also been shown to express high levels of chemokine (C-C motif) receptor 7 (CCR7) (119), nitric oxide synthase 2 (NOS2) (122), calprotectin (121), and CCR2 (120). Conversely, M2 macrophages are characterised by the production of high levels of IL-10 (123), transforming growth factor beta (TGF-β) (118), and high expression of the scavenger receptor CD163 (122) (123), mannose receptor (MR, CD206) (119) (123) and IL-1 receptor antagonist (IL-1RA) (124).

In terms of gene expression and transcription factor activation, the main characteristics of human M1 macrophages are high levels of prostaglandin-endoperoxide synthase 2 (Ptgs2 or Cox2) and IL23a (IL23p19) gene expression, and signal transducer and activator of transcription 3 (STAT3) and/or STAT1 phosphorylation. In addition, high levels of SOCS3 and IRF5 expression have also been associated with pro-inflammatory M1 macrophages *in vitro* (139,141,142,187). Human M2 macrophages, on the other hand, can be identified by high levels of Kruppel-like factor 4 (Klf4) and chitinase 3-like 2 (Chi3l2 or Ykl39) gene expression and STAT6 phosphorylation (79). Furthermore, SOCS1 (142,143) and IRF4 expression are generally linked to the development of the M2 phenotype (149,188).

In human macrophages, some overlapping in the expression of cell markers between M1 and M2 phenotype states in their marker profiles can be observed. In addition, some morphological differences of different macrophage have been observed in

number of studies (See **chapter one**, general introduction). The complexity of M1/M2 identification in human macrophages has encouraged to investigate an alternative approach, that would be simpler, less resource-intensive, and hence, more widely adoptable. By depending on hypothesise that cell morphology could be an indicator of macrophage activation status.

The aim of the present study was to further investigate the relationship between morphology and activation status in human primary monocyte-derived macrophages. High content, automated image analysis approach was selected in order to determine whether cell size and morphology could be used to reliably determine the activation status of the cell. Machine learning has found numerous applications in biology in recent years (189-192), from RNA screening studies detecting over 50 phenotypes (193) down to the simple classification of two cell types from a population (48). Methods applying such high content image analysis to the detection and classification of various cell types have been demonstrated, including mesenchymal stem cells (194) and endothelial/fibroblast cells (195). Beyond this, machine learning methods have also been used to classify the specific stage of the cell cycle, e.g. M-phase (196), and to assist clinicians in diagnostic settings (191). In this study, in collaboration with Gadegaard's group (University of Glasgow), the use of a Bayesian classifier to distinguish between M1 and M2 macrophages was examined. Machine learning effectively substitutes the manual classification of cell phenotype by researchers and clinical practitioners, and offloads the decision making to an algorithm. The reasons automated image processing, segmentation, and analysis have found such interest are that they offer huge possibilities to free up researchers time, and to ensure consistent interpretation of results free from any bias.

5.2. Material and method

5.2.1. Macrophage culture and activation

Monocytes were isolated from Buffy coats of 6 independent donors (see **chapter 2.5.**). Purified monocytes were suspended in RPMI-1640 medium supplemented with 10% foetal bovine serum (FBS), 2 mM L-glutamine, 100 U/ml penicillin, and 100 µg/ml streptomycin (all from Sigma-Aldrich) (henceforth referred to as "complete RPMI medium") and seeded at 1 x 10^6 cells/ml/well in 24-well tissue culture-treated polystyrene (TCP) plates (Corning Life Sciences). The following cytokines were added to the monocytes to obtain different activation states: M1 - 20 ng/ml IFN-γ (R&D Systems) and 50 ng/ml GM-CSF (Miltenyi Biotec); M2 - 20 ng/ml of IL-4 (Miltenyi Biotec) and 50 ng/ml M-CSF (Miltenyi Biotec) (197); naïve (unpolarised) macrophages - 50 ng/ml GM-CSF. Monocytes not treated with any cytokines served as untreated controls. The cells were incubated at 37ºC, 5% CO_2 in a humidified incubator for 6 days. On Day 3 of incubation, 500 µl of the medium in the wells was replaced with fresh complete RPMI medium containing the same concentration and mix of cytokines that were used for cell stimulation on Day 0.

M1 and M2 cell supernatants were collected after six days of incubation for IL-6, IL-10, IL-1β and CCL18 cytokine analyses (see **chapter 2.7.**) In addition, mRNA were harvested from day 6 M1 and M2 cells to perform STAT1, SCS1, SOCS3, IRF4 and IRF5 transcription factors analysis by quantitative real-time OPCR (qRT-PCR) (see **chapter 2.8.**).

For microscopy, round coverslips with 12 mm diameter, thickness #2 (VWR International) coated with 20 µg/ml Poly-L-lysine hydrobromide (Sigma-Aldrich) (198) were put inside each well of a 24-well TCP plate. Monocytes were then seeded and stimulated on the coverslips as described above. On Day 6 cells were washed once with PBS and fixed.

Fixed cells for each phenotype were stained with fluorescent antibodies calprotectin (M1 cell marker) and MR (M2 cell marker) (see **chapter 2.6.1.**). In addition, cells from different samples for each phenotype but from the same donor were used for observing the morphological differences by fixing them and staining the actin cytoskeleton of the cells with phalloidin Alexa Flour 488 and their nucleus with DAPI (see **chapter 2.6.2.**). A fluorescent microscope with 60X objective was used for imaging.

5.2.2. Image analysis and machine learning for phenotype identification

Composite images of f-actin and DAPI staining were loaded into CellProfiler, and metadata detailing the cell type in the image was extracted from the file name. After optimisation of the primary detection of the cell nucleus (DAPI channel), followed by secondary detection of the cell body (f-actin channel) the full dataset of 93 images was analysed in 4 h on a high spec desktop computer (Dell XPS). The extent of each cell was then morphologically analysed for a broad range of descriptors such as area, orientation, extent, shape, intensity, etc. A total of 228 measurements were acquired for each cell, and a database was established for the full experiment, which was comprised of 93 images. The machine learning step was then carried out in CellProfiler Analyst. Here, 50 cells were randomly selected from the training data set representing each of the different phenotypes. The software then performed a GentleBoosting algorithm to establish a set of 25 rules capable of identifying the different phenotypes based on individual morphometric values for each cell. Progress was checked by cross validation of the classifier, after which the user could add further training data to improve accuracy.

5.2.3. Statistical analysis

Statistical significance of differences between different expression profiles was assessed using Student's t-test with GraphPad Prism 6 Differences were considered statistically significant if the p-value was less than 0.05.

5.3. Results

5.3.1 Characterisation of Macrophage Activation Status

Human peripheral blood monocytes were differentiated into macrophages *in vitro* in the presence of GM-CSF (naïve macrophages), IFN-γ and GM-CSF (M1 macrophages), or IL-4 and M-CSF (M2 macrophages) for 6 days. In order to establish the activation status of these monocyte-derived macrophages by traditional methods, immunofluorescent staining for the M1 and M2 markers, calprotectin and MR respectively, was performed. Untreated monocytes cultured *in vitro* for 6 days were used as controls. In addition, further characterisation of M1 and M2 macrophages was carried out by analysing the cytokine profiles of supernatants from these cells after 6 days of culture, and determining their transcription factor expression profile by qRT-PCR.

5.3.1.1. Immunofluorescent staining

Immunofluorescent staining for the activation markers calprotectin and MR (CD206) demonstrated that M1 macrophages had the highest expression of calprotectin, while expression of this marker was much lower on M2 macrophages and naïve macrophages and not detected in untreated monocytes (**Figure 5.1**). On the other hand, expression of MR measured by mean fluorescent intensity (MFI) was found to be highest on M2 macrophages followed by M1 macrophages, naïve macrophages and untreated monocytes in that order (**Figure 5.1**). CD68, a macrophage marker that was

included in order determine macrophage differentiation, was expressed in all the macrophage types after 6 days in culture, but not in untreated monocytes.

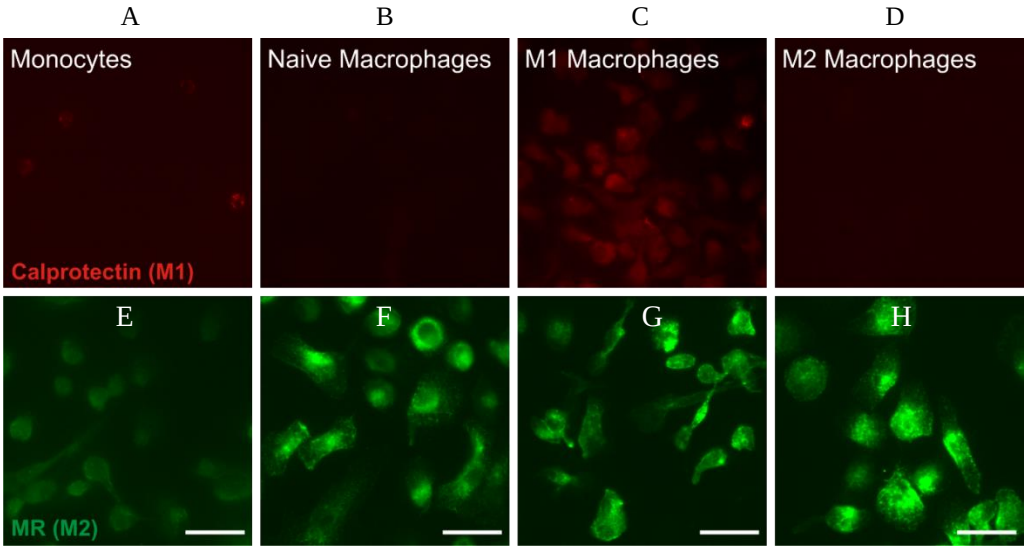

Figure 5.1: Fluorescent images of monocytes and macrophages stained for calprotectin (Calprotectin antigen, red, A-D), and mannose receptor (MR, green, E-H). Scale bar = 25 µm. Representative images from *n*=3 different experiment, for three different donors are shown. Images were taken with 60X objectives.

5.3.1.2. Cytokine analysis

Cytokine analysis of supernatants obtained from M1 and M2 macrophages after 6 days of culture demonstrated that M1 macrophages produced significantly higher amounts of the pro-inflammatory cytokines IL-6 ($p<0.0001$), IL-1β ($p<0.0001$), and TNF-γ ($p<0.0001$) (**Figure 5.2**). By comparison, M2 macrophages produced significantly higher levels of the cytokines IL-10 and IL-1RA ($p=0.0115$), and the chemokine CCL18 ($p=0.0245$) (**Figure 5.2**), which play a role in the reduction of inflammation and wound-healing.

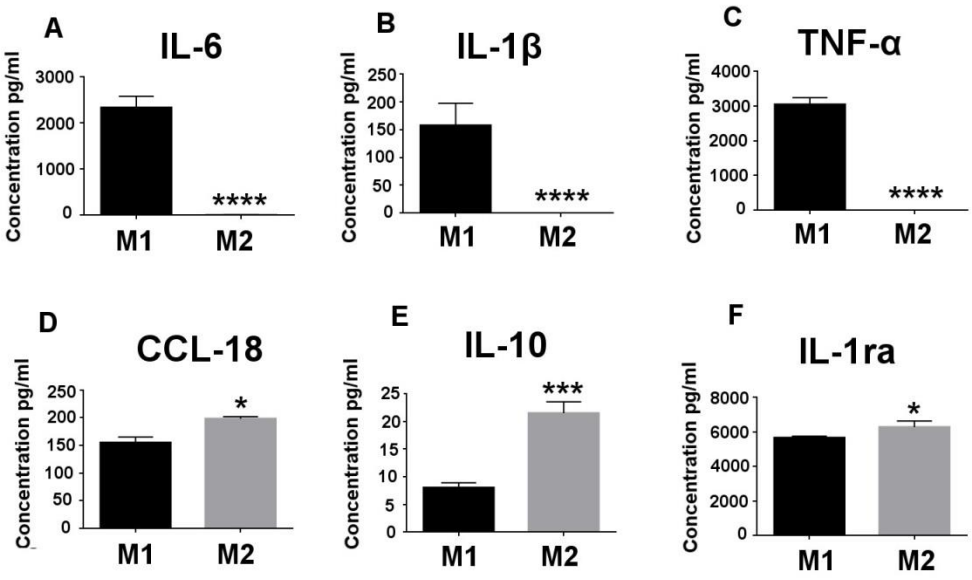

Figure 5.2: Comparison of cytokine profiles of M1 and M2 macrophages. Cytokines in the supernatants of human monocyte-derived M1 and M2 macrophages cultured for 6 days were measured by means of a bead-based flow cytometric system (for (**A**)IL-6, (**B**)IL-1β, (**C**)TNF-α), ELISA (for (**D**)CCL-18), and a bead-based luminex system (for (**E**)IL-10 and (**F**)IL-1RA). Data presented are the mean ± SD of at least 5 independent experiments, each experiment with one donor and 2 repeats. Statistical significance was assessed using paired Student's t-test (*= P<0.05, ** = p<0.01, *** = p<0.001).

5.3.1.3. PCR

To further characterise the phenotype of polarised macrophages, qRT-PCR was used to determine the relative mRNA expression of a panel of transcription factors. There was significantly higher expression of STAT1 (p<0.0050) (**Figure 5.3A**)**,** suppressor of cytokine signalling 3 **(**SOCS3 (p<0.0005), **Figure 5.3E)**, and interferon regulatory factor **(**IRF5 (p<0.0055), **Figure 5.3C**) mRNA in M1 macrophages in comparison with M2 macrophages. SOCS1 mRNA expression was also higher in M1 compared to M2 macrophages; however, this was not significant (**Figure 5.3B**). M2 macrophages, on the other hand, expressed significantly more STAT6 (p<0.0053) mRNA than M1

macrophages (**Figure 5.3D**)**.** A small, non-significant increase in IRF4 mRNA was also noted in M2 macrophages compared to M1 macrophages (**Figure 5.3F**).

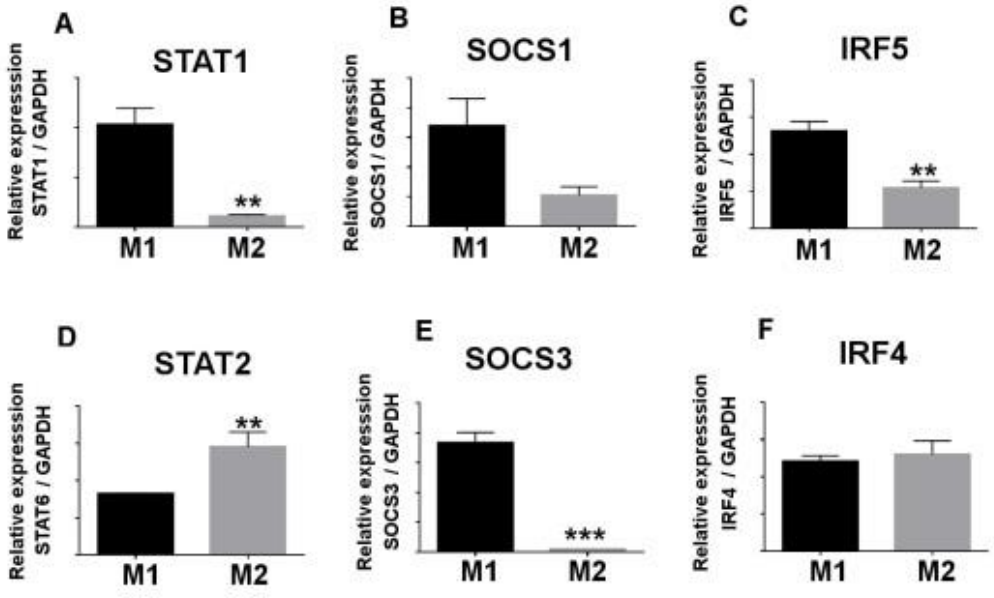

Figure 5.3: Comparison of transcription factor mRNA expression in M1 and M2 macrophages. qRT-PCR analysis of (**A**) STAT1, (**B**) SOCS1, (**C**) IRF5, (**D**) STAT6, (**E**) SOCS3, (**F**) IRF4 relative mRNA expression in M1 and M2 macrophages after 6 days of culture. All values are reported relative to the house-keeping gene GAPDH. Data show mean values ± SEM of 3 independent experiments using macrophages from 3 different donors with 2 repeats. Statistical significance was assessed using student's t-test (** = $p<0.01$, *** = $p<0.001$).

5.3.2. Characterisation of Macrophage Morphology

In order to visualise the morphology of naïve, M1 and M2 macrophages, cells were stained for their nuclei and f-actin filaments using DAPI and fluorescently labelled phalloidin, respectively. Untreated monocytes cultured for 2 h and 6 days were used as controls. Morphological differences were observed between the different cell types. Monocytes cultured for 2 h were found to be small rounded cells (**Figure 5.4A**)**.** After 6 days in culture, monocytes appeared as larger rounded cells, whilst naïve macrophages were larger and more irregular in shape (**Figure 5.4B and C,** respectively**)**. M2 macrophages were the largest of the five cell types, showing a

flattened, expanded phenotype (**Figure 5.4E**). M1 macrophages, on the other hand, were smaller, irregular-shaped cells, some of which adopted an elongated spindle-shaped appearance (**Figure 5.4D**). These images were analysed to obtain different parameters (e.g. nuclei to cytoplasm ratio, cell perimeter) for each cell phenotype which were processed in the CellProfiler software suite (Broad Institute, Harvard, USA).

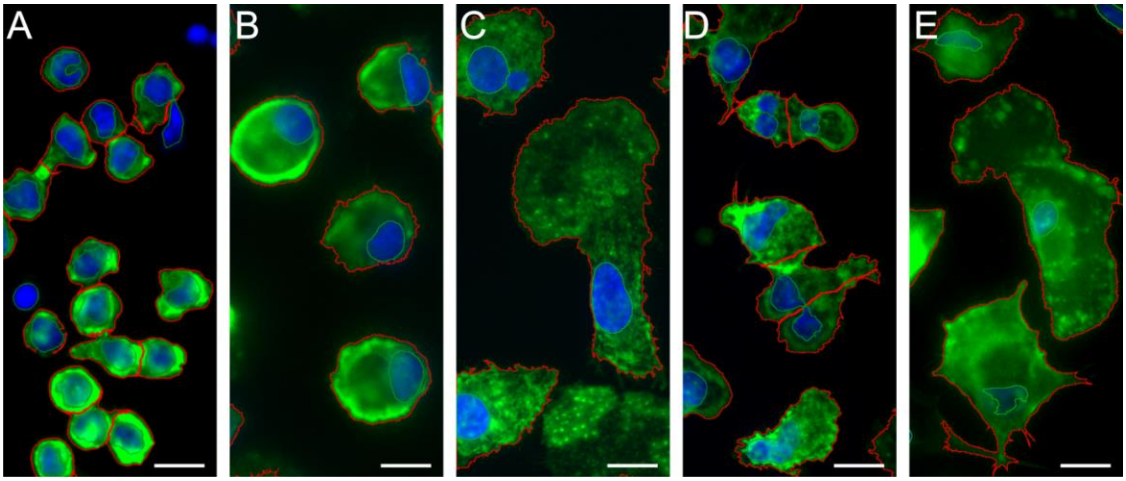

Figure 5.4: Immunofluorescent staining of monocytes and macrophages. (A) Monocytes cultured for 2 h; **(B)** monocytes cultured for 6 days; **(C)** naïve macrophages; **(D)** M1 macrophages; **(E)** M2 macrophages. F-actin and cell nuclei were stained with phalloidin Alexa Fluor 488 (green) and DAPI (blue), respectively. The detected nucleus and cell outlines are shown as green and red lines respectively. Scale bar = 10 µm. Images were taken with 40X objectives. Representative images from *n*= 6 independent experiments, each experiment with one donor and 3 repeats.

Visual inspection of cytoskeletal staining of macrophages showed immediate differences in their respective morphologies. Beyond basic descriptors such as size and shape, there were differences in the distribution and granular texture of the cell cytoskeleton. These differences can be quantified and described in detail by various image processing methods (41). Significant differences emerged between M1 and M2 macrophages. M1 macrophages were smaller, more rounded cells with tightly packed dotted texture of actin, **Figure 5.4D**. M2 macrophages exhibited larger, more irregular

cell bodies with smoother actin granules staining and more distributed localised spots. Various metrics of nucleus/cell size, texture, and staining intensity show differences in M1 and M2 phenotypes, as shown in **Figure 5.5** Differences in cell size (**Figure 5.5A**) and shape (**Figure 5.5B**) were confirmed, whilst other metrics emerged as key differences between the two phenotypes such as the intensity of actin staining around the cell periphery (**Figure 5.5D**) and the granular texture of actin staining (**Figure 5.5E**).

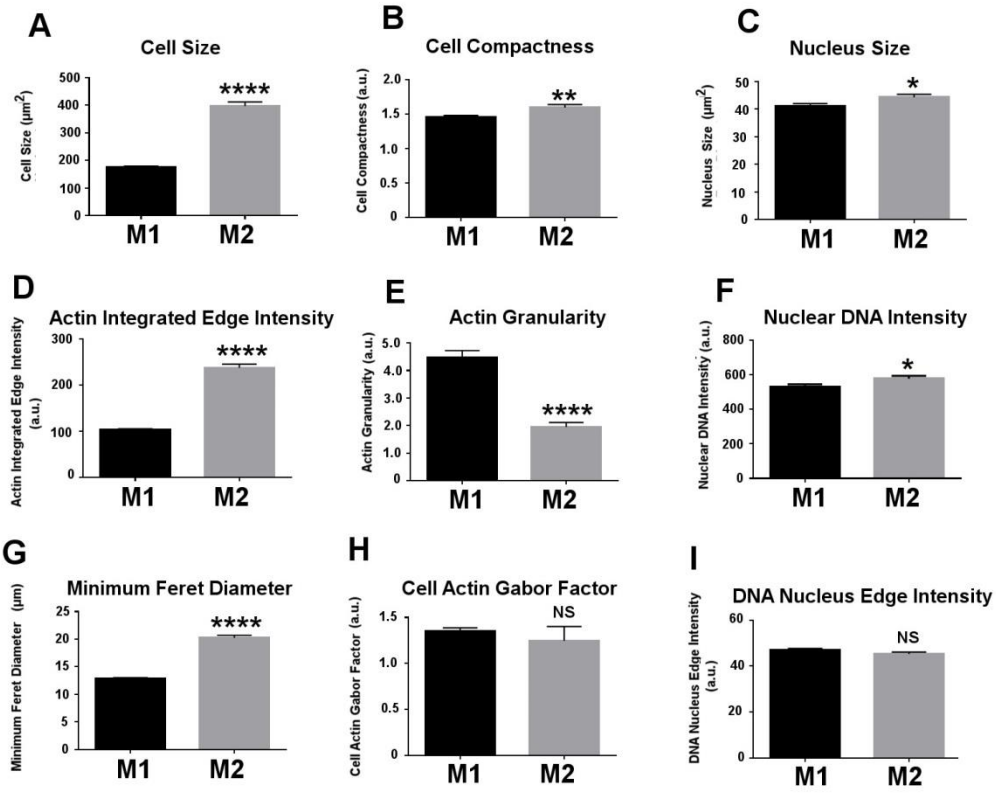

Figure 5.5: Comparison of key morphometric measurements of M1 and M2 macrophages. Measurement of **(A)** nucleus size, **(B)** cell compactness, **(C)** the minimum Feret diameter, **(D)** the summed intensity of actin around the cell edge, **(E)** the granularity of the actin stain, and **(F)** the summed intensity of DNA within the nucleus. Data is presented for at least *n*=250 for each cell type. Bars show average, with error bars denoting the S.E.M. * = $p<0.05$, ** = $p<0.01$, *** = $p<0.001$ by student's t-test. Measurements are described in (**Error! Reference source not found.**)

Figure 5.6: Measurements used to form the cytoprofile, as plotted in (Figure 5.5)

5.3.3. Classification of Cell Type by Machine Learning

Alongside the ability of PCR and immunostaining to confirm M1/M2 phenotype (**Figure 5.3** and **Figure 5.4** respectively**)** it has been demonstrated that simple descriptors of cell shape also hold sufficient information to allow accurate identification of macrophage polarisation states. The inherent heterogeneity of the cell system requires that multiple nuances in cell shape within individual phenotypes can be identified and classified. To avoid any bias, fluorescent images raw intensity were

used without any scaling, and they have not been through the normalisation process. Of the 228 measurements collected for each cell, some were found to significantly differ between phenotypes, whilst others did not, **Figure 5.9** the Bayesian classifier provided as part of the CellProfiler software suite was configured to construct a 25-rule classifier for both 4 and 2 classes of immune cell phenotypes. The rules generated for each classifier are included in the **Figure 5.7** and **Figure 5.8** for reference, and make use of measurements which were found to bear stark differences between cell phenotypes, as well as measurements which did not appear to be statistically different. The classifier was trained using a subset of the image data collected, by extracting 50 random cells of each phenotype. This was done in collaboration with Nikolaj Gadegaard's group (University of Glasgow) who performed some of the image analyses using the classifiers. From the 50 randomly selected cells for each of the phenotypes, a rule set (25 rules) was generated. The graphical user interface provided by CellProfiler Analyst makes the task of building a machine learning based classifier accessible to even novice users.

Table 5.1 Confusion matrix showing machine learning classification of immune cell phenotypes. Data is presented for all cells as a percentage of correctly classified cells. At least 500 cells were classified for each cell type across 93 images. Using the same dataset, 4-way and 2-way classifiers were built and their performance analysed. The number of correctly classified cells is presented as a percentage, with true positives highlighted on the diagonal in red.

			Measurement < Threshold		Measurement > Threshold	
Rule #	Measurement	Threshold	M1	M2	M1	M2
1	Cells_AreaShape_Area	10979.000	-0.939	0.939	0.463	-0.463
2	Cells_Granularity_12_Actin	2.865	0.693	-0.693	-0.461	0.461
3	Cells_Intensity_UpperQuartileIntensity_DNA	0.090	0.288	-0.288	-0.911	0.911
4	Cells_RadialDistribution_RadialCV_Actin_3of10	0.057	0.561	-0.561	-0.688	0.688
5	Cells_Granularity_6_Actin	5.016	1.000	-1.000	-0.280	0.280
6	Cells_Intensity_IntegratedIntensityEdge_Actin	204.459	-0.854	0.854	0.338	-0.338
7	Cells_RadialDistribution_RadialCV_Actin_9of10	0.172	0.547	-0.547	-0.600	0.600
8	Cells_Intensity_MeanIntensityEdge_Actin	0.142	-0.455	0.455	0.654	-0.654
9	Cells_Granularity_2_Actin	0.724	0.274	-0.274	-1.000	1.000
10	Cells_Intensity_StdIntensityEdge_DNA	0.040	0.702	-0.702	-0.403	0.403
11	Cells_Texture_Gabor_Actin_5	0.645	0.295	-0.295	-0.822	0.822
12	Cells_RadialDistribution_RadialCV_Actin_2of10	0.026	0.261	-0.261	-1.000	1.000
13	Cells_Granularity_10_Actin	3.818	0.754	-0.754	-0.460	0.460
14	Nuclei_Intensity_MinIntensityEdge_DNA	0.259	-0.976	0.976	0.280	-0.280
15	Cells_Intensity_UpperQuartileIntensity_DNA	0.212	0.714	-0.714	-0.421	0.421
16	Cells_Granularity_7_Actin	2.750	0.722	-0.722	-0.329	0.329
17	Cells_RadialDistribution_RadialCV_Actin_1of10	0.021	0.324	-0.324	-0.938	0.938
18	Cells_Granularity_4_Actin	2.519	0.663	-0.663	-0.464	0.464
19	Cells_Texture_Gabor_Actin_5	0.645	0.310	-0.310	-0.914	0.914
20	Cells_Granularity_1_Actin	36.031	-0.574	0.574	0.492	-0.492
21	Nuclei_Intensity_LowerQuartileIntensity_Actin	0.196	-0.678	0.678	0.375	-0.375
22	Cells_RadialDistribution_RadialCV_Actin_2of10	0.042	0.448	-0.448	-0.660	0.660
23	Nuclei_AreaShape_Zernike_7_1	0.011	-0.703	0.703	0.309	-0.309
24	Cells_AreaShape_Zernike_7_7	0.004	-0.441	0.441	0.499	-0.499
25	Cells_AreaShape_Zernike_3_1	0.020	-0.390	0.390	0.657	-0.657

Figure 5.7: 1 Rules for binary classifier, built using CellProfiler Analyst, to classify M1 and M2 macrophages. For a cell of an unknown type, its measured characteristics are compared against the threshold value, and a value added to the 'score' for both M1 and M2 possibilities. The largest value after 25 rules determines the classifier's estimation of the cell type, with larger values in favour of a given cell type generally indicating a higher confidence.

			Value < Threshold				Value > Threshold			
Rule #	Measurement	Threshold Value	Day6	Naïve	M1	M2	Day6	Naïve	M1	M2
1	Cells_Intensity_IntegratedIntensityEdge_Actin	186.5843	-0.876	-0.2	-0.907	-0.015	-0.318	-0.644	-0.303	-0.733
2	Nuclei_AreaShape_Area	1443.0000	0.1441	0.1405	-0.32	-0.522	-0.711	-0.611	0.2017	0.4104
3	Cells_Intensity_UpperQuartileIntensity_DNA	0.0863	-0.069	0.1032	0.1514	-0.346	0.0658	-0.507	-0.846	0.6322
4	Cells_Granularity_11_Actin	1.7314	0.3399	-0.35	0.0415	-0.483	-0.58	0.2839	-0.13	0.3167
5	Cells_Intensity_MinIntensity_Actin	0.1333	0.0337	0.4618	-0.839	-0.129	-0.042	-0.337	0.2637	0.0406
6	Nuclei_Intensity_MeanIntensityEdge_DNA	0.2463	0.3791	-0.41	0.0018	-0.264	-0.536	0.3115	-0.104	0.1739
7	Cells_AreaShape_Compactness	1.1930	-0.501	0.0413	0.2865	-0.056	0.436	-0.077	-0.465	0.0849
8	Cells_Number_Object_Number	16.0000	-0.385	0.2885	0.0463	-0.069	0.3862	-0.551	-0.092	0.0883
9	Cells_RadialDistribution_MeanFrac_Actin_1of10	0.8447	-0.354	0.2209	0.0667	0.0045	0.5295	-0.543	-0.155	-0.013
10	Cells_RadialDistribution_FracAtD_Actin_6of10	0.1089	0.3172	-0.859	-0.001	0.5659	-0.076	0.178	1	-0.242
11	Nuclei_AreaShape_Zernike_9_9	0.0019	0.1187	-0.395	0.1503	0.0953	-0.361	0.4625	-0.469	-0.193
12	Cells_Granularity_3_Actin	1.4869	-0.105	-0.302	0.4118	-0.141	0.1016	0.2526	-0.605	0.13
13	Cells_Texture_Gabor_Actin_5	0.9134	-0.488	-0.052	0.3661	-0.174	0.2009	0.0349	-0.508	0.1253
14	Cells_RadialDistribution_RadialCV_Actin_2of10	0.0479	-0.02	-0.213	0.3623	-0.3	0.0025	0.2043	-0.599	0.2354
15	Nuclei_Granularity_9_DNA	1.9377	0.1681	0.1589	-0.433	-0.068	-0.425	-0.469	0.4238	0.0886
16	Cells_AreaShape_Zernike_0_0	0.4867	0.0988	0.2041	0.1566	-0.52	-0.272	-0.205	-0.159	0.4393
17	Cells_Intensity_MeanIntensityEdge_Actin	0.2932	-0.82	0.916	0.2966	-1	0.1083	-0.188	-0.016	0.0408
18	Nuclei_AreaShape_Zernike_7_1	0.0119	-0.479	-0.235	-0.485	0.6469	0.0504	0.0927	0.1528	-0.269
19	Cells_Granularity_12_Actin	7.7103	-0.528	-1	0.9206	-1	0.0297	0.0271	-0.241	0.089
20	Nuclei_AreaShape_Zernike_9_7	0.0023	-0.119	-0.172	0.3167	0.0045	0.3198	0.3254	-0.751	-0.096
21	Cells_AreaShape_FormFactor	0.4333	0.4865	-0.864	-0.221	0.4466	-0.166	0.1937	0.0031	-0.088
22	Cells_AreaShape_MaxFeretDiameter	181.8186	-0.003	-0.571	-0.17	0.5165	0.0151	0.2255	0.0511	-0.344
23	Nuclei_Intensity_MinIntensity_DNA	0.2588	0.5996	0.1428	-0.96	0.3948	-0.174	-0.055	0.2197	-0.096
24	Cells_Granularity_5_Actin	2.4500	0.3008	-0.628	0.2367	-0.309	-0.163	0.2372	-0.262	0.0943
25	Nuclei_Granularity_4_DNA	5.1012	-0.392	0.0392	0.2351	0.169	0.3653	-0.105	-0.463	-0.294

Figure 5.8: 2 Rule set for a 4-way classifier to estimate the phenotype of unknown cells as either Day 6 monocytes, or Naïve, M1, or M2 macrophages.

Table 5.1: Confusion matrix showing machine learning classification of five cell phenotypes. Data is presented for all cells as a percentage of correctly classified cells. At least 500 cells were classified for each cell type across 93 images.

		Predicted				
		Monocyte Day 0	Monocyte Day 6	Naïve Macrophage	M1 Macrophage	M2 Macrophage
Actual	Monocyte Day0	95%	1%	1%	3%	0%
	Monocyte Day 6	3%	67%	16%	8%	7%
	Naïve Macrophage	3%	17%	54%	10%	17%
	M1 Macrophage	4%	15%	7%	69%	5%
	M2 Macrophage	4%	6%	7%	17%	66%

To examine the ability of the software to correctly identify different immune cell phenotypes, the accuracy of 2-way and 4-way classifier was compared using a confusion matrix, **Table 5.1** All images in the dataset were scored using each classifier, and the percentage of cells classified into each bin is listed. On a cell by cell basis, it appears that misclassification is high, with naïve macrophages, for example, only being correctly classified 58% of the time across the whole dataset. The average accuracy across all cell types was 64.8% for the 4-way classifier and 88.8% for a 2 way classifier analysing only M1 and M2 phenotypes. When whole images or groups of images are considered, however, as in **Figure 5.9**, the spread of misclassifications across the other classes increases the accuracy to 76%.

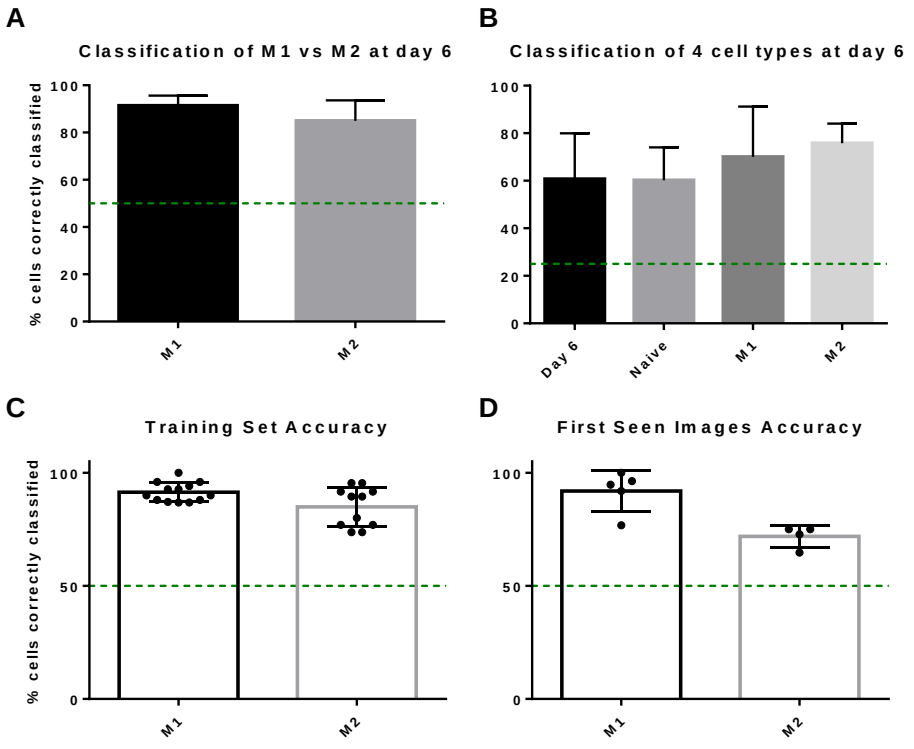

Figure 5.9: Classifier accuracy in determining M1 and M2 phenotype. (A) Classification of M1 and M2 cells based on morphometric features using a binary classifier. **(B)** Classification of all cell types found after 6 days culture using a 4-way classifier. Classification of the images used to train the classifier **(C)** gives an accuracy of 91% for M1 cells and 85% for M2 when these cells are then returned to the classifier for scoring. Subsequent classification of 5 blinded images for each cell type were 92% accurate for M1 cells and 65% accurate for M2 cells **(D)**. Images of cells from multiple patients were used, data is presented as an average (bar), individual image data (dot plot) and standard deviation (error bars). Green dashed line indicates the accuracy of a random classifier.

5.4. Discussion

In previous chapter, although there was no significant difference between cells on M1 and M2 biased polymers, there was significant difference between cell morphology incubated on different polymers. This supported the hypothesis that following exposure to cytokines and subsequent polarisation of the cells, there was a difference in cell size between M1 and M2 macrophages (**Appendix II**).

Macrophages perform their myriad functions via the adoption of different activation states (123). Determination of macrophage activation can provide important information about disease status, inflammation, and the outcome of therapeutic interventions. Current methods for assessing macrophage activation include analysis of marker and transcription factor expression, cytokine profiling, and functional assays such as phagocytosis. However, these methods are laborious, resource-intensive, and require a range of skills. Here, a simple, single-assay method was developed for the automated identification of different macrophage functional phenotypes using their cell size and morphology. This is the first time such method is used for characterisation of the immune cells.

Monocytes were stimulated *in vitro* with M1 or M2-inducing cytokines for 6 days following which macrophage phenotype was confirmed by immunofluorescent staining for calprotectin and MR expression (M1 and M2 surface markers respectively), measurement of cytokines in culture supernatants, and analysis of transcription factors by quantitative real-time PCR (qRT-PCR). Unpolarised (naïve) macrophages, freshly isolated monocytes, and monocytes cultured for 6 days without cytokines were also included as controls. Macrophage morphology was assessed microscopically by staining the cells with fluorescently labelled phalloidin in order to visualise the actin cytoskeleton. Cell images were analysed using CellProfiler (193,199) in order to measure different dimensions of the cells and their nuclei, and create a specific profile with shared characteristics for each cell type. These profiles formed the basis for M1 and M2 phenotype identification. From the automated CellProfiler analysis a so-called ‘cytoprofile’ was established which described the characteristics of the individual cells from the different phenotypes. This profile included size, shape, intensity, and texture of the actin and nuclear stain. With the

cytoprofile established for the different cell types, this large multivariate dataset was used to create a classifier based on a Bayesian machine learning algorithm. CellProfiler Analyst provides a graphical user interface, allowing users to visually build training sets for each cell type, followed by classifier training and generation of a set of rules. From the established rules, it was possible to identify key characteristics separating the individual phenotypes. Beyond simply visualising the cell body, fluorescent labelling of the nucleus and actin cytoskeleton provides a wealth of information (199). Common descriptors of cell morphology such as cell area, perimeter, and elongation can be combined with more specific metrics of texture and intensity to create a robust 'fingerprint' of a given phenotype – referred to as the 'cytoprofile'. A number of open source packages have been released in recent years which allow researchers to utilise this 'cytoprofile' to perform multivariate and machine learning analyses (199,200). In this study a supervised Bayesian classifier (193) was used available in CellProfiler Analyst to construct a 5-way classifier capable of distinguishing between monocyte and macrophage phenotypes.

The accuracy of the classifier can be further improved through accumulation of larger training sets and increased image quality. Inclusion of some slightly out of focus images can skew the machine learning algorithm and so care should be taken to understand the impact that imaging artefacts can have on classifier performance. For example, a fine texture may be lost if the image is only slightly out of focus. To combat this, filters could be generated to detect out of focus images, and either discard the data or recapture the image if automated image acquisition methods were used.

The CellProfiler Analyst software package generates an enrichment score for each image, and a probability that an image is enriched for a given phenotype. This takes into account the distribution of morphologies within a given image. Whilst some cells

may be classified into one bin when compared to the training set, if the vast majority of cells in an image fall into a given class, the software will identify the image as enriched and one can infer that all cells in the image belong to said phenotype. In this instance, with raw data provided in the form of images with only a single phenotype in each, this was a strong measurement of performance and yielded high accuracies of over 85% when using a 2-way classifier. In a clinical setting wherein a heterogeneous cell population is analysed within a given image, the headline accuracy may fall as the power of analysing an image as a collection of the same phenotype is lost. After training the classifier using known data,–each classifier with 40 blind images was presented introducing new instances of each phenotype not seen in the machine learning training phase - 6. This method was found to have an accuracy of 82% for a binary classifier looking only at M1 and M2 phenotypes, and an accuracy of 49% for a 4-way classifier. A 10-fold cross validation included in CellProfiler Analyst was used to determine classifier accuracy across the full image dataset (training data and blind images), which reported 85% accuracy for a binary classifier, and 52% for a 4 way classifier. Both of these values are significantly higher than the baseline value for each classifier configuration. This correlates with the confusion matrix shown in **Table 5.1**, which shows a lower classification accuracy for the 4-way classifier as compared to the 2-way. Furthermore, it was observed that the 2-way classifier was less accurate in detecting M2 macrophages, 6D, which may indicate that M2 macrophages display a more heterogeneous phenotype. This is reinforced by considering the larger error bars on specific cell shape measurements such as cell size.

Identifying M1 and M2 macrophage by machine learning depending on cell morphology with accuracy of about 88% was important finding in this experiment.

5.5. Conclusions

Image based machine learning using a broad array of metrics of the cell nucleus and cytoskeleton is an effective means of classifying M1 and M2 macrophages. These results demonstrate that an 'off the shelf' Bayesian classifier is capable of achieving accuracies in excess of 85% in classifying M1 and M2 macrophages. It was confirmed the phenotypical difference between Naïve, M1 and M2 macrophages isolated from peripheral blood by classical techniques as found in the literature, namely qRT-PCR, cytokine profiling and immunostaining. In addition, new means of classifying macrophage populations using image based machine learning was demonstrated. Given the heterogeneity of macrophage phenotype and current limitations of the machine learning approach, it may be too early to suggest use of image analysis as an alternative to conventional cell phenotyping. However, presented data provide strong evidence for the ability of high content and automated image analysis approaches for accurate, less resource intensive and fast phenotyping of functionally diverse cell populations.

Chapter Six: General Discussion

6.1. General discussion

Macrophages as antigen presenting cell play a crucial role against foreign bodies. These cells are able to secrete chemokine and cytokines after stimulation, which are essential in regulating inflammation, inducing and recruiting of other immune cells. These processes are necessary for tissue healing and remodelling after injury caused by implanting biomaterials (106,149,150), Biomaterial surface chemistry modification has previously been shown to modulate macrophage function(201,202).

Materials with anti-protein adsorbent properties have been an issue for most of the biocompatible material related studies. They tried to reduce biomaterial-protein-immune cell interaction to the minimum. Instead, modulating biomaterials by changing surface chemistry to stimulate immune cells (macrophage), and polarise them towards pro-healing/anti-inflammatory (M2) phenotype, can be an alternative approach for research. In addition, identifying proteins (amino acids) that are associated with surface chemistry (with hydrophilic or hydrophobic properties) and a particular macrophage (M1 or M2) phenotype is another important point to be considered.

It is known that etching polystyrene with oxygen plasma cause change in surface chemistry of the biomaterial, consequently that will reflect on adsorbed protein identity. That in turn can stimulate downstream signal pathways of macrophages and stimulate them to a particular phenotype.

Thus one of the aims of this study was to develop polystyrene with different surface chemistry by oxygen plasma etching of polystyrene. Data presented here show that polystyrene with a particular chemistry (hydrophilic or hydrophobic) can polarise adherent macrophages towards a pro-inflammatory/anti-tumour (M1) or toward an

anti-inflammatory/pro-healing phenotype (M2) macrophage phenotype. Furthermore, the identity of adsorbed protein particles was investigated using surface chemistry characterisation technique, such as Tof-SIMS and XPS.

Interestingly data presented in this study show differentiation of monocytes towards different macrophage phenotypes in the absence of any polarising cytokines and in response to different surface chemistries. Hydrophilic oxygen plasma etched surfaces (i.e. O_2-PS40) stimulated monocyte polarisation towards a pro-inflammatory M1-like phenotype in comparison with hydrophobic surfaces (i.e. untreated PS). The observation of alterations in surface chemistry can induce such polarised macrophage profiles which have important implications for biomaterial design and function.

6.1. The impact of surface chemistry on macrophage polarisation

6.1.1 The impact Polystyrene surface chemistry on macrophage polarisation

In this study there was monocyte differentiation towards different macrophage phenotypes in response to altered surface chemistry without using of exogenous polarising cytokines. Given its widespread use for tissue culture, polystyrene was used for surface modification studies. By using O_2 plasma etching 4 surfaces with distinct chemistries were developed, which were classified by their surface wettability (measured as WCA). O_2-PS40 was the most hydrophilic and untreated PS the most hydrophobic. It was found that the hydrophilic surface O_2-PS40 stimulated monocyte polarisation towards a pro-inflammatory M1-like phenotype while the hydrophobic surface PS had the opposite impact.

MR (M2-marker) $cell^+$/Calprotectin (M1-marker) $cell^+$ ratio on polystyrene surfaces, the most hydrophobic PS (un-treated) was around 3, while on hydrophilic surface (O_2-PS40) decreased to around 1. Also a significant amount of anti-inflammatory

cytokine, IL-10 secretion was secreted by seeded monocyte on non-treated PS surfaces in comparison with those on the other polystyrene surfaces. Also, there was higher phagocytic activity on cultured cells on O_2-PS40 in comparison with PS-cultured cells. Phagocytosis mediated by Fc-receptor and specific pathogen recognition receptors have various effects on macrophage polarisation (77,137). For example, a study has shown an increase of non-Fc-mediated phagocytosis of yeast and decrease of Fc-mediated phagocytosis in M1 (77) in this study, phagocytosis was mediated by Fc-receptors due to exist of FBS in the cell culture medium and also by zymosan-specific receptors such as complement receptors, mannose receptors and β-glucan receptors (138).

Furthermore, transcription factor analysis showed similar level of IRF4 in monocytes on both O_2-PS40 and PS surfaces. Previous study reported a similar IRF4 gene expression in M-CSF and GM-CSF-induced human macrophages (139). It was found high levels of pro-inflammatory M1 related transcription factors, STAT1 (77,140) and IRF5 (139,141) expression on monocytes cultured on hydrophilic O_2-PS40 surfaces when compared to cells seeded on hydrophobic PS (203). However, in cells cultured on PS there was less SOCS1 (M2 related cytokine suppressor signalling protein) expression (142,143) in comparison with O_2-PS40. Interestingly, Whyte *et al*. reported IL-10 secretion can be inhibiting by SOCS1 (143). This, possibly explain why there was lower IL-10 secretion on O_2-PS40 surfaces and higher IL-10 production by cell on PS vs. SOCS1-hi cells. Suggesting that SOCS1/SOCS3 expression balance in macrophage affects their activation state (142). This study suggested polystyrene surface wettability modification can stimulate seeded macrophage to display a unique phenotype directed towards a more pro-inflammatory or anti-inflammatory state. That

can be due to identity of adsorbed proteins, which were influenced by surface chemistry, that can guide macrophage differentiation towards different phenotypes.

6.1.2 How surfaces chemistry affect macrophage polarisation

The mechanism of how surface chemistry stimulates macrophage polarisation still unclear (127). Here, it has been hypothesised that the impact of different surface chemistries of polystyrene surfaces on macrophage polarisation without using cytokines can be due to the difference in type and amount of the adsorbed proteins on different polystyrene surfaces (126), to assess that, XPS and ToF-SIMS used to characterise surface chemistry of all surfaces. The XPS data showed that hydrophilic polystyrene (O_2-PS40) was with the highest amount of total amount of adsorbed protein in comparison with other surfaces. Grinnell and Feld reported similar results when they found that hydrophilic glass was stimulated to adsorb fibronectin more than to hydrophobic functionalised glass. However, other study have reported that fibronectin adhere to hydrophobic polystyrene surfaces more than to hydrophilic surfaces (144). In addition, adsorbed protein was proportional with the hydrophilicity and oxygen atomic percentage before incubation. Also a correlation was found between oxygen atomic percentage and hydrophilicity of polystyrene surfaces. This suggests that, protein thickness can be related to oxygen atomic percentage. Furthermore, ToF-SIMS assigned to O_2-PS40 surface was prevalent with amino acids arginine, alanine, and proline, while PS surfaces were more prevalent ions assigned to tyrosine, phenylalanine, lysine, histidine, valine, and methionine.

From this surface characterisation has been proposed that, polystyrene surface chemistry controls the adsorbed protein which in turn influences the macrophage response. Macrophage engage with adsorbed protein such as fibronectin and

fibrinogen on implanted biomaterial surfaces through leukocyte β2 integrin receptors (particularly αMβ2 (Mac-1) mediator (145,146)). This causes signalling pathways initiation leading to macrophage stimulation of inflammatory cytokines (IL-6, IL-1α, TNF-β) secretion (204), and secretion of chemotactic factors such as IL-8 and macrophage inflammatory protein 1 beta (MIP-1β) (63). Not only the type of adsorbed proteins, but also their orientation on a surface can affect the type of macrophage response (148).

6.2. The impact of Acrylamides and Acrylates polymers on macrophage attachment, phenotype and morphology

The interface between the biology and biomaterials is extremely complex, therefore no starting points to hypothesise from which materials elicit immunomodulatory behaviour. That way, Douglas Kell bioassay approach was taken, by using inductive or data high driven strategy to determine the initial point, to investigate for immunomodulatory potential materials (170). Polymer microarray was suitable for this approach in combination with commercially available libraries. Therefore, available acrylate and acrylamide were used without considering their identity and without any bias to a particular available chemistry (171).

Thus, this study aimed to investigate libraries of acrylates and acrylamide polymer for their ability to modulate monocyte differentiation to different macrophage subsets using a high throughput screening strategy.

In this study, ǂ it was observed that incubated monocytes on co-polymers 217 (35-co-141) and 123 (24-co-113) for six days were polarised toward pro-inflammatory M1-like phenotype. However, co-polymer 157(117-co-121) stimulated macrophages to express MR (M2 marker). These observations indicate that alterations in surface

chemistry can induce polarised macrophage profiles which have important implications for biomaterial design and function.

High throughput screening has proven a highly sufficient strategy to identify new materials with distinct functional properties such as promoting stem cells differentiation towards cardiomyocytes, hepatocyte-like cells, and neural progenitors (205). Here, a high throughput screening strategy of an acrylamide and acrylate polymer library was used, to investigate the effect of a combinatorial library of polymers on human monocyte differentiation. A range of macrophage responses were observed to the various polymers including changes in cell attachment, cell morphology and macrophage phenotype.

Data from the first generation array library, which consists of 141 different homo-polymers with higher chemical diversity, showed less cell attachment than the second generation co-polymers, for instance, Homo-polymer 42 (230±65 cells) ,133 (209±47 cells) , 90 (197±69cells) were the most adherent polymers, while co-polymer 56 (50-co- 29) (411±143 cells), 386 (71-co-126) (363±99 cells) and 32 (25-co-67) (357±166 cells) from the second generation of the array were the most adherent polymers.

Homo-polymer 29 (81±40) and co-polymer 263 (88-co-24) (276±66) were the most adherent M2 and M1 biased polymers respectively, while M2 biased homo-polymer 39 (9.8±3.9 cells) and M1 biased co-polymer 123 (24-co-113) (113.2±48 cells) were the least adherent biased polymers. The nature of the surface chemistry of polymers can stimulate cell attachment (63,128,174), via the differences in adsorbed proteins (127).

Although co-polymers from second generation array such as 56 (50-co-29) (411.2±143.3 cells), 386 (71-co-126) (362.7±99 cells), 32 (25-co-67), 347 (3-co-126)

(328.2±125.5 cells) and 295 (94-co-71) (346.9±165.6 cells) had the highest number of attached cells, non-of their constituents had a significant high rate of cell attachment in the first generation array. In addition, co-polymers 358 (29-co-115) (18.8±5.6 cells), 209(35-co-126) (46.8±22.1cells), 434 (35-co-123) (51.2±16.9 cells), 94(35-co-47) (54.1±8.6 cells) and 48(50-co-47) (55.7±18.5 cells) had the fewest attached cells in the second generation array. Their constituent homo-polymers in the first generation had no significant cell attachment data. Interestingly, the second, third and fourth least adherent co-polymers had monomer 35 (hexyl acrylate) as one of their two constituents. Also, the cell attachment in the second generation was higher than the first generation. That possibly due to the synergic effect of the individual monomers when combined as a co-polymer.

Macrophage attachment depends on adsorbed protein to surfaces (175). Protein adsorption can be induce by anionic carboxylate groups, which have been observed to be particularly effective at inducing macrophage adhesion (176). Carboxylate ions from meth acrylates (178) or acrylamides (173) may play a role in macrophage adhesion. Previous studies reported that co-polymers and homo-polymers of methacrylamides can stimulate antibody production in mice when they linked oligopeptide side chains (179). Also, poly(ethylene glycol) and poly(lactide) (MPEG-b-PLLA) co-polymers were observed to stimulate human bone marrow stromal cells (hBMSCs) proliferation and adhesion via upregulation of the adhesion molecule complex, cadherin-catenin (180).

In this study, number of polymers were identified which can stimulate monocyte differentiation towards distinct macrophage phenotypes. Co-polymer 157 (117-co-121) enhanced seeded monocytes to express the highest level of MR (M2 marker)

while, co-polymers 217 (35-co-141) and 123 (24-co-113) in influenced incubated cells high level of calprotectin (M1 marker) expression.

Chemical properties of each polymer spot can influence the nature of bio-adsorbate layers themselves. Also, it has crucial impact on quality and quantity of adsorbed protein (57,63,64,66,128). FBS in RPMI media consist of great variety of protein (181) and adsorbed protein identity to the surface is a key mediator of cell activity and behaviour (182). Therefore macrophage polarisation toward a particular phenotype can be under influence of specific type of protein. As instance, M1-biased on polystyrene surfaces were found related with arginine, proline and alanine, while M2-biased surfaces were more associated with phenylalanine, tyrosine, histidine, lysine, methionine and valine (see **chapter 3**). This means that distinct bio-adsorbate from cell-secreted biomolecules and media proteins on each of these polymer spots are responsible for cell polarisation toward a specific phenotype. Therefore it is important to find the exact molecular basis of such polymer stimulate macrophage differentiation toward either M1 or M2.

The polarisation ability to a particular phenotype by a number of co-polymers from the second generation of the microarray was improved by copolymerisation. Co-polymers 217 (35-co-141) (made from 66% monomer 35 and 33% monomer 141) and 123 (24-co-113), were induced M1 inter donor cell ratio by 3.5 and 2.5 folds respectively, while their constituent in the first generation had no significant effect on inter donor M2/M1 cell ratio. However, homo-polymers 141, 24 and 113 were M1biased and homo-polymer 35 was M2 biased in one third of all 3 donors. However, co-polymer 157 (117-co-121) in the second generation microarray polarised cells towards an M2 phenotype as evidenced by 2 times higher expression of MR than

calprotectin (M1 marker). In the first generation microarrays both its constituent had no significant impact on macrophage polarisation.

The most consistent macrophage phenotypical biased polymer were; co-polymers 217 (M1 biased), 123 (M1 biased) and 157 (M2 biased). They were biased to a particular phenotype in the inter donor M2/M1 ratio, and in intra donor M2/M1 ratio in 2/3 of all 3 donors.

Macrophage M1 and M2 phenotypical polarisation efficiency by polymers was lower than cytokines (GM-CSF+IFN-γ for M1 and M-CSF+IL-4 for M2) by about 6 and 2 times respectively. However, in the second donor M-biased copolymer 222 (22-co-126) and M2-biased 255(88-co-25) stimulated macrophage polarisation towards their phenotype, by about double more than cytokines.

That mean they can be considered M1 biased co-polymers (217 and 123) and M2 biased 157 as robust polymers, which can used in design of biomaterials that are able to trigger desired immunological outcomes and thus support either pro-healing (M2) or anti-tumour (M1) process .

Biomaterials surface chemistry has been reported to have influence on changing macrophage morphology (86,183).

Here in this study, the main morphological parameters such as cell area, nucleus area, major axis length, and minor axis length have been reported.

There was significant differences between a group of top 10 homo-polymers influenced the cells to have large cell area (122-165 μm^2) and other group of which stimulated cell with smaller cell area (52-94 μm^2). Furthermore, a group of 10 co-polymers with large cell area (210-220 μm^2) had significant differences with other group of polymers with small cell area (78-107 μm^2). Interestingly, the cell area of

incubated cells on both co-polymers hit groups, were larger than their counterpart on homo-polymer hit groups. That can be due to the synergic effects of copolymerisation. However, there was not significant morphological difference between cells on M1 and M2 biased hit polymers.

6.3. M1 and M2 macrophages identification by Image based Machine Learning

Although there were no significant differences between cells on M1 and M2 biased polymers, there was a significant difference between cells morphology seeded on different polymers. From initial observations of polarised M1 and M2 macrophages following exposure to cytokines which were used as controls in the experiment, there were some differences between both phenotypes in terms of cell size. M2 cells had larger cell area than M1 cells. That proposed the idea that, investigating possible differences in morphology of polarised macrophage (following exposure to cytokines) could lead to developing a machine learning algorithm for M1 and M2 phenotype identification, depending on differences of phenotypical cell morphology.

Macrophages perform their myriad functions via the adoption of different activation states (123). Determination of macrophage activation can provide important information about disease status, inflammation, and the outcome of therapeutic interventions. Current methods for assessing macrophage activation include analysis of marker and transcription factor expression, cytokine profiling, and functional assays such as phagocytosis. However, these methods are laborious, resource-intensive, and require a range of skills. Here, in collaboration with the University of Glasgow a simple, single-assay method has been developed for the automated identification of different macrophage functional phenotypes using their cell size and morphology

Significant differences in cell morphology of M1 and M2 on microarray polymers were observed. In addition, other research shows some morphological differences between M1 and M2 macrophage (see general introduction). That way it was hypothesised to build up morphological data for M1 and M2 aiming to use them for M1and M2 phenotype identification, depending on their morphological differences. Therefore, a simple, single-assay method has been developed for the automated identification of different macrophage functional phenotypes using their cell size and morphology.

In vitro monocytes were stimulated with M1 (IFNγ+GM-CSF) or M2 (IL4+M-CSF)-inducing cytokines for 6 days, then polarised macrophage phenotypes were confirmed by immunofluorescent staining for calprotectin (M1-marker) and MR (M2 marker) expression. Also pro-and anti-inflammatory cytokines were measured in culture supernatants, and transcription factors STAT1 and STAT6 for the each phenotype were analysed by performing quantitative real-time PCR (qRT-PCR). In addition, unpolarised (naïve) macrophages, freshly isolated monocytes, and monocytes cultured for 6 days without adding cytokines were also included as controls.

To assess macrophage morphology microscopically, the cytoskeleton of the cells were stained with fluorescently labelled phalloidin which stains the actin and DAPI stain was used for the nucleus. Cell images were analysed by using CellProfiler (193,199) in order to measure different cell and nucleus dimensions, and then was created a specific profile with shared characteristics for each cell phenotype. These profiles formatted on bases of M1 and M2 phenotype identification. Also the individual cells characteristics from the different phenotypes described in an automated CellProfiler analysis called ‘cytoprofile’, which included morphological information about cell size, shape, intensity, and texture of the actin and nuclear stain for different

macrophage phenotypes. By depending on those profiles, which were the source of a large multivariate dataset and by using Bayesian machine learning algorithm, a classifier was created. CellProfiler Analyst provided graphical user interface, that allowed the users to visually create training sets for each cell phenotype, then followed by training of classifier and generation of a set of rules. After establishing of those rules, key characteristics for separating the individual phenotypes were identified. In this study supervised Bayesian classifier was used (193) which is available in CellProfiler Analyst to build a 5-way classifier capable of distinguishing between macrophage phenotypes and monocytes.

The accuracy of the classifier was further improved, by increasing the number of training sets, also by improving the image quality, and by introducing enrichment score for each image and a probability that an image is enriched for a given phenotype generated by the package of CellProfiler Analyst software. Also, morphological distribution of cell phenotype within a given image is taken into account. For instance, by using a 2-way classifier with raw data provided in the form of images with only a single phenotype in each, there was a strong measurement of performance that yielded high accuracies of about 85%. Furthermore, M2 macrophage detection was less accurate in the 2-way classifier, due to a high phenotypical heterogeneity of the cell. This was evidenced by the larger error bars on specific cell shape measurements such as cell size.

Polarizing cells with chemically modified polystyrene surfaces, or by copolymers without using exogenous cytokines, and discovering the amino acids that correlated with each surface, were important findings in this experiment. In addition, identifying M1 and M2 macrophage by machine learning depending on cell morphology with accuracy of about 88%, was a significant finding.

6.4. Conclusions

To conclude, this study shows the changes in surface chemistry with O_2 plasma etching affect protein adsorption on the material. This subsequently appears to stimulate monocyte polarisation towards macrophages with distinct phenotypes. Hydrophobic PS shown to promote M2-associated markers and anti-inflammatory cytokines, while supressing M1-associated markers. However, hydrophilic O_2-PS40 had contrary impact.

Moreover, co-polymer 157 from the second generation microarray was the most potent polymer for induction of M2-associated marker (MR) while co-polymers 217 and 123 influenced high levels of calprotectin (M1 marker) expression. In addition, synergic effect of co-polymers influenced the cell attachment by double in comparison with the first generation homo-polymers.

Therefore, it is reasonable to suggest that changes in the surface chemistry of biomaterial can be a powerful tool for modulating macrophage phenotype and function without using polarising cytokines. This has clear implications in biomaterial design and function with applications in cell culture, medical device fabrication and implant medicine.

Furthermore, automated image analysis approaches can be used as accurate, less resource intensive and fast phenotyping of functionally diverse macrophage populations.

6.5. Future work

Future studies should focus on screening a more diverse set of chemical libraries for their immune modulatory properties. In addition, in this study macrophage surface marker expression was used as a surrogate for their functional phenotype. While such

an approach is informative, future studies should examine the possibility of using more functional readouts such as phagocytic ability or cytokine profile with high throughput screening. The focus on function will clearly make the screening more powerful. Another important area is developing a better understanding of the molecular basis for polymer induced changes in macrophage phenotype/function. Such information could provide new insight on signalling pathways that control macrophage polarisation towards pro or anti-inflammatory phenotypes. Clearly better characterisation of protein adsorbates on polymer surfaces will be the first step in achieving this goal.

References

References

1. Abraham, C. M. (2014) A brief historical perspective on dental implants, their surface coatings and treatments. The open dentistry journal 8, 50-55

2. Saini, M., Singh, Y., Arora, P., Arora, V., and Jain, K. (2015) Implant biomaterials: A comprehensive review. World journal of clinical cases 3, 52-57

3. Rahyussalim, A. J., Marsetio, A. F., Saleh, I., Kurniawati, T., and Whulanza, Y. (2016) The Needs of Current Implant Technology in Orthopaedic Prosthesis Biomaterials Application to Reduce Prosthesis Failure Rate. Journal of Nanomaterials 2016, 9

4. Chee, W., and Jivraj, S. (2007) Failures in implant dentistry. Brit Dent J 202, 123-129

5. Rodriguez-Merchan, E. C. (2011) Instability following total knee arthroplasty. HSS journal : the musculoskeletal journal of Hospital for Special Surgery 7, 273-278

6. Pye, A. D., Lockhart, D. E., Dawson, M. P., Murray, C. A., and Smith, A. J. (2009) A review of dental implants and infection. The Journal of hospital infection 72, 104-110

7. Landgraeber, S., Jaeger, M., Jacobs, J. J., and Hallab, N. J. (2014) The Pathology of Orthopedic Implant Failure Is Mediated by Innate Immune System Cytokines. Mediators of Inflammation, Article No.: 185150

8. Anderson, J. M., Rodriguez, A., and Chang, D. T. (2008) Foreign body reaction to biomaterials. Semin Immunol 20, 86-100

9. Wei, Q., Becherer, T., Angioletti-Uberti, S., Dzubiella, J., Wischke, C., Neffe, A. T., Lendlein, A., Ballauff, M., and Haag, R. (2014) Protein interactions with polymer coatings and biomaterials. Angewandte Chemie 53, 8004-8031

10. Swartzlander, M. D., Barnes, C. A., Blakney, A. K., Kaar, J. L., Kyriakides, T. R., and Bryant, S. J. (2015) Linking the foreign body response and protein adsorption to PEG-based hydrogels using proteomics. Biomaterials 41, 26-36

11. Wilson, C. J., Clegg, R. E., Leavesley, D. I., and Pearcy, M. J. (2005) Mediation of biomaterial-cell interactions by adsorbed proteins: A review. Tissue Eng 11, 1-18

12. Lee, J. M., and Kim, Y. J. (2015) Foreign Body Granulomas after the Use of Dermal Fillers: Pathophysiology, Clinical Appearance, Histologic Features, and Treatment. Arch Plast Surg 42, 232-239

13. Trindade, R., Albrektsson, T., Tengvall, P., and Wennerberg, A. (2016) Foreign Body Reaction to Biomaterials: On Mechanisms for Buildup and Breakdown of Osseointegration. Clinical implant dentistry and related research 18, 192-203

14. Sheikh, Z., Brooks, P. J., Barzilay, O., Fine, N., and Glogauer, M. (2015) Macrophages, Foreign Body Giant Cells and Their Response to Implantable Biomaterials. Materials 8, 5671-5701

15. Lemperle, G., Romano, J. J., and Busso, M. (2003) Soft tissue augmentation with artecoll: 10-year history, indications, techniques, and complications. Dermatologic surgery : official publication for American Society for Dermatologic Surgery [et al.] 29, 573-587; discussion 587

16. Zaveri, T. D., Lewis, J. S., Dolgova, N. V., Clare-Salzler, M. J., and Keselowsky, B. G. (2014) Integrin-directed modulation of macrophage responses to biomaterials. Biomaterials 35, 3504-3515

17. Anderson, J. M. (2000) Multinucleated giant cells. Current Opinion in Hematology 7, 40-47

18. Xia, Z., and Triffitt, J. T. (2006) A review on macrophage responses to biomaterials. Biomed Mater 1, R1-R9

19. Abensee, J. E. B. (2008) Interaction of dendritic cells with biomaterials. Seminars in Immunology 20, 101-108

20. Kou, P. M., and Babensee, J. E. (2011) Macrophage and dendritic cell phenotypic diversity in the context of biomaterials. J Biomed Mater Res A 96A, 239-260

21. Solheim, E., Sudmann, B., Bang, G., and Sudmann, E. (2000) Biocompatibility and effect on osteogenesis of poly(ortho ester) compared to poly(DL-lactic acid). J Biomed Mater Res 49, 257-263

22. de Mel, A., Cousins, B. G., and Seifalian, A. M. (2012) Surface modification of biomaterials: a quest for blood compatibility. International journal of biomaterials 2012, 707863

23. Zaveri, T. D., Dolgova, N. V., Chu, B. H., Lee, J., Wong, J., Lele, T. P., Ren, F., and Keselowsky, B. G. (2010) Contributions of surface topography and cytotoxicity to the macrophage response to zinc oxide nanorods. Biomaterials 31, 2999-3007

24. Unadkat, H. V., Hulsman, M., Cornelissen, K., Papenburg, B. J., Truckenmuller, R. K., Carpenter, A. E., Wessling, M., Post, G. F., Uetz, M., Reinders, M. J., Stamatialis, D., van Blitterswijk, C. A., and de Boer, J. (2011) An algorithm-based topographical biomaterials library to instruct cell fate. Proceedings of the National Academy of Sciences of the United States of America 108, 16565-16570

25. McCoy, C. P., Craig, R. A., McGlinchey, S. M., Carson, L., Jones, D. S., and Gorman, S. P. (2012) Surface localisation of photosensitisers on intraocular lens biomaterials for prevention of infectious endophthalmitis and retinal protection. Biomaterials 33, 7952-7958

26. Karagkiozaki, V., Karagiannidis, P. G., Kalfagiannis, N., Kavatzikidou, P., Patsalas, P., Georgiou, D., and Logothetidis, S. (2012) Novel nanostructured biomaterials: implications for coronary stent thrombosis. Int J Nanomedicine 7, 6063-6076

27. Cao, Y., and Wang, B. (2009) Biodegradation of silk biomaterials. Int J Mol Sci 10, 1514-1524

28. Smith, R. S., Zhang, Z., Bouchard, M., Li, J., Lapp, H. S., Brotske, G. R., Lucchino, D. L., Weaver, D., Roth, L. A., Coury, A., Biggerstaff, J., Sukavaneshvar, S., Langer, R., and Loose, C. (2012) Vascular catheters with a nonleaching poly-sulfobetaine surface modification reduce thrombus formation and microbial attachment. Sci Transl Med 4, 153ra132

29. Xue, L., and Greisler, H. P. (2003) Biomaterials in the development and future of vascular grafts. J Vasc Surg 37, 472-480

30. Katti, K. S. (2004) Biomaterials in total joint replacement. Colloids Surf B Biointerfaces 39, 133-142

31. Stover, T., and Lenarz, T. (2009) [Biomaterials in cochlear implants]. Laryngorhinootologie 88 Suppl 1, S12-31

32. Taguchi, T., Maeba, S., and Sueda, T. (2014) Prevention of pacemaker-associated contact dermatitis by polytetrafluoroethylene sheet and conduit coating of the pacemaker system. J Artif Organs 17, 285-287

33. Place, E. S., Evans, N. D., and Stevens, M. M. (2009) Complexity in biomaterials for tissue engineering. Nat Mater 8, 457-470

34. Kratky, W., Sousa, C. R. E., Oxenius, A., and Sporria, R. (2011) Direct activation of antigen-presenting cells is required for CD8(+) T-cell priming and tumor vaccination. Proc Natl Acad Sci U S A 108, 17414-17419

35. Wilke, C. M., Kryczek, I., and Zou, W. (2011) Antigen-presenting cell (APC) subsets in ovarian cancer. Int Rev Immunol 30, 120-126

36. Guermonprez, P., Valladeau, J., Zitvogel, L., Thery, C., and Amigorena, S. (2002) Antigen presentation and T cell stimulation by dendritic cells. Annu Rev Immunol 20, 621-667

37. Zhu, J., and Paul, W. E. (2010) Heterogeneity and plasticity of T helper cells. Cell Res 20, 4-12

38. Meuret, G. (1976) Origin, ontogeny, and kinetics of mononuclear phagocytes. Adv Exp Med Biol 73 PT-A, 71-81

39. Shi, C., and Pamer, E. G. (2011) Monocyte recruitment during infection and inflammation. Nat Rev Immunol 11, 762-774

40. Randolph, G. J., Jakubzick, C., and Qu, C. (2008) Antigen presentation by monocytes and monocyte-derived cells. Curr Opin Immunol 20, 52-60

41. Schmid, H., Sauerbrei, R., Schwarz, G., Weber, E., Kalbacher, H., and Driessen, C. (2002) Modulation of the endosomal and lysosomal distribution of cathepsins B, L and S in human monocytes/macrophages. Biological Chemistry 383, 1277-1283

42. Steinman, R. M., and Cohn, Z. A. (1973) Identification of a novel cell type in peripheral lymphoid organs of mice. I. Morphology, quantitation, tissue distribution. J Exp Med 137, 1142-1162

43. Liu, K., and Nussenzweig, M. C. (2010) Development and homeostasis of dendritic cells. Eur J Immunol 40, 2099-2102

44. Medzhitov, R., and Janeway, C. A., Jr. (2002) Decoding the patterns of self and nonself by the innate immune system. Science 296, 298-300

45. Banchereau, J., Briere, F., Caux, C., Davoust, J., Lebecque, S., Liu, Y. J., Pulendran, B., and Palucka, K. (2000) Immunobiology of dendritic cells. Annu Rev Immunol 18, 767-811

46. Ohteki, T. (2007) The dynamics of dendritic cell: mediated innate immune regulation. Allergology international : official journal of the Japanese Society of Allergology 56, 209-214

47. Roncarolo, M. G., Levings, M. K., and Traversari, C. (2001) Differentiation of T regulatory cells by immature dendritic cells. J Exp Med 193, F5-9

48. Chau, D. Y., Brown, S. V., Mather, M. L., Hutter, V., Tint, N. L., Dua, H. S., Rose, F. R., and Ghaemmaghami, A. M. (2012) Tissue transglutaminase (TG-2) modified amniotic membrane: a novel scaffold for biomedical applications. Biomedical materials 7, 045011

49. Zheng, W., Zhang, W., and Jiang, X. (2013) Precise control of cell adhesion by combination of surface chemistry and soft lithography. Adv Healthc Mater 2, 95-108

50. Roach, P., Parker, T., Gadegaard, N., and Alexander, M. R. (2013) A bio-inspired neural environment to control neurons comprising radial glia, substrate chemistry and topography. Biomater Sci-Uk 1, 83-93

51. Rakic, P. (2003) Developmental and evolutionary adaptations of cortical radial glia. Cereb Cortex 13, 541-549

52. Evans, M. D., and Steele, J. G. (1998) Polymer surface chemistry and a novel attachment mechanism in corneal epithelial cells. J Biomed Mater Res 40, 621-630

53. Yang, J., Rose, F. R. A. J., Gadegaard, N., and Alexander, M. R. (2009) A High-Throughput Assay of Cell-Surface Interactions using Topographical and Chemical Gradients. Advanced Materials 21, 300-304

54. Liu, X., He, J., Zhang, S., Wang, X. M., Liu, H. Y., and Cui, F. Z. (2013) Adipose stem cells controlled by surface chemistry. J Tissue Eng Regen Med 7, 112-117

55. Hofstetter, W., Sehr, H., de Wild, M., Portenier, J., Gobrecht, J., and Hunziker, E. B. (2013) Modulation of human osteoblasts by metal surface chemistry. Journal of Biomedical Materials Research Part A 101, 2355-2364

56. Ranella, A., Barberoglou, M., Bakogianni, S., Fotakis, C., and Stratakis, E. (2010) Tuning cell adhesion by controlling the roughness and wettability of 3D micro/nano silicon structures. Acta Biomater 6, 2711-2720

57. Cantini, M., Sousa, M., Moratal, D., Mano, J. F., and Salmeron-Sanchez, M. (2013) Non-monotonic cell differentiation pattern on extreme wettability gradients. Biomaterials Science 1, 202-212

58. Shen, Y., Wang, G. X., Huang, X. L., Zhang, Q., Wu, J., Tang, C. J., Yu, Q. S., and Liu, X. H. (2012) Surface wettability of plasma SiOx:H nanocoating-induced endothelial cells' migration and the associated FAK-Rho GTPases signalling pathways. J R Soc Interface 9, 313-327

59. Park, J., and Babensee, J. E. (2012) Differential functional effects of biomaterials on dendritic cell maturation. Acta Biomater 8, 3606-3617

60. Kou, P. M., Pallassana, N., Bowden, R., Cunningham, B., Joy, A., Kohn, J., and Babensee, J. E. (2012) Predicting biomaterial property-dendritic cell phenotype

relationships from the multivariate analysis of responses to polymethacrylates. Biomaterials 33, 1699-1713

61. Zhu, M., Tian, X., Song, X., Li, Y., Tian, Y., Zhao, Y., and Nie, G. (2012) Nanoparticle-induced exosomes target antigen-presenting cells to initiate Th1-type immune activation. Small 8, 2841-2848

62. Hume, P. S., He, J., Haskins, K., and Anseth, K. S. (2012) Strategies to reduce dendritic cell activation through functional biomaterial design. Biomaterials 33, 3615-3625

63. Jones, J. A., Chang, D. T., Meyerson, H., Colton, E., Kwon, I. K., Matsuda, T., and Anderson, J. M. (2007) Proteomic analysis and quantification of cytokines and chemokines from biomaterial surface-adherent macrophages and foreign body giant cells. J Biomed Mater Res A 83A, 585-596

64. McBane, J. E., Matheson, L. A., Sharifpoor, S., Santerre, J. P., and Labow, R. S. (2009) Effect of polyurethane chemistry and protein coating on monocyte differentiation towards a wound healing phenotype macrophage. Biomaterials 30, 5497-5504

65. Schutte, R. J., Parisi-Amon, A., and Reichert, W. M. (2009) Cytokine profiling using monocytes/macrophages cultured on common biomaterials with a range of surface chemistries. J Biomed Mater Res A 88A, 128-139

66. Dadsetan, M., Jones, J. A., Hiltner, A., and Anderson, J. M. (2004) Surface chemistry mediates adhesive structure, cytoskeletal organization, and fusion of macrophages. J Biomed Mater Res A 71A, 439-448

67. Jenney, C. R., DeFife, K. M., Colton, E., and Anderson, J. M. (1998) Human monocyte/macrophage adhesion, macrophage motility, and IL-4-induced foreign body giant cell formation on silane-modified surfaces in vitro. Student Research Award in the Master's Degree Candidate Category, 24th Annual Meeting of the Society for Biomaterials, San Diego, CA, April 22-26, 1998. J Biomed Mater Res 41, 171-184

68. Alfarsi, M. A., Hamlet, S. M., and Ivanovski, S. (2014) Titanium surface hydrophilicity modulates the human macrophage inflammatory cytokine response. Journal of Biomedical Materials Research Part A 102, 60-67

69. Morais, J., Papadimitrakopoulos, F., and Burgess, D. (2010) Biomaterials/Tissue Interactions: Possible Solutions to Overcome Foreign Body Response. AAPS J 12, 188-196

70. Williams, D. F. (2008) On the mechanisms of biocompatibility. Biomaterials 29, 2941-2953

71. Waldeck, H., Wang, X., Joyce, E., and Kao, W. J. (2012) Active leukocyte detachment and apoptosis/necrosis on PEG hydrogels and the implication in the host inflammatory response. Biomaterials 33, 29-37

72. Zhi, Z. L., Liu, B., Jones, P. M., and Pickup, J. C. (2010) Polysaccharide multilayer nanoencapsulation of insulin-producing beta-cells grown as pseudoislets for potential cellular delivery of insulin. Biomacromolecules 11, 610-616

73. Sutterwala, F. S., Noel, G. J., Clynes, R., and Mosser, D. M. (1997) Selective suppression of interleukin-12 induction after macrophage receptor ligation. Journal of Experimental Medicine 185, 1977-1985

74. Mosser, D. M., and Edwards, J. P. (2008) Exploring the full spectrum of macrophage activation. Nature Reviews Immunology 8, 958-969

75. Bradding, P., Feather, I. H., Howarth, P. H., Mueller, R., Roberts, J. A., Britten, K., Bews, J. P., Hunt, T. C., Okayama, Y., Heusser, C. H., and et al. (1992) Interleukin 4 is localized to and released by human mast cells. The Journal of experimental medicine 176, 1381-1386

76. Gordon, S., and Martinez, F. O. (2010) Alternative Activation of Macrophages: Mechanism and Functions. Immunity 32, 593-604

77. Martinez, F. O., and Gordon, S. (2014) The M1 and M2 paradigm of macrophage activation: time for reassessment. F1000Prime Rep 6, 13

78. Murray, P. J., Allen, J. E., Biswas, S. K., Fisher, E. A., Gilroy, D. W., Goerdt, S., Gordon, S., Hamilton, J. A., Ivashkiv, L. B., Lawrence, T., Locati, M., Mantovani, A., Martinez, F. O., Mege, J. L., Mosser, D. M., Natoli, G., Saeij, J. P., Schultze, J. L., Shirey, K. A., Sica, A., Suttles, J., Udalova, I., van Ginderachter, J. A., Vogel, S. N., and Wynn, T. A. (2014) Macrophage Activation and Polarization: Nomenclature and Experimental Guidelines. Immunity 41, 14-20

79. Murray, P. J., and Wynn, T. A. (2011) Protective and pathogenic functions of macrophage subsets. Nature Reviews Immunology 11, 723-737

80. El Kasmi, K. C., Qualls, J. E., Pesce, J. T., Smith, A. M., Thompson, R. W., Henao-Tamayo, M., Basaraba, R. J., Konig, T., Schleicher, U., Koo, M. S., Kaplan, G., Fitzgerald, K. A., Tuomanen, E. I., Orme, I. M., Kanneganti, T. D., Bogdan, C., Wynn, T. A., and Murray, P. J. (2008) Toll-like receptor-induced arginase 1 in macrophages thwarts effective immunity against intracellular pathogens. Nat Immunol 9, 1399-1406

81. Porcheray, F., Viaud, S., Rimaniol, A. C., Leone, C., Samah, B., Dereuddre-Bosquet, N., Dormont, D., and Gras, G. (2005) Macrophage activation switching: an asset for the resolution of inflammation. Clin Exp Immunol 142, 481-489

82. Davis, M. J., Tsang, T. M., Qiu, Y., Dayrit, J. K., Freij, J. B., Huffnagle, G. B., and Olszewski, M. A. (2013) Macrophage M1/M2 polarization dynamically adapts to changes in cytokine microenvironments in Cryptococcus neoformans infection. MBio 4, e00264-00213

83. Chinetti-Gbaguidi, G., Baron, M., Bouhlel, M. A., Vanhoutte, J., Copin, C., Sebti, Y., Derudas, B., Mayi, T., Bories, G., Tailleux, A., Haulon, S., Zawadzki, C., Jude, B., and Staels, B. (2011) Human Atherosclerotic Plaque Alternative Macrophages Display Low Cholesterol Handling but High Phagocytosis Because of Distinct Activities of the PPAR gamma and LXR alpha Pathways. Circulation Research 108, 985-995

84. Leitinger, N., and Schulman, I. G. (2013) Phenotypic Polarization of Macrophages in Atherosclerosis. Arteriosclerosis Thrombosis and Vascular Biology 33, 1120-1126

85. Pelegrin, P., and Surprenant, A. (2009) Dynamics of macrophage polarization reveal new mechanism to inhibit IL-1beta release through pyrophosphates. EMBO J 28, 2114-2127

86. Lee, H. S., Stachelek, S. J., Tomczyk, N., Finley, M. J., Composto, R. J., and Eckmann, D. M. (2013) Correlating macrophage morphology and cytokine production resulting from biomaterial contact. J Biomed Mater Res A 101, 203-212

87. McWhorter, F. Y., Wang, T. T., Nguyen, P., Chung, T., and Liu, W. F. (2013) Modulation of macrophage phenotype by cell shape. Proceedings of the National Academy of Sciences of the United States of America 110, 17253-17258

88. Vereyken, E. J., Heijnen, P. D., Baron, W., de Vries, E. H., Dijkstra, C. D., and Teunissen, C. E. (2011) Classically and alternatively activated bone marrow derived macrophages differ in cytoskeletal functions and migration towards specific CNS cell types. J Neuroinflammation 8, 58

89. Cejudo-Guillen, M., Ramiro-Gutierrez, M. L., Labrador-Garrido, A., Diaz-Cuenca, A., and Pozo, D. (2012) Nanoporous silica microparticle interaction with toll-like receptor agonists in macrophages. Acta Biomater 8, 4295-4303

90. Majani, R., Zelzer, M., Gadegaard, N., Rose, F. R., and Alexander, M. R. (2010) Preparation of Caco-2 cell sheets using plasma polymerised acrylic acid as a weak boundary layer. Biomaterials 31, 6764-6771

91. Anderson, D. G., Levenberg, S., and Langer, R. (2004) Nanoliter-scale synthesis of arrayed biomaterials and application to human embryonic stem cells. Nat Biotechnol 22, 863-866

92. Burridge, P. W., Anderson, D., Priddle, H., Munoz, M. D. B., Chamberlain, S., Allegrucci, C., Young, L. E., and Denning, C. (2007) Improved human embryonic stem cell embryoid body homogeneity and cardiomyocyte differentiation from a novel V-96 plate aggregation system highlights interline variability. Stem Cells 25, 929-938

93. Denning, C., Allegrucci, C., Priddle, H., Barbadillo-Munoz, M. D., Anderson, D., Self, T., Smith, N. M., Parkin, C. T., and Young, L. E. (2006) Common culture conditions for maintenance and cardiomyocyte differentiation of the human embryonic stem cell lines, BG01 and HUES-7. Int J Dev Biol 50, 27-37

94. Hook, A. L., Chang, C. Y., Yang, J., Scurr, D. J., Langer, R., Anderson, D. G., Atkinson, S., Williams, P., Davies, M. C., and Alexander, M. R. (2012) Polymer microarrays for high throughput discovery of biomaterials. Journal of visualized experiments : JoVE, e3636

95. Taylor, M., Urquhart, A. J., Zelzer, M., Davies, M. C., and Alexander, M. R. (2007) Picoliter water contact angle measurement on polymers. Langmuir 23, 6875-6878

96. Ray, S., and Shard, A. G. (2011) Quantitative Analysis of Adsorbed Proteins by X-ray Photoelectron Spectroscopy. Anal Chem 83, 8659-8666

97. Miranda, A. A., Le Borgne, Y. A., and Bontempi, G. (2008) New routes from minimal approximation error to principal components. Neural Process Lett 27, 197-207

98. Harrington, H., Cato, P., Salazar, F., Wilkinson, M., Knox, A., Haycock, J. W., Rose, F., Aylott, J. W., and Ghaemmaghami, A. M. (2014) Immunocompetent 3D model of human upper airway for disease modeling and in vitro drug evaluation. Molecular pharmaceutics 11, 2082-2091

99. Garcia-Nieto, S., Johal, R. K., Shakesheff, K. M., Emara, M., Royer, P. J., Chau, D. Y., Shakib, F., and Ghaemmaghami, A. M. (2010) Laminin and fibronectin treatment leads to generation of dendritic cells with superior endocytic capacity. PloS one 5, e10123

100. Wong, C. K., Li, M. L., Wang, C. B., Ip, W. K., Tian, Y. P., and Lam, C. W. (2006) House dust mite allergen Der p 1 elevates the release of inflammatory cytokines and

expression of adhesion molecules in co-culture of human eosinophils and bronchial epithelial cells. Int Immunol 18, 1327-1335

101. Horlock, C., Shakib, F., Mahdavi, J., Jones, N. S., Sewell, H. F., and Ghaemmaghami, A. M. (2007) Analysis of proteomic profiles and functional properties of human peripheral blood myeloid dendritic cells, monocyte-derived dendritic cells and the dendritic cell-like KG-1 cells reveals distinct characteristics. Genome biology 8, R30

102. Sharquie, I. K., Al-Ghouleh, A., Fitton, P., Clark, M. R., Armour, K. L., Sewell, H. F., Shakib, F., and Ghaemmaghami, A. M. (2013) An investigation into IgE-facilitated allergen recognition and presentation by human dendritic cells. Bmc Immunology 14

103. Kuchipudi, S. V., Tellabati, M., Nelli, R. K., White, G. A., Perez, B. B., Sebastian, S., Slomka, M. J., Brookes, S. M., Brown, I. H., Dunham, S. P., and Chang, K. C. (2012) 18S rRNA is a reliable normalisation gene for real time PCR based on influenza virus infected cells. Virology journal 9, 230

104. Firbank, M. J., Coulthard, A., Harrison, R. M., and Williams, E. D. (1999) A comparison of two methods for measuring the signal to noise ratio on MR images. Physics in medicine and biology 44, N261-264

105. He, Z., and Zhou, J. (2008) Empirical evaluation of a new method for calculating signal-to-noise ratio for microarray data analysis. Applied and environmental microbiology 74, 2957-2966

106. Higgins, D. M., Basaraba, R. J., Hohnbaum, A. C., Lee, E. J., Grainger, D. W., and Gonzalez-Juarrero, M. (2009) Localized immunosuppressive environment in the foreign body response to implanted biomaterials. Am J Pathol 175, 161-170

107. Bartoli, C. R., and Godleski, J. J. (2010) Blood flow in the foreign-body capsules surrounding surgically implanted subcutaneous devices. J Surg Res 158, 147-154

108. Shen, M., Garcia, I., Maier, R. V., and Horbett, T. A. (2004) Effects of adsorbed proteins and surface chemistry on foreign body giant cell formation, tumor necrosis factor alpha release and procoagulant activity of monocytes. J Biomed Mater Res A 70, 533-541

109. Sica, A., and Mantovani, A. (2012) Macrophage plasticity and polarization: in vivo veritas. J Clin Invest 122, 787-795

110. Ogle, M. E., Segar, C. E., Sridhar, S., and Botchwey, E. A. (2016) Monocytes and macrophages in tissue repair: Implications for immunoregenerative biomaterial design. Exp Biol Med 241, 1084-1097

111. Garcia, S., Krausz, S., Ambarus, C. A., Fernandez, B. M., Hartkamp, L. M., van Es, I. E., Hamann, J., Baeten, D. L., Tak, P. P., and Reedquist, K. A. (2014) Tie2 Signaling Cooperates with TNF to Promote the Pro-Inflammatory Activation of Human Macrophages Independently of Macrophage Functional Phenotype. Plos One 9

112. Mills, C. D., Kincaid, K., Alt, J. M., Heilman, M. J., and Hill, A. M. (2000) M-1/M-2 macrophages and the Th1/Th2 paradigm. Journal of Immunology 164, 6166-6173

113. Hamilton, J. A. (2002) GM-CSF in inflammation and autoimmunity. Trends Immunol 23, 403-408

114. Hamilton, J. A. (2008) Colony-stimulating factors in inflammation and autoimmunity. Nat Rev Immunol 8, 533-544

115. Verreck, F. A. W., de Boer, T., Langenberg, D. M. L., Hoeve, M. A., Kramer, M., Vaisberg, E., Kastelein, R., Kolk, A., de Waal-Malefyt, R., and Ottenhoff, T. H. M. (2004) Human IL-23-producing type 1 macrophages promote but IL-10-producing type 2, macrophages subvert, immunity to (myco)bacteria. Proceedings of the National Academy of Sciences of the United States of America 101, 4560-4565

116. Mantovani, A., Sica, A., Sozzani, S., Allavena, P., Vecchi, A., and Locati, M. (2004) The chemokine system in diverse forms of macrophage activation and polarization. Trends Immunol 25, 677-686

117. Hofkens, W., Storm, G., van den Berg, W., and van Lent, P. (2011) Inhibition of M1 Macrophage Activation in Favour of M2 Differentiation by Liposomal Targeting of Glucocorticoids to the Synovial Lining during Experimental Arthritis. Annals of the Rheumatic Diseases 70, A40-A40

118. Hao, N. B., Lu, M. H., Fan, Y. H., Cao, Y. L., Zhang, Z. R., and Yang, S. M. (2012) Macrophages in tumor microenvironments and the progression of tumors. Clinical & developmental immunology 2012, 948098

119. Agrawal, H. (2012) Macrophage phenotypes correspond with remodeling outcomes of various acellular dermal matrices. Open Journal of Regenerative Medicine 01, 51-59

120. Willenborg, S., Lucas, T., van Loo, G., Knipper, J. A., Krieg, T., Haase, I., Brachvogel, B., Hammerschmidt, M., Nagy, A., Ferrara, N., Pasparakis, M., and Eming, S. A. (2012) CCR2 recruits an inflammatory macrophage subpopulation critical for angiogenesis in tissue repair. Blood 120, 613-625

121. Bartneck, M., Schulte, V. A., Paul, N. E., Diez, M., Lensen, M. C., and Zwadlo-Klarwasser, G. (2010) Induction of specific macrophage subtypes by defined micro-patterned structures. Acta biomaterialia 6, 3864-3872

122. Edin, S., Wikberg, M. L., Dahlin, A. M., Rutegard, J., Oberg, A., Oldenborg, P. A., and Palmqvist, R. (2012) The distribution of macrophages with a M1 or M2 phenotype in relation to prognosis and the molecular characteristics of colorectal cancer. Plos One 7, e47045

123. Mantovani, A. (2006) Macrophage diversity and polarization: in vivo veritas. Blood 108, 408-409

124. Baitsch, D., Bock, H. H., Engel, T., Telgmann, R., Muller-Tidow, C., Varga, G., Bot, M., Herz, J., Robenek, H., von Eckardstein, A., and Nofer, J. R. (2011) Apolipoprotein E induces antiinflammatory phenotype in macrophages. Arterioscler Thromb Vasc Biol 31, 1160-1168

125. Choi, K. M., Kashyap, P. C., Dutta, N., Stoltz, G. J., Ordog, T., Donohue, T. S., Bauer, A. J., Linden, D. R., Szurszewski, J. H., Gibbons, S. J., and Farrugia, G. (2010) CD206-Positive M2 Macrophages That Express Heme Oxygenase-1 Protect Against Diabetic Gastroparesis in Mice. Gastroenterology 138, 2399-U2261

126. Sigal, G. B., Mrksich, M., and Whitesides, G. M. (1998) Effect of surface wettability on the adsorption of proteins and detergents. Journal of the American Chemical Society 120, 3464-3473

127. McNally, A. K., and Anderson, J. M. (2015) Phenotypic expression in human monocyte-derived interleukin-4-induced foreign body giant cells and macrophages in vitro: Dependence on material surface properties. J Biomed Mater Res A 103, 1380-1390

128. Brodbeck, W. G., Nakayama, Y., Matsuda, T., Colton, E., Ziats, N. P., and Anderson, J. M. (2002) Biomaterial surface chemistry dictates adherent monocyte/macrophage cytokine expression in vitro. Cytokine 18, 311-319

129. Murphy, W. L., McDevitt, T. C., and Engler, A. J. (2014) Materials as stem cell regulators. Nat Mater 13, 547-557

130. Celiz, A. D., Smith, J. G. W., Patel, A. K., Hook, A. L., Rajamohan, D., George, V. T., Flatt, L., Patel, M. J., Epa, V. C., Singh, T., Langer, R., Anderson, D. G., Allen, N. D., Hay, D. C., Winkler, D. A., Barrett, D. A., Davies, M. C., Young, L. E., Denning, C., and Alexander, M. R. (2015) Discovery of a Novel Polymer for Human Pluripotent Stem Cell Expansion and Multilineage Differentiation. Advanced Materials 27, 4006-4012

131. Sun, T., Han, D., Riehemann, K., Chi, L. F., and Fuchs, H. (2007) Stereospecific interaction between immune cells and chiral surfaces (vol 129, pg 1496, 2007). Journal of the American Chemical Society 129, 4853-4853

132. Senaratne, W., Sengupta, P., Jakubek, V., Holowka, D., Ober, C. K., and Baird, B. (2006) Functionalized surface arrays for spatial targeting of immune cell signaling. Journal of the American Chemical Society 128, 5594-5595

133. Zamora, P. O., Osaki, S., and Chen, M. (2003) Plasma-deposited coatings, devices and methods. Google Patents

134. Grate, J. W., Dehoff, K. J., Warner, M. G., Pittman, J. W., Wietsma, T. W., Zhang, C., and Oostrom, M. (2012) Correlation of oil-water and air-water contact angles of diverse silanized surfaces and relationship to fluid interfacial tensions. Langmuir : the ACS journal of surfaces and colloids 28, 7182-7188

135. Samuel, N. T., Wagner, M. S., Dornfeld, K. D., and Castner, D. G. (2001) Analysis of Poly(amino acids) by Static Time-of-Flight Secondary Ion Mass Spectrometry (TOF-SIMS). Surface Science Spectra 8, 163-184

136. Aderem, A., and Underhill, D. M. (1999) Mechanisms of phagocytosis in macrophages. Annual review of immunology 17, 593-623

137. Martinez, F. O., Helming, L., and Gordon, S. (2009) Alternative Activation of Macrophages: An Immunologic Functional Perspective. Annual review of immunology 27, 451-483

138. Underhill, D. M. (2003) Macrophage recognition of zymosan particles. J Endotoxin Res 9, 176-180

139. Krausgruber, T., Blazek, K., Smallie, T., Alzabin, S., Lockstone, H., Sahgal, N., Hussell, T., Feldmann, M., and Udalova, I. A. (2011) IRF5 promotes inflammatory macrophage polarization and TH1-TH17 responses. Nat Immunol 12, 231-238

140. Sica, A., and Bronte, V. (2007) Altered macrophage differentiation and immune dysfunction in tumor development. J Clin Invest 117, 1155-1166

141. Weiss, M., Blazek, K., Byrne, A. J., Perocheau, D. P., and Udalova, I. A. (2013) IRF5 is a specific marker of inflammatory macrophages in vivo. Mediators Inflamm 2013, 245804

142. Wilson, H. M. (2014) SOCS Proteins in Macrophage Polarization and Function. Frontiers in immunology 5, 357

143. Whyte, C. S., Bishop, E. T., Ruckerl, D., Gaspar-Pereira, S., Barker, R. N., Allen, J. E., Rees, A. J., and Wilson, H. M. (2011) Suppressor of cytokine signaling (SOCS)1 is a key determinant of differential macrophage activation and function. J Leukocyte Biol 90, 845-854

144. Grinnell, F., and Feld, M. K. (1982) Fibronectin adsorption on hydrophilic and hydrophobic surfaces detected by antibody binding and analyzed during cell adhesion in serum-containing medium. J Biol Chem 257, 4888-4893

145. Flick, M. J., Du, X. L., and Degen, J. L. (2004) Fibrin(ogen)alpha(M)beta(2) interactions regulate leukocyte function and innate immunity in vivo. Experimental Biology and Medicine 229, 1105-1110

146. Tang, L., Ugarova, T. P., Plow, E. F., and Eaton, J. W. (1996) Molecular determinants of acute inflammatory responses to biomaterials. J Clin Invest 97, 1329-1334

147. Duque, G. A., and Descoteaux, A. (2014) Macrophage cytokines: involvement in immunity and infectious diseases. Front Immunol 5, 1-12

148. Garcia, A. J., Vega, M. D., and Boettiger, D. (1999) Modulation of cell proliferation and differentiation through substrate-dependent changes in fibronectin conformation. Mol Biol Cell 10, 785-798

149. Lehtonen, A., Veckman, V., Nikula, T., Lahesmaa, R., Kinnunen, L., Matikainen, S., and Julkunen, I. (2005) Differential expression of IFN regulatory factor 4 gene in human monocyte-derived dendritic cells and macrophages. J Immunol 175, 6570-6579

150. Fujiwara, N., and Kobayashi, K. (2005) Macrophages in inflammation. Current drug targets. Inflammation and allergy 4, 281-286

151. Dominguez-Medina, S., Kisley, L., Tauzin, L. J., Hoggard, A., Shuang, B., Indrasekara, A. S. D. S., Chen, S. S., Wang, L. Y., Derry, P. J., Liopo, A., Zubarev, E. R., Landes, C. F., and Link, S. (2016) Adsorption and Unfolding of a Single Protein Triggers Nanoparticle Aggregation. Acs Nano 10, 2103-2112

152. Gref, R., Luck, M., Quellec, P., Marchand, M., Dellacherie, E., Harnisch, S., Blunk, T., and Muller, R. H. (2000) 'Stealth' corona-core nanoparticles surface modified by polyethylene glycol (PEG): influences of the corona (PEG chain length and surface density) and of the core composition on phagocytic uptake and plasma protein adsorption. Colloid Surface B 18, 301-313

153. Mazur, A., Holthoff, E., Vadali, S., Kelly, T., and Post, S. R. (2016) Cleavage of Type I Collagen by Fibroblast Activation Protein-alpha Enhances Class A Scavenger Receptor Mediated Macrophage Adhesion. Plos One 11, e0150287

154. Springer, N. L., and Fischbach, C. (2016) Biomaterials approaches to modeling macrophage-extracellular matrix interactions in the tumor microenvironment. Current opinion in biotechnology 40, 16-23

155. Moore, L. B., and Kyriakides, T. R. (2015) Molecular Characterization of Macrophage-Biomaterial Interactions. Advances in experimental medicine and biology 865, 109-122

156. Multhaupt, H. A., Leitinger, B., Gullberg, D., and Couchman, J. R. (2016) Extracellular matrix component signaling in cancer. Advanced drug delivery reviews 97, 28-40

157. Parekh, A., and Weaver, A. M. (2016) Regulation of invadopodia by mechanical signaling. Experimental cell research 343, 89-95

158. Yu, F. X., Zhao, B., and Guan, K. L. (2015) Hippo Pathway in Organ Size Control, Tissue Homeostasis, and Cancer. Cell 163, 811-828

159. Sridharan, R., Cameron, A. R., Kelly, D. J., Kearney, C. J., and O'Brien, F. J. (2015) Biomaterial based modulation of macrophage polarization: a review and suggested design principles. Mater Today 18, 313-325

160. Sanders, J. E., Stiles, C. E., and Hayes, C. L. (2000) Tissue response to single-polymer fibers of varying diameters: evaluation of fibrous encapsulation and macrophage density. Journal of biomedical materials research 52, 231-237

161. Cao, H., McHugh, K., Chew, S. Y., and Anderson, J. M. (2010) The topographical effect of electrospun nanofibrous scaffolds on the in vivo and in vitro foreign body reaction. J Biomed Mater Res A 93, 1151-1159

162. Schulte, V. A., Diez, M., Moller, M., and Lensen, M. C. (2009) Surface topography induces fibroblast adhesion on intrinsically nonadhesive poly(ethylene glycol) substrates. Biomacromolecules 10, 2795-2801

163. Fink, J., Fuhrmann, R., Scharnweber, T., and Franke, R. P. (2008) Stimulation of monocytes and macrophages: possible influence of surface roughness. Clinical hemorheology and microcirculation 39, 205-212

164. Spiller, D., Mirtelli, C., Losi, P., Briganti, E., Sbrana, S., Counoupas, S., Kull, S., Tonlorenzi, S., and Soldani, G. (2009) In vitro evaluation of the PEtU-PDMS material immunocompatibility: the influence of surface topography and PDMS content. Journal of materials science. Materials in medicine 20, 2511-2520

165. Chen, S., Jones, J. A., Xu, Y., Low, H. Y., Anderson, J. M., and Leong, K. W. (2010) Characterization of topographical effects on macrophage behavior in a foreign body response model. Biomaterials 31, 3479-3491

166. Boersema, G. S. A., Grotenhuis, N., Bayon, Y., Lange, J. F., and Bastiaansen-Jenniskens, Y. M. (2016) The Effect of Biomaterials Used for Tissue Regeneration Purposes on Polarization of Macrophages. Bioresearch Open Acc 5, 6-14

167. Hook, A. L., Chang, C. Y., Yang, J., Luckett, J., Cockayne, A., Atkinson, S., Mei, Y., Bayston, R., Irvine, D. J., Langer, R., Anderson, D. G., Williams, P., Davies, M. C., and Alexander, M. R. (2014) Combinatorial discovery of polymers resistant to bacterial attachment (vol 30, pg 868, 2012). Nat Biotechnol 32, 592-592

168. Celiz, A. D., Smith, J. G. W., Patel, A. K., Langer, R., Anderson, D. G., Barrett, D. A., Young, L. E., Davies, M. C., Denning, C., and Alexander, M. R. (2014) Chemically diverse polymer microarrays and high throughput surface characterisation: a method for discovery of materials for stem cell culture. Biomaterials Science 2, 1604-1611

169. Tourniaire, G., Collins, J., Campbell, S., Mizomoto, H., Ogawa, S., Thaburet, J. F., and Bradley, M. (2006) Polymer microarrays for cellular adhesion. Chem. Comm., 2118-2120

170. Kell, D. B., and Oliver, S. G. (2004) Here is the evidence, now what is the hypothesis? The complementary roles of inductive and hypothesis-driven science in the post-genomic era. BioEssays 26, 99-105

171. Celiz, A. D., Smith, J. G. W., Langer, R., Anderson, D. G., Winkler, D. A., Barrett, D. A., Davies, M. C., Young, L. E., Denning, C., and Alexander, M. R. (2014) Materials for stem cell factories of the future. Nature Materials 13, 570-579

172. Collier, T. O., Thomas, C. H., Anderson, J. M., and Healy, K. E. (2000) Surface chemistry control of monocyte and macrophage adhesion, morphology, and fusion. Journal of biomedical materials research 49, 141-145

173. Kadajji, V. G., and Betageri, G. V. (2011) Water Soluble Polymers for Pharmaceutical Applications. Polymers-Basel 3, 1972-2009

174. Jones, J. A., Dadsetan, M., Collier, T. O., Ebert, M., Stokes, K. S., Ward, R. S., Hiltner, P. A., and Anderson, J. M. (2004) Macrophage behavior on surface-modified polyurethanes. J Biomater Sci Polym Ed 15, 567-584

175. Godek, M. L., Michel, R., Chamberlain, L. M., Castner, D. G., and Grainger, D. W. (2009) Adsorbed serum albumin is permissive to macrophage attachment to perfluorocarbon polymer surfaces in culture. J Biomed Mater Res A 88A, 503-519

176. Smetana, K., Vacik, J., Houska, M., Souckova, D., and Lukas, J. (1993) Macrophage Recognition of Polymers - Effect of Carboxylate Groups. J Mater Sci-Mater M 4, 526-529

177. Rapado, M., and Peniche, C. (2015) Synthesis and characterization of pH and temperature responsive poly(2-hydroxyethyl methacrylate-co-acrylamide) hydrogels. Polimeros 25, 547-555

178. Nickle, S. K., and Werner, E. R. (1992) Waterbased coating composition of methylol (meth)acrylamide acrylic polymer, acrylic hydrosol and melamine crosslinking agent. Google Patents

179. Rihova, B., Kopecek, J., Ulbrich, K., Pospisil, M., and Mancal, P. (1984) Effect of the chemical structure of N-(2-hydroxypropyl)methacrylamide copolymers on their ability to induce antibody formation in inbred strains of mice. Biomaterials 5, 143-148

180. Mao, X., Chen, Z., Ling, J., Quan, J., Peng, H., and Xiao, Y. (2014) Methoxy-Poly(ethylene glycol) Modified Poly(L-lactide) Enhanced Cell Affinity of Human Bone Marrow Stromal Cells by the Upregulation of 1-Cadherin and Delta-2-catenin. Biomed Res Int 2014, 9

181. Zheng, X. Y., Baker, H., Hancock, W. S., Fawaz, F., McCaman, M., and Pungor, E. (2006) Proteomic analysis for the assessment of different lots of fetal bovine serum as a raw material for cell culture. Part IV. Application of proteomics to the manufacture of biological drugs. Biotechnol Progr 22, 1294-1300

182. Mpoyi, E. N., Cantini, M., Reynolds, P. M., Gadegaard, N., Dalby, M. J., and Salmeron-Sanchez, M. (2016) Protein Adsorption as a Key Mediator in the Nanotopographical Control of Cell Behavior. Acs Nano 10, 6638-6647

183. Rice, J. M., Fisher, A. C., and Hunt, J. A. (1998) Macrophage - polymer interactions. J Biomat Sci-Polym E 9, 833-847

184. Goerdt, S., and Orfanos, C. E. (1999) Other functions, other genes: alternative activation of antigen-presenting cells. Immunity 10, 137-142

185. Fleming, B. D., and Mosser, D. M. (2011) Regulatory macrophages: Setting the Threshold for Therapy. European Journal of Immunology 41, 2498-2502

186. Sindrilaru, A., Peters, T., Wieschalka, S., Baican, C., Baican, A., Peter, H., Hainzl, A., Schatz, S., Qi, Y., Schlecht, A., Weiss, J. M., Wlaschek, M., Sunderkotter, C., and Scharffetter-Kochanek, K. (2011) An unrestrained proinflammatory M1 macrophage population induced by iron impairs wound healing in humans and mice. J Clin Invest 121, 985-997

187. Arnold, C. E., Whyte, C. S., Gordon, P., Barker, R. N., Rees, A. J., and Wilson, H. M. (2014) A critical role for suppressor of cytokine signalling 3 in promoting M1 macrophage activation and function in vitro and in vivo. Immunology 141, 96-110

188. Gauzzi, M. C., Purificato, C., Conti, L., Adorini, L., Belardelli, F., and Gessani, S. (2005) IRF-4 expression in the human myeloid lineage: up-regulation during dendritic cell differentiation and inhibition by 1alpha,25-dihydroxyvitamin D3. J Leukoc Biol 77, 944-947

189. Sommer, C., and Gerlich, D. W. (2013) Machine learning in cell biology - teaching computers to recognize phenotypes. J Cell Sci 126, 5529-5539

190. Tarca, A. L., Carey, V. J., Chen, X. W., Romero, R., and Draghici, S. (2007) Machine learning and its applications to biology. Plos Comput Biol 3, 953-963

191. Wei, L. Y., Yang, Y. Y., Nishikawa, R. M., and Jiang, Y. L. (2005) A study on several machine-learning methods for classification of malignant and benign clustered microcalcifications. Ieee T Med Imaging 24, 371-380

192. Wang, N., Liang, H. W., and Zen, K. (2014) Molecular mechanisms that influence the macrophage M1-M2 polarization balance. Front Immunol 5, 9

193. Jones, T. R., Carpenter, A. E., Lamprecht, M. R., Moffat, J., Silver, S. J., Grenier, J. K., Castoreno, A. B., Eggert, U. S., Root, D. E., Golland, P., and Sabatini, D. M. (2009) Scoring diverse cellular morphologies in image-based screens with iterative feedback and machine learning. Proceedings of the National Academy of Sciences of the United States of America 106, 1826-1831

194. Matsuoka, F., Takeuchi, I., Agata, H., Kagami, H., Shiono, H., Kiyota, Y., Honda, H., and Kato, R. (2013) Morphology-Based Prediction of Osteogenic Differentiation Potential of Human Mesenchymal Stem Cells. Plos One 8, 12

195. Reynolds, P. M., Pedersen, R. H., Stormonth-Darling, J., Dalby, M. J., Riehle, M. O., and Gadegaard, N. (2013) Label-Free Segmentation of Co-cultured Cells on a Nanotopographical Gradient. Nano Lett 13, 570-576

196. Neumann, B., Held, M., Liebel, U., Erfle, H., Rogers, P., Pepperkok, R., and Ellenberg, J. (2006) High-throughput RNAi screening by time-lapse imaging of live human cells. Nat Methods 3, 385-390

197. Sierra-Filardi, E., Vega, M. A., Sanchez-Mateos, P., Corbi, A. L., and Puig-Kroger, A. (2010) Heme Oxygenase-1 expression in M-CSF-polarized M2 macrophages contributes to LPS-induced IL-10 release. Immunobiology 215, 788-795

198. Vadillo-Rodriguez, V., Busscher, H. J., Norde, W., De Vries, J., Dijkstra, R. J., Stokroos, I., and Van Der Mei, H. C. (2004) Comparison of atomic force microscopy interaction forces between bacteria and silicon nitride substrata for three commonly used immobilization methods. Appl Environ Microbiol 70, 5441-5446

199. Carpenter, A. E., Jones, T. R., Lamprecht, M. R., Clarke, C., Kang, I. H., Friman, O., Guertin, D. A., Chang, J. H., Lindquist, R. A., Moffat, J., Golland, P., and Sabatini, D. M. (2006) CellProfiler: image analysis software for identifying and quantifying cell phenotypes. Genome Biol 7, 11

200. Held, M., Schmitz, M. H., Fischer, B., Walter, T., Neumann, B., Olma, M. H., Peter, M., Ellenberg, J., and Gerlich, D. W. (2010) CellCognition: time-resolved phenotype annotation in high-throughput live cell imaging. Nat Methods 7, 747-754

201. Lee, C. H., Kim, Y. J., Jang, J. H., and Park, J. W. (2016) Modulating macrophage polarization with divalent cations in nanostructured titanium implant surfaces. Nanotechnology 27, 085101

202. Qie, Y. Q., Yuan, H. F., von Roemeling, C. A., Chen, Y. X., Liu, X. J., Shih, K. D., Knight, J. A., Tun, H. W., Wharen, R. E., Jiang, W., and Kim, B. Y. S. (2016) Surface modification of nanoparticles enables selective evasion of phagocytic clearance by distinct macrophage phenotypes. Sci Rep-Uk 6, 10

203. Chaves de Souza, J. A., Nogueira, A. V., Chaves de Souza, P. P., Kim, Y. J., Silva Lobo, C., Pimentel Lopes de Oliveira, G. J., Cirelli, J. A., Garlet, G. P., and Rossa, C., Jr. (2013) SOCS3 expression correlates with severity of inflammation, expression of proinflammatory cytokines, and activation of STAT3 and p38 MAPK in LPS-induced inflammation in vivo. Mediators of inflammation 2013, 650812

204. Sprague, A. H., and Khalil, R. A. (2009) Inflammatory cytokines in vascular dysfunction and vascular disease. Biochemical pharmacology 78, 539-552

205. Engle, S. J., and Vincent, F. (2014) Small molecule screening in human induced pluripotent stem cell-derived terminal cell types. The Journal of biological chemistry 289, 4562-4570

Appendices

Appendix I: The conditions for O_2 plasma etching and water contact angles (WCAs) of un-treated polystyrene (PS), oxygen plasma-etched polystyrene (O_2-PS40), oxygen plasma-etched polystyrene (O_2-PS8), and tissue culture well plate (TCP).

Surface	Power (W)	Duration (s)	Pressure (mTorr)
PS	-	-	-
O_2-PS8	8	5	300
TCP	-	-	-
O_2-PS40	40	60	300

Appendix II: M1(A-B) and M2(C-D)threshold controls. (A) M1 phenotype polarised with IFN-γ + GM-CSF and incubated for six days (B) Mean of maximum intensity of MR in M1 measured by CellProfiler per image (C) M2 phenotype polarised wit M-CSF+IL-4 and incubated for six days (D) Mean of maximum intensity of MR in M1 per image (B,C) X axis (pixel intensity), y axis (pixels). *n*= 2 sample for each phenotype, 9 images for each sample (mean maximum pexil intensity of =2(samples)X9(repeats)) . (A,C) Fluorescent images of cells stained for calprotectin (27E10 antigen, red), and mannose receptor (MR, green). Scale bar = 200 µm.

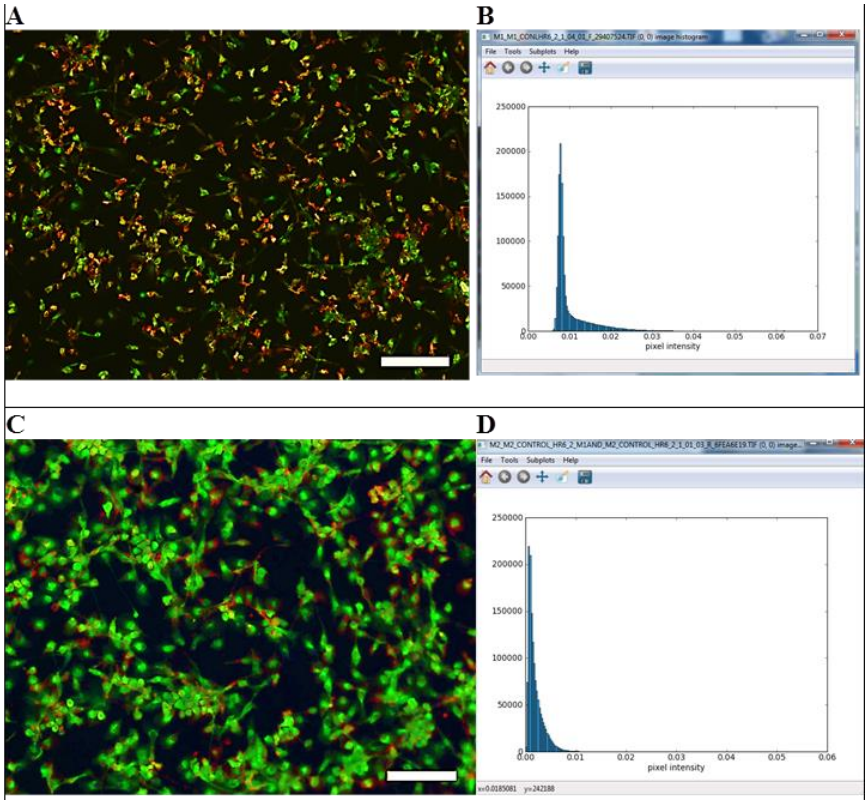

Appendix III. (A-D) **Immunofluorescent Staining of monocytes seeded on polystyrene and TCP surfaces for 6 days**. (**A**) PS, (**B**) TCP, (**C**) O2PS8, (**D**) O2PS40. Cells were stained with rabbit anti-human MR primary antibody and goat anti-rabbit secondary antibody conjugated with Alexa Fluor 488 (green), mouse anti-human 27E10 primary antibody (against calprotectin) and goat anti-mouse secondary antibody conjugated with Rhodamine red-X (red), and DAPI (blue) to visualise the nucleus. Scale bar=200 µm.

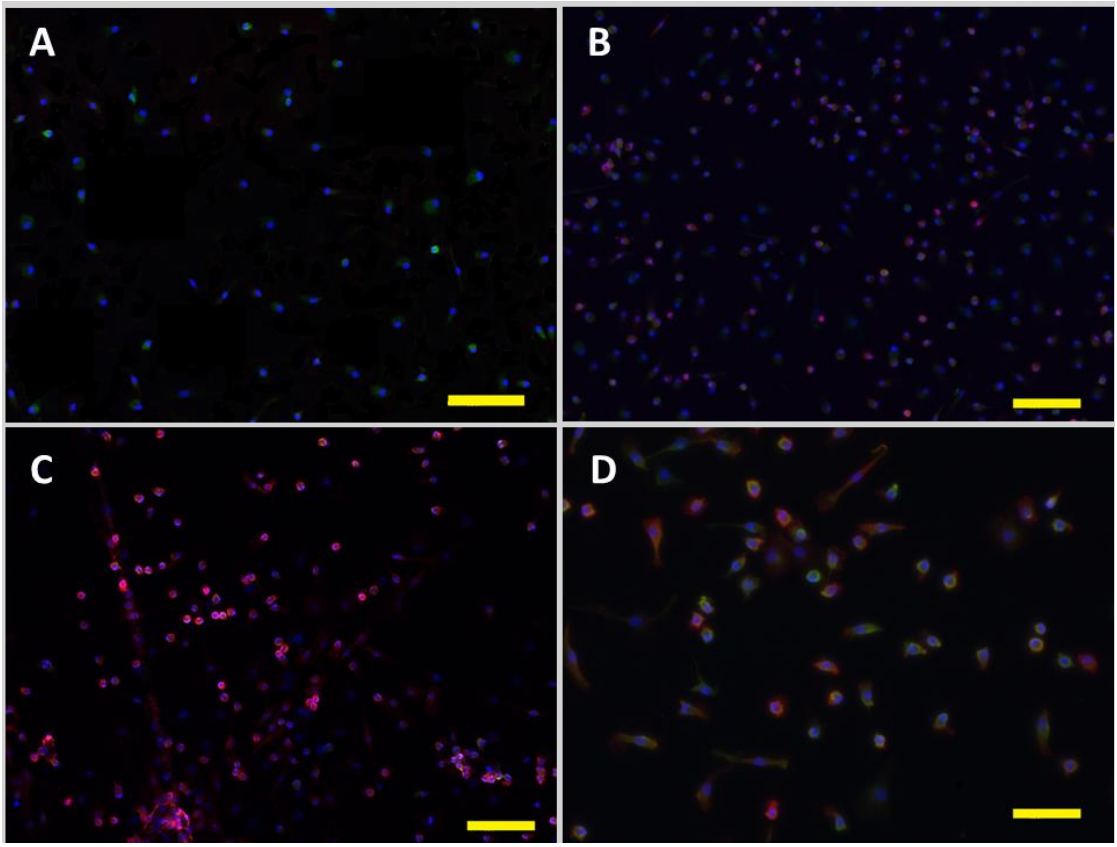

Appendix IV: The first generation microarray libraries with their code.

1	N-(4-Hydroxyphenyl)methacrylamide	**73**	N-Phenylmethacrylamide
2	N,N'-Methylenebismethacrylamide	**74**	N,N'-Methylenebisacrylamide
3	Octafluoro-2-hydroxy-6-(trifluoromethyl)heptyl methacrylate	**75**	Hexafluorobutyl methacrylate
4	Ethyl methacrylate	**76**	Allyl methacrylate
5	Octafluoropentyl acrylate	**77**	Hexadecafluoro-9-(trifluoromethyl)decyl acrylate
6	Benzyl methacrylate	**78**	Methacryloyloxy)ethyl acetoacetate
7	Octafluoropentyl methacrylate	**79**	Hexafluoropent-1,5-diyl diacrylate
8	Neopentyl glycol propoxylate diacrylate	**80**	Isodecyl acrylate
9	Tridecafluorooctyl acrylate	**81**	Hexafluoroisopropyl acrylate
10	Acrylamide	**82**	N-(3-(Dimethylamino)propyl)acrylamide
11	Diacetone acrylamide	**83**	N-tert-Butylacrylamide
12	Trimethylhexyl acrylate	**84**	Poly(ethylene glycol) phenyl ether acrylate
13	Ter-butyl methacrylate	**85**	Acryloyloxy-2-hydroxypropyl methacrylate
14	Poly(propylene glycol) acrylate	**86**	Methyl 3-hydroxy-2-methylenebutyrate
15	Ethylene glycol dimethacrylate	**87**	Poly(ethylene glycol) methyl ether acrylate
16	Tetrahydrofurfuryl acrylate	**88**	Phenyl methacrylate
17	Lauryl acrylate	**89**	Glycidyl acrylate
18	Tetra(ethylene glycol) diacrylate	**90**	Di(ethylene glycol) diacrylate
19	N-Methylmethacrylamide	**91**	N-Hydroxyethyl acrylamide
20	N-Isopropylacrylamide	**92**	N-Dodecylacrylamide
21	Tetraethylene glycol dimethacrylate	**93**	Sulfopropyl acrylate potassium salt
22	Ethoxyethyl methacrylate	**94**	3-Hydroxy-2,2-dimethylpropyl 3-hydroxy-2,2-dimethylpropionate diacrylate
23	Di(ethylene glycol) 2-ethylhexyl ether acrylate	**95**	Hydroxyethyl methacrylate
24	t-Butyl cyclohexyl methacrylate	**96**	Carboxyethyl acrylate
25	Isodecyl methacrylate	**97**	Isobornyl methacrylate
26	Butyl acrylate	**98**	Hydroxypropyl acrylate
27	Trimethylolpropane ethoxylate triacrylate	**99**	Methyl-1,2-ethanediyl bis(oxy(methyl-2,1-ethanediyl))diacrylate
28	N-(3-(Dimethylamino)propyl)methacrylamide	**100**	Blank
29	N-(1,1,3,3-tetramethylbutyl)acrylamide	**101**	N,N'-Methylenebismethacrylamide
30	3-Sulfopropyl methacrylate potassium salt	**102**	1,3,5-Triacryloylhexahydro-1,3,5-triazine
31	Bisphenol A ethoxylate diacrylate	**103**	Hexyl methacrylate
32	Butyl methacrylate	**104**	Hydroxybutyl methacrylate
33	Hexanediol ethoxylate diacrylate	**105**	Poly(propylene glycol) diacrylate
34	Tetrahydrofurfuryl methacrylate	**106**	Lauryl methacrylate
35	Hexyl acrylate	**107**	Ethylene glycol methyl ether methacrylate
36	Trimethylolpropane triacrylate	**108**	Isobornyl acrylate
37	Methacrylamide	**109**	N-(3-Aminopropyl)methacrylamide hydrochloride
38	N,N'-(1,2-Dihydroxyethylene)bisacrylamide	**110**	1,4-Bis(acryloyl)piperazine
39	Tridecafluorooctyl methacrylate	**111**	Hexafluoroisopropyl methacrylate
40	Di(ethylene glycol) methyl ether methacrylate	**112**	Acryloyloxy-ß,ß-dimethyl-Y-butyrolactone
41	Hexafluorobutyl acrylate	**113**	Heptadecafluorodecyl methacrylate
42	Cyclohexyl methacrylate	**114**	Stearyl methacrylate
43	Heptafluorobutyl methacrylate	**115**	Dodecafluoro-7-(trifluoromethyl)-octyl acrylate
44	Neopentyl glycol diacrylate	**116**	Isooctyl acrylate
45	Dodecafluoroheptyl acrylate	**117**	Heptafluorobutyl acrylate

46	N-(Isobutoxymethyl)acrylamide	**118**	N,N'-Dimethylacrylamide
47	N-(Tris(hydroxymethyl)methyl)acrylamide	**119**	N-(Butoxymethyl)acrylamide
48	Ethoxyethyl acrylate	**120**	Glycerol dimethacrylate
49	Hydroxypropyl methacrylate	**121**	Butoxyethyl methacrylate
50	Decyl methacrylate	**122**	Ethylene glycol diacrylate
51	Hydroxy-3-phenoxypropyl acrylate	**123**	Chloro-2-hydroxy-propyl methacrylate
52	Methylthioethyl methacrylate	**124**	Caprolactone 2-(methacryloyloxy)ethyl ester
53	Ethyl acrylate	**125**	Di(ethylene glycol) ethyl ether acrylate
54	Trimethylolpropane ethoxylate methyl ether diacrylate	**126**	Isobutyl acrylate
55	N-(3-Methoxypropyl)acrylamide	**127**	N,N'-Dimethylmethacrylamide
56	Acrylamide	**128**	N-(Hydroxymethyl)acrylamide
57	Tri(ethylene glycol) dimethacrylate	**129**	[2-(Methacryloyloxy)ethyl]dimethyl-(3-sulfopropyl) ammonium hydroxide
58	Hydroxypivalyl hydroxypivalate bis(6-(acryloyloxy)hexanoate)	**130**	Tris(2-(acryloyloxy)ethyl) isocyanurate
59	Ethyl 2-ethylacrylate	**131**	Glycidyl methacrylate
60	Tricyclodecane-dimethanol diacrylate	**132**	Benzyl acrylate
61	Ethylhexyl methacrylate	**133**	Norbornyl methacrylate
62	Propargyl acrylate	**134**	Ethylene glycol phenyl ether methacrylate
63	Hexamethylene diacrylate	**135**	Ethylene glycol phenyl ether methacrylate
64	Blank	**136**	Blank
65	N-(2-(1H-indol-3-yl)ethyl)acrylamide	**137**	N-tert-Butylmethacrylamide
66	2-Methacryloyloxyethyl phosphorylcholine	**138**	Dimethylamino-ethyl acrylate
67	Tert-butylcyclohexylacrylate	**139**	Cyanoethyl acrylate
68	Vinyl methacrylate	**140**	Tert-butylamino-ethyl methacrylate
69	Butanediol diacrylate	**141**	Dimethylamino-ethyl methacrylate
70	Furfuryl methacrylate	**142**	Diethylaminoethyl methacrylate
71	Ethylhexyl acrylate	**143**	Dimethylamino-propyl acrylate
72	Butanediol-1,3 diacrylate	**144**	Diethylamino ethyl acrylate

Appendix V: The most 10 effective homo-polymers on inter donor average number of M1 or M2 cell+ with highest cell adherence.

M1(bias) monomer			M2(bias) monomer		
Code	**Monomer name**	**Monomer structure**	**Code**	**Monomer name**	**Monomer structure**
98	Hydroxypropyl acrylate	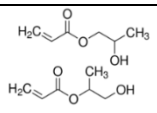	50	Decyl methacrylate	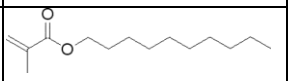
126	Isobutyl acrylate	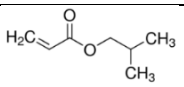	35	Hexyl acrylate	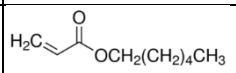
135	Glycerol propoxylate triacrylate	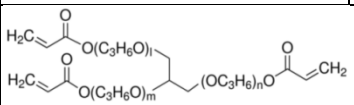	94	Poly(propylene glycol) diacrylate	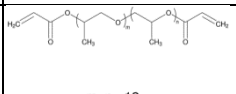 m+n= 12
117	Heptafluorobutyl acrylate	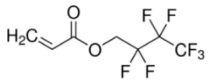	47	N-[Tris(hydroxymethyl)methyl]acrylamide	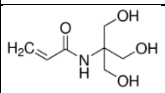
113	Heptadecafluorodecyl methacrylate	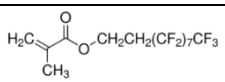	37	Methacrylamide	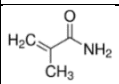
141	Dimethylamino-ethyl methacrylate	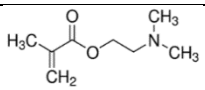	9	Tridecafluorooctyl acrylate	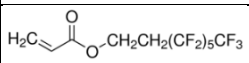
125	Di(ethylene glycol) ethyl ether acrylate	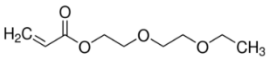	29	N-(1,1,3,3-tetramethylbutyl)acrylamide	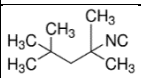
115	Dodecafluoro-7-(trifluoromethyl)-octyl acrylate	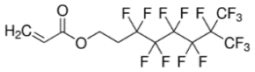	3	Octafluoro-2-hydroxy-6-(trifluoromethyl)heptyl methacrylate	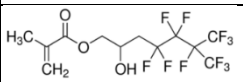
123	Chloro-2-hydroxy-propyl methacrylate	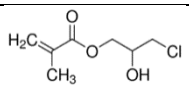	121	Butoxyethyl methacrylate	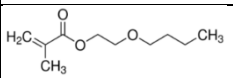
73	N-Phenylmethacrylamide	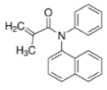	71	Ethylhexyl acrylate	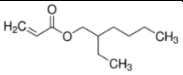

Appendix VI: Second generation polymer library with their code and their constituent.

231-253	208-230	185-207	162-184	139-161	116-138	93-115	70-92	47-69	24-46	1-23
66% (67) 33% (88)	66% (90) 33% (126)	66% (15) 33% (126)	66% (42) 33% (126)	66% (25) 33% (126)	66% (88) 33% (126)	66% (90) 33% (88)	66% (15) 33% (88)	66% (42) 33% (88)	66% (25) 33% (88)	66% (88) 33% (88)
66% (3) 33% (47)	66% (35) 33% (126)	66% (29) 33% (126)	66% (50) 33% (126)	66% (94) 33% (126)	66% (9) 33% (126)	66% (35) 33% (47)	66% (29) 33% (47)	66% (50) 33% (47)	66% (94) 33% (47)	66% (9) 33% (47)
66% (37) 33% (37)	66% (47) 33% (98)	66% (61) 33% (98)	66% (24) 33% (98)	66% (67) 33% (98)	66% (90) 33% (98)	66% (47) 33% (37)	66% (61) 33% (25)	66% (24) 33% (25)	66% (67) 33% (25)	66% (90) 33% (25)
66% (15) 33% (42)	66% (42) 33% (135)	66% (25) 33% (135)	66% (88) 33% (135)	66% (3) 33% (98)	66% (35) 33% (98)	66% (42) 33% (42)	66% (25) 33% (42)	66% (88) 33% (42)	66% (3) 33% (37)	66% (35) 33% (37)
66% (29) 33% (9)	66% (50) 33% (135)	66% (94) 33% (135)	66% (9) 33% (135)	66% (37) 33% (135)	66% (47) 33% (135)	66% (50) 33% (9)	66% (94) 33% (9)	66% (9) 33% (9)	66% (37) 33% (9)	66% (47) 33% (9)
66% (61) 33% (15)	66% (24) 33% (117)	66% (67) 33% (117)	66% (90) 33% (117)	66% (15) 33% (117)	66% (42) 33% (117)	66% (24) 33% (15)	66% (67) 33% (15)	66% (90) 33% (15)	66% (15) 33% (15)	66% (42) 33% (15)
66% (25) 33% (90)	66% (88) 33% (113)	66% (3) 33% (117)	66% (35) 33% (117)	66% (29) 33% (117)	66% (50) 33% (117)	66% (88) 33% (90)	66% (3) 33% (94)	66% (35) 33% (94)	66% (29) 33% (94)	66% (50) 33% (94)
66% (94) 33% (50)	66% (9) 33% (113)	66% (37) 33% (113)	66% (47) 33% (113)	66% (61) 33% (113)	66% (24) 33% (113)	66% (9) 33% (50)	66% (37) 33% (50)	66% (47) 33% (50)	66% (61) 33% (90)	66% (24) 33% (90)
66% (67) 33% (67)	66% (90) 33% (141)	66% (15) 33% (141)	66% (42) 33% (141)	66% (25) 33% (141)	66% (88) 33% (141)	66% (90) 33% (67)	66% (15) 33% (67)	66% (42) 33% (67)	66% (25) 33% (67)	66% (88) 33% (67)
66% (3) 33% (29)	66% (35) 33% (141)	66% (29) 33% (141)	66% (50) 33% (141)	66% (94) 33% (141)	66% (9) 33% (141)	66% (35) 33% (29)	66% (29) 33% (29)	66% (50) 33% (29)	66% (94) 33% (29)	66% (9) 33% (29)
66% (37) 33% (35)	66% (47) 33% (125)	66% (61) 33% (125)	66% (24) 33% (125)	66% (67) 33% (125)	66% (90) 33% (125)	66% (47) 33% (35)	66% (61) 33% (24)	66% (24) 33% (24)	66% (67) 33% (24)	66% (90) 33% (24)
66% (15) 33% (61)	66% (42) 33% (115)	66% (25) 33% (115)	66% (88) 33% (115)	66% (3) 33% (125)	66% (35) 33% (125)	66% (42) 33% (61)	66% (25) 33% (61)	66% (88) 33% (61)	66% (3) 33% (35)	66% (35) 33% (35)
66% (29) 33% (3)	66% (50) 33% (115)	66% (94) 33% (115)	66% (9) 33% (115)	66% (37) 33% (115)	66% (47) 33% (115)	66% (50) 33% (3)	66% (94) 33% (3)	66% (9) 33% (3)	66% (37) 33% (3)	66% (47) 33% (3)
66% (133) 33% (61)	66% (133) 33% (125)	66% (133) 33% (141)	66% (133) 33% (113)	66% (133) 33% (117)	66% (133) 33% (135)	66% (133) 33% (24)	66% (133) 33% (67)	66% (133) 33% (90)	66% (133) 33% (15)	66% (133) 33% (42)
66% (22) 33% (25)	66% (22) 33% (126)	66% (115) 33% (133)	66% (125) 33% (133)	66% (141) 33% (133)	66% (113) 33% (133)	66% (22) 33% (88)	66% (61) 33% (133)	66% (24) 33% (133)	66% (67) 33% (133)	66% (90) 33% (133)
66% (15) 33% (22)	66% (135) 33% (22)	66% (98) 33% (22)	66% (126) 33% (22)	66% (22) 33% (115)	66% (22) 33% (125)	66% (42) 33% (22)	66% (25) 33% (22)	66% (88) 33% (22)	66% (22) 33% (61)	66% (22) 33% (24)
66% (121) 33% (29)	66% (121) 33% (113)	66% (121) 33% (117)	66% (121) 33% (135)	66% (121) 33% (98)	66% (121) 33% (126)	66% (121) 33% (50)	66% (121) 33% (94)	66% (121) 33% (9)	66% (121) 33% (37)	66% (121) 33% (47)
66% (3) 33% (121)	66% (125) 33% (121)	66% (141) 33% (121)	66% (113) 33% (121)	66% (117) 33% (121)	66% (135) 33% (121)	66% (35) 33% (121)	66% (29) 33% (121)	66% (50) 33% (121)	66% (94) 33% (121)	66% (9) 33% (121)
66% (37) 33% (71)	66% (126) 33% (71)	66% (71) 33% (115)	66% (71) 33% (125)	66% (71) 33% (141)	66% (71) 33% (113)	66% (47) 33% (71)	66% (71) 33% (3)	66% (71) 33% (35)	66% (71) 33% (29)	66% (71) 33% (50)
66% (15) 33% (123)	66% (9) 33% (123)	66% (37) 33% (123)	66% (47) 33% (123)	66% (115) 33% (71)	66% (125) 33% (71)	66% (42) 33% (123)	66% (25) 33% (123)	66% (88) 33% (123)	66% (3) 33% (71)	66% (35) 33% (71)
66% (67) 33% (73)	66% (50) 33% (73)	66% (94) 33% (73)	66% (9) 33% (73)	66% (37) 33% (73)	66% (47) 33% (73)	66% (90) 33% (73)	66% (15) 33% (73)	66% (42) 33% (73)	66% (25) 33% (73)	66% (88) 33% (73)
100% (125)	100% (141)	100% (117)	100% (98)	66% (71) 33% (73)	66% (22) 33% (73)	100% (113)	100% (135)	100% (126)	66% (121) 33% (73)	66% (133) 33% (73)
					66% (71) 33% (121)					66% (121) 33% (71)

438-460	415-437	392-414	369-391	346-368	323-345	300-322	277-299	254-276	
66% (37) 33% (126)	66% (47) 33% (126)	66% (61) 33% (126)	66% (24) 33% (126)	66% (67) 33% (126)	66% (37) 33% (47)	66% (47) 33% (47)	66% (61) 33% (88)	66% (24) 33% (88)	
66% (15) 33% (98)	66% (42) 33% (98)	66% (25) 33% (98)	66% (88) 33% (98)	66% (3) 33% (126)	66% (15) 33% (25)	66% (42) 33% (25)	66% (25) 33% (25)	66% (88) 33% (25)	
66% (29) 33% (98)	66% (50) 33% (98)	66% (94) 33% (98)	66% (9) 33% (98)	66% (37) 33% (98)	66% (29) 33% (37)	66% (50) 33% (37)	66% (94) 33% (37)	66% (9) 33% (37)	
66% (61) 33% (135)	66% (24) 33% (135)	66% (67) 33% (135)	66% (90) 33% (135)	66% (15) 33% (135)	66% (61) 33% (42)	66% (24) 33% (42)	66% (67) 33% (42)	66% (90) 33% (42)	
66% (25) 33% (117)	66% (88) 33% (117)	66% (3) 33% (135)	66% (35) 33% (135)	66% (29) 33% (135)	66% (25) 33% (15)	66% (88) 33% (15)	66% (3) 33% (9)	66% (35) 33% (9)	
66% (94) 33% (117)	66% (9) 33% (117)	66% (37) 33% (117)	66% (47) 33% (117)	66% (61) 33% (117)	66% (94) 33% (94)	66% (9) 33% (94)	66% (37) 33% (94)	66% (47) 33% (94)	
66% (67) 33% (113)	66% (90) 33% (113)	66% (15) 33% (113)	66% (42) 33% (113)	66% (25) 33% (113)	66% (67) 33% (90)	66% (90) 33% (90)	66% (15) 33% (90)	66% (42) 33% (90)	
66% (3) 33% (113)	66% (35) 33% (113)	66% (29) 33% (113)	66% (50) 33% (113)	66% (94) 33% (113)	66% (3) 33% (50)	66% (35) 33% (50)	66% (29) 33% (50)	66% (50) 33% (50)	
66% (37) 33% (141)	66% (47) 33% (141)	66% (61) 33% (141)	66% (24) 33% (141)	66% (67) 33% (141)	66% (37) 33% (29)	66% (47) 33% (29)	66% (61) 33% (67)	66% (24) 33% (67)	
66% (15) 33% (125)	66% (42) 33% (125)	66% (25) 33% (125)	66% (88) 33% (125)	66% (3) 33% (141)	66% (15) 33% (24)	66% (42) 33% (24)	66% (25) 33% (24)	66% (88) 33% (24)	
66% (29) 33% (125)	66% (50) 33% (125)	66% (94) 33% (125)	66% (9) 33% (125)	66% (37) 33% (125)	66% (29) 33% (35)	66% (50) 33% (35)	66% (94) 33% (35)	66% (9) 33% (35)	
66% (61) 33% (115)	66% (24) 33% (115)	66% (67) 33% (115)	66% (90) 33% (115)	66% (15) 33% (115)	66% (61) 33% (61)	66% (24) 33% (61)	66% (67) 33% (61)	66% (90) 33% (61)	
66% (133) 33% (98)	66% (133) 33% (126)	66% (3) 33% (115)	66% (35) 33% (115)	66% (29) 33% (115)	66% (133) 33% (25)	66% (133) 33% (88)	66% (3) 33% (3)	66% (35) 33% (3)	
66% (117) 33% (133)	66% (135) 33% (133)	66% (98) 33% (133)	66% (126) 33% (133)	66% (133) 33% (115)	66% (15) 33% (133)	66% (42) 33% (133)	66% (25) 33% (133)	66% (88) 33% (133)	
66% (22) 33% (141)	66% (22) 33% (113)	66% (22) 33% (117)	66% (22) 33% (135)	66% (22) 33% (98)	66% (22) 33% (67)	66% (22) 33% (90)	66% (22) 33% (15)	66% (22) 33% (42)	
66% (115) 33% (22)	66% (125) 33% (22)	66% (141) 33% (22)	66% (113) 33% (22)	66% (117) 33% (22)	66% (61) 33% (22)	66% (24) 33% (22)	66% (67) 33% (22)	66% (90) 33% (22)	
66% (98) 33% (121)	66% (126) 33% (121)	66% (121) 33% (115)	66% (121) 33% (125)	66% (121) 33% (141)	66% (37) 33% (121)	66% (47) 33% (121)	66% (121) 33% (3)	66% (121) 33% (35)	
66% (71) 33% (117)	66% (71) 33% (135)	66% (71) 33% (98)	66% (71) 33% (126)	66% (115) 33% (121)	66% (71) 33% (94)	66% (71) 33% (9)	66% (71) 33% (37)	66% (71) 33% (47)	
66% (141) 33% (71)	66% (113) 33% (71)	66% (117) 33% (71)	66% (135) 33% (71)	66% (98) 33% (71)	66% (29) 33% (71)	66% (50) 33% (71)	66% (94) 33% (71)	66% (9) 33% (71)	
66% (3) 33% (123)	66% (35) 33% (123)	66% (29) 33% (123)	66% (50) 33% (123)	66% (94) 33% (123)	66% (61) 33% (123)	66% (24) 33% (123)	66% (67) 33% (123)	66% (90) 33% (123)	
66% (71) 33% (123)	66% (22) 33% (123)	66% (3) 33% (73)	66% (35) 33% (73)	66% (29) 33% (73)	66% (121) 33% (123)	66% (133) 33% (123)	66% (61) 33% (73)	66% (24) 33% (73)	
100 % (71)	66% (22) 33% (133)	100 % (22)	100% (73)	100% (115)	100 % (121)	66% (133) 33% (22)	100 % (133)	100% (123)	

Appendix VII: Polarised macrophage by cytokines (**A**) M1 phenotype polarised with IFN-γ + GM-CSF **(B)** M2 phenotype polarised wit M-CSF+IL-4. (**A,B)**. Fluorescent images of cells stained for calprotectin (27E10 antigen, red), and mannose receptor (MR, green). Scale bar = 200 µm .(**C)** Scatter plot for number of M2 /M1polarised cells with cytokines on glass slide, X-axis average total cell number of the adherent cells ,Y-axis is number of cells expressed MR^+(M2- phenotype)/ number of cell expressed calprotectin (M1- phenotype)on glass slide. Dotted line is cells with M2-cells (MR^+ cells)/M2-cells ($Calprotectin^+$ cells) =1 . *n*=3 of different samples (M1 and M2) for each sample with 20 replicates. (M1 mean and M2 mean) are mean of M1 and M2 samples respectively.